NASA
National Aeronautics and
Space Administration

Lyndon B. Johnson Space Center
Houston, Texas 77058

LUNAR CURATORIAL BRANCH
PUBLICATION NUMBER 61

JSC 17172

CATALOG OF THE APOLLO 16 LUNAR CORE 60009/60010

R. M. Fruland
NATIONAL AERONAUTICS AND SPACE ADMINISTRATION
LYNDON B. JOHNSON SPACE CENTER
HOUSTON, TEXAS

J. S. Nagle
J. H. Allton
NORTHOP SERVICES, INCORPORATED
HOUSTON, TEXAS

MARCH 1982

ACKNOWLEDGEMENTS

Many people contributed to the effort that went into this catalog, beginning with the astronauts Charles Duke and John Young, who collected the 60009/60010 core. Lunar Curatorial Laboratory people who provided for the core's safe-keeping and its non-destructive removal of the soil column from the core tube were William Parkan, Steve Waltz, Ed Miller, and Wayne Walton. The soil column was processed, beginning to end, by J. Stewart Nagle.

During preparation of the catalog, Judy Allton provided creative as well as physical support. Claudine Robb, Sherry Feicht, and Gary Kitmacher are responsible for the majority of the graphics (the other figures and tables were lifted from published papers). The essential typing support was provided by Diana Luis in the early stage of compilation, and by Alene Simmons, during the middle and final stages. Jeanette Simon helped with typing when brush fires arose. The final layout was done by Claudine Robb. Helpful comments and suggestions were given by many people including Richard Morris, Dave Walker, Jeff Taylor, Fred Horz, Dave McKay, and Janet Nieber-Reimold. Finally, I would like to thank Pat Butler for his guidance and encouragement during the time that he was the curator when I first started to compile this catalog.

TABLE OF CONTENTS

LIST OF FIGURES

LIST OF TABLES

1.0 INTRODUCTION TO THE 60009/10 CORE

1.1 COLLECTION

A core tube was scheduled to be taken on the return from North Ray Crater at the base of the Smokey Mountains. This would have given another "Descartes" sample for comparison with the 64001/64002 Stone Mountain core. When the third Extravehicular Activity (EVA) was shortened by two hours, this was not possible, and so a sampling site in the Lunar Module/Apollo Lunar Surface Experiment Package area (LM/ALSEP) was chosen instead. The site for this core, 60009/60010, and those of the two previously collected cores, 60001 through 60007 (the deep drill core) and 60013/60014, form a rough equilateral triangle having approximately 50 meter sides. The spatial arrangement is illustrated in Figure 1.1.

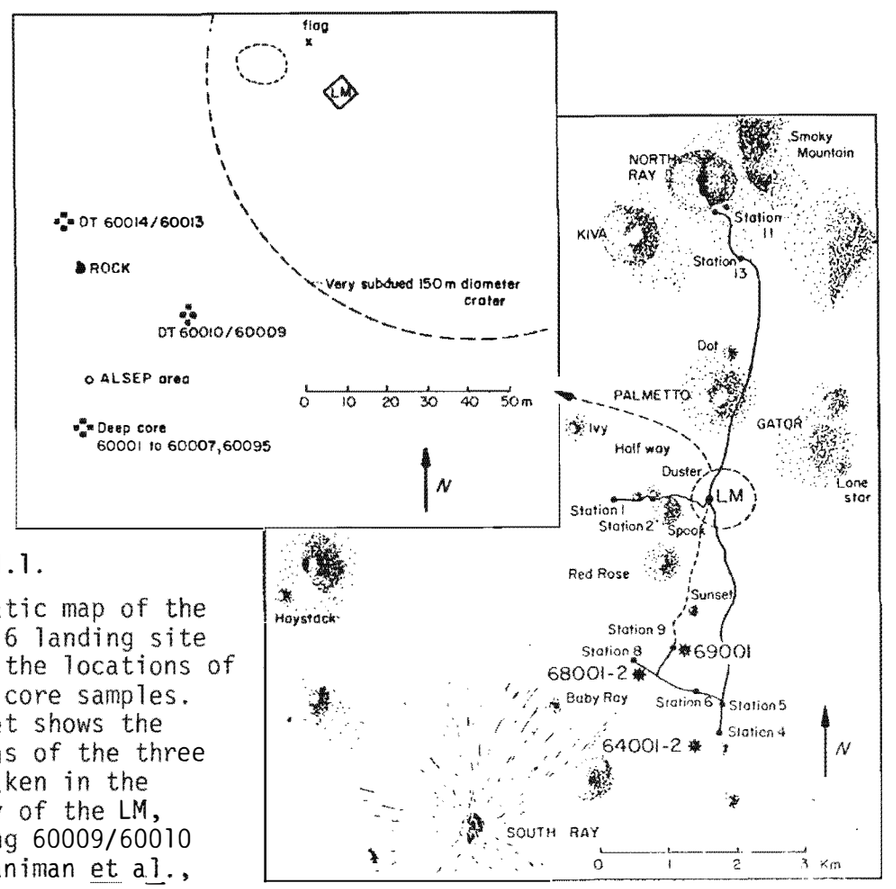

Figure 1.1.

A schematic map of the Apollo 16 landing site showing the locations of the six core samples. The inset shows the locations of the three cores taken in the vicinity of the LM, including 60009/60010 (from Vaniman et al., 1976).

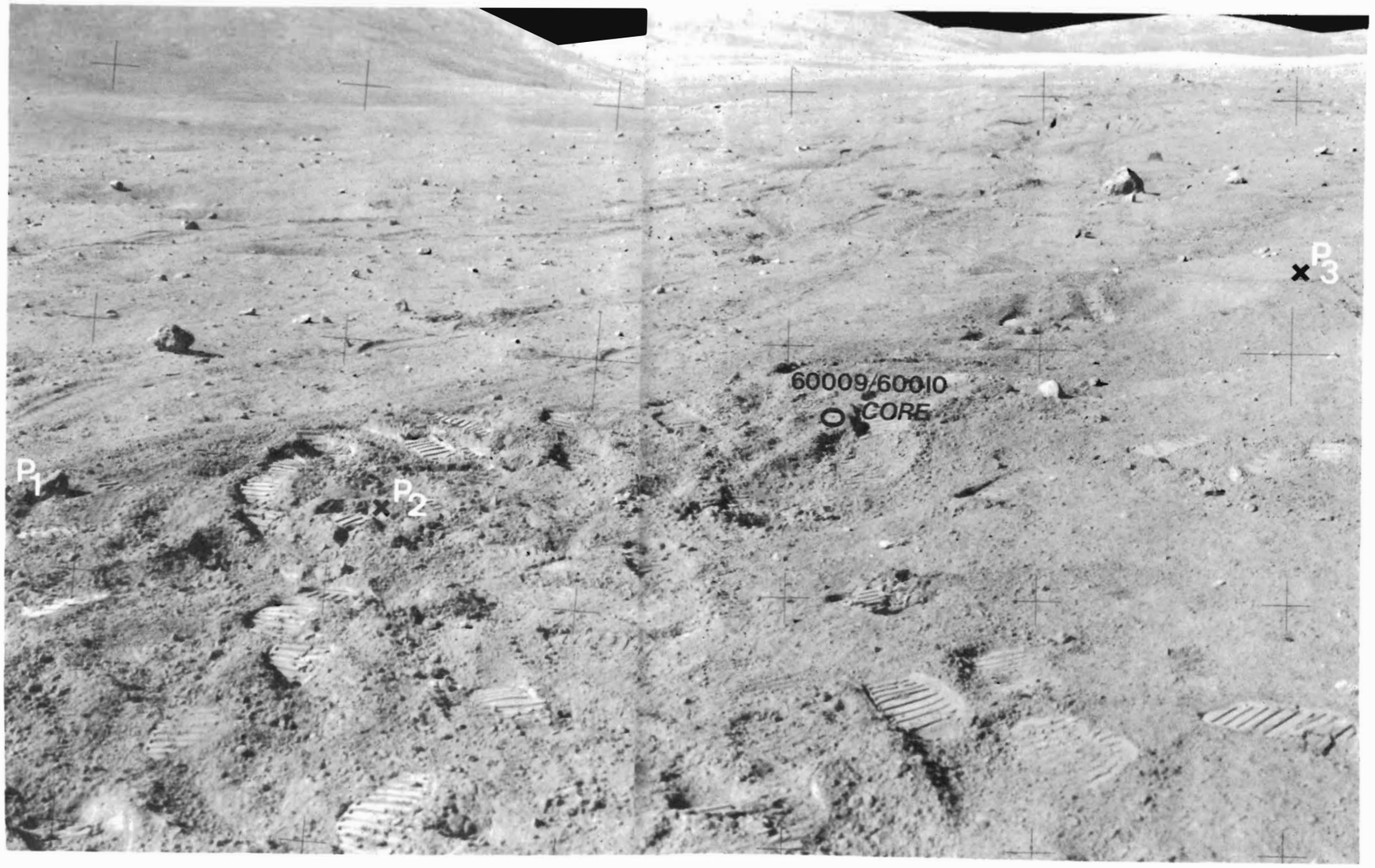

Figure 1.2 shows the general appearance of the Cayley Plains, including the area where the 60009/60010 core and several penetrometer tests were taken. (AS16-114-18464,65)

The general appearance of the Cayley Plains is seen in Figure 1.2. The location of the 60009/60010 core and associated penetrometer test locations are shown. According to astronauts' descriptions, this area was not as rocky on the surface (although there were more rake samples) as where the 60013/60014 core was collected. There were numerous meter-sized craters. Core 60009/60010 was collected on the rim of a 0.6 meter crater, shown in Figure 1.3. Although the crater is subdued, there is the possibility that some of the stratigraphy in the core is from the cratering event. According to the astronauts' transcripts, the core went about 18 centimeters into the regolith with little difficulty. Then, it required so many hammer blows to drive it completely in, that J. Young, who collected the sample,

Figure 1.3 shows the 60009/60010 core in place. The slight depression to the left of the core tube is a 0.6 meter subdued crater. (AS16-115-18557)

was not sure he was going to be successful (Bailey and Ulrich, 1975).

1.2 PENETROMETER TESTS

An intriguing observation connected with the collection of the 60009/60010 core is the apparent correlation with several penetrometer results. SRP tests (self-recording penetrometer) nearby indicated a resistant layer in the regolith about 20 centimeters beneath the surface, corresponding to the depth at which the core tube could no longer be pushed into the soil; one test indicated a rocky layer at about 50 centimeters (Mitchell et al., 1972). The latter corresponds to a rocky layer observed in the opened core, and was apparently the cause of Young's difficulty in collecting the sample. After the core tube and the soil column were examined (Figure 1.4), it became evident that Young had cut a large rock fragment into pieces during his hammering on the core tube: some of the rock was sampled; the rest remains at the Apollo 16 site.

1.3 CONDITION OF THE CORE UPON RETURN TO THE EARTH

The core was placed in Apollo Lunar Sample Return Container (ALSRC) #2 by the astronauts for the trip home. This was vacuum-sealed on the lunar surface, so that the core would not be exposed to the spacecraft environment during the return trip to Earth. Both core tube sections were measured to be at 80 μm pressure upon examination in the Lunar Receiving Laboratory (LRL).

1.4 X-RADIOGRAPHY

Both core tubes appeared to be filled with lunar soil in the x-radiographs taken shortly after their return to the LRL. Units of coarser and finer components, as well as numerous rock fragments could be discerned. Previous catalogs (Duke and Nagle, 1974; Duke and Nagle, 1976) and the Apollo 16 Preliminary Science Report have described and discussed the results. The x-radiographs were primarily an aid for extrusion and dissection planning. Because the core has since been opened and studied, these early results are not repeated here. These x-radiographs are available through the Curator's office.

1.5 MAGNETICS EXPERIMENT

An additional experiment was conducted on the unopened 60010 core tube by D. Strangway and G.W. Pearce. It

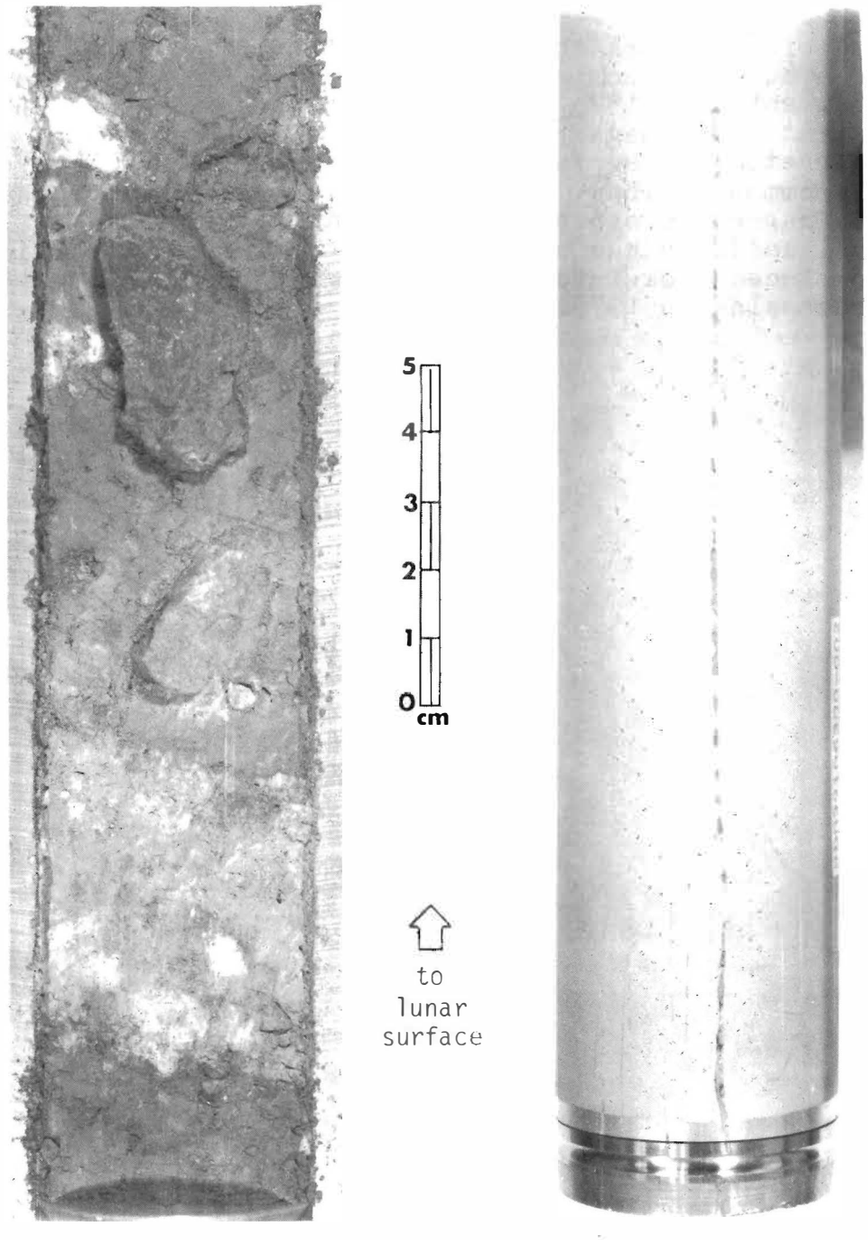

Figure 1.4 The core tube on the right was scratched inside and outside to approximately 16 cm from the bottom. This corresponds to one large and numerous small rocks at the 42 cm depth point. On the left, the 60009 soil column is shown before the third dissection pass. (S-75-26667, S-75-30840)

consisted of isolating the core from the Earth's magnetic field in a mu-metal container from the 16th of August to the 4th of September in 1973. This was to enable measurement of the remanent lunar magnetism. The core was found to be highly magnetic, as surface soils usually are (G.W. Pearce, personal communication). The core tube was x-radiographed after the magnetics experiment to confirm that the additional handling had not caused any internal disruption, and then placed back into storage in the Curatorial Facility until processing in 1975.

2.0 REMOVAL OF THE SAMPLES FROM THE CORE TUBE

2.1 EXTRUSION OF SOIL COLUMN

The processing of the 60009/60010 core was delayed until 1975 because procedures and equipment had to be developed that would minimize disturbance to the soil column. The equipment used for extruding large diameter cores is shown in Figure 2.1.

Each section was dissected in two stages, and the lower section, 60009 was dissected first. For stage one, the core was oriented vertically in the same direction as during collection on the lunar surface. A series of 1 mm thick soil discs were then removed from the top five millimeters (see Figure 2.2). The purpose in doing this for 60009 was to test the procedure before dissecting the top part of the 60010 soil column, which was contiguous with the lunar surface.

The second phase involved slowly extruding the soil column into a special cylindrical receptacle made out of a series of removable aluminum side plates and a top silica-glass plate (Figures 2.1, 2.2). The core extruder seen in Figure 2.1 gently pushed the soil column into the receptacle, and after the fused silica cover was taken off, successive longitudinal soil layers were then removed or "dissected" (Figure 2.2). The soil columns were extruded with the same direction of motion as the initial entry of material (i.e., out the top of the core tube section). Although the relative positions of particles and stratigraphy appeared to be preserved during extrusion, some compaction did occur. The extruded length of the soil column was about 3 cm less for each section than the length indicated by the x-radiographs (Duke and Nagle, 1974). Additional compaction and/or extension may have occurred during collection on the Moon and subsequent handling before the samples were returned to the LRL.

A photograph of the freshly extruded 60009 soil column is shown in Figure 2.3 (left view). The surface appeared nearly uniform from the smearing that resulted from pushing the soil column from the core tube into the dissection cylinder. The smeared surface was also contaminated chemically from being adjacent to the inner wall of the core tube. Therefore, the smeared exterior, to about a millimeter depth, was scraped off with clean tools revealing the stratigraphy of the soil column, Figure 2.3 (right view). From observations of this surface, the initial dissection plan for the soil column was prepared.

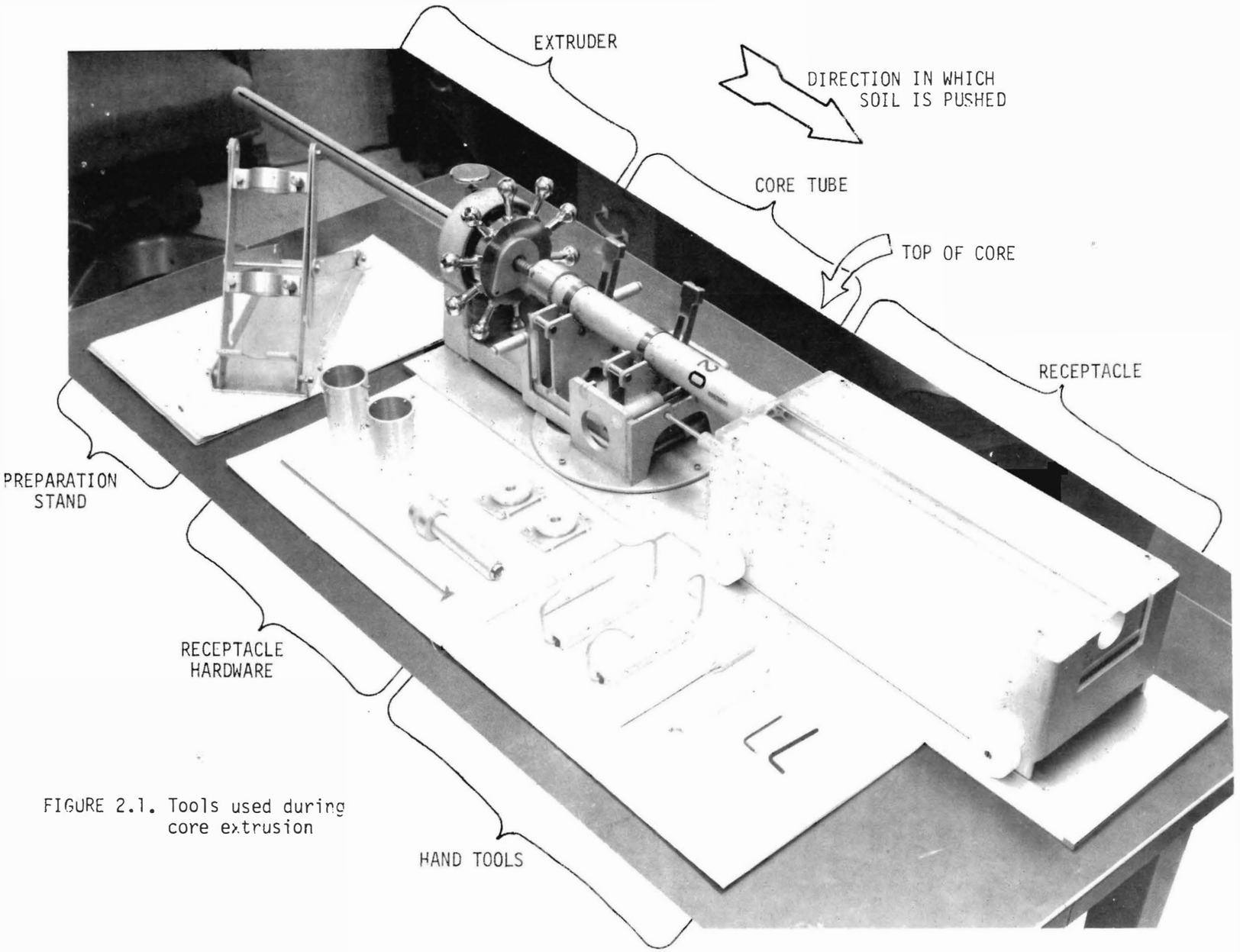

FIGURE 2.1. Tools used during core extrusion

Removal of Samples from Core Tubes

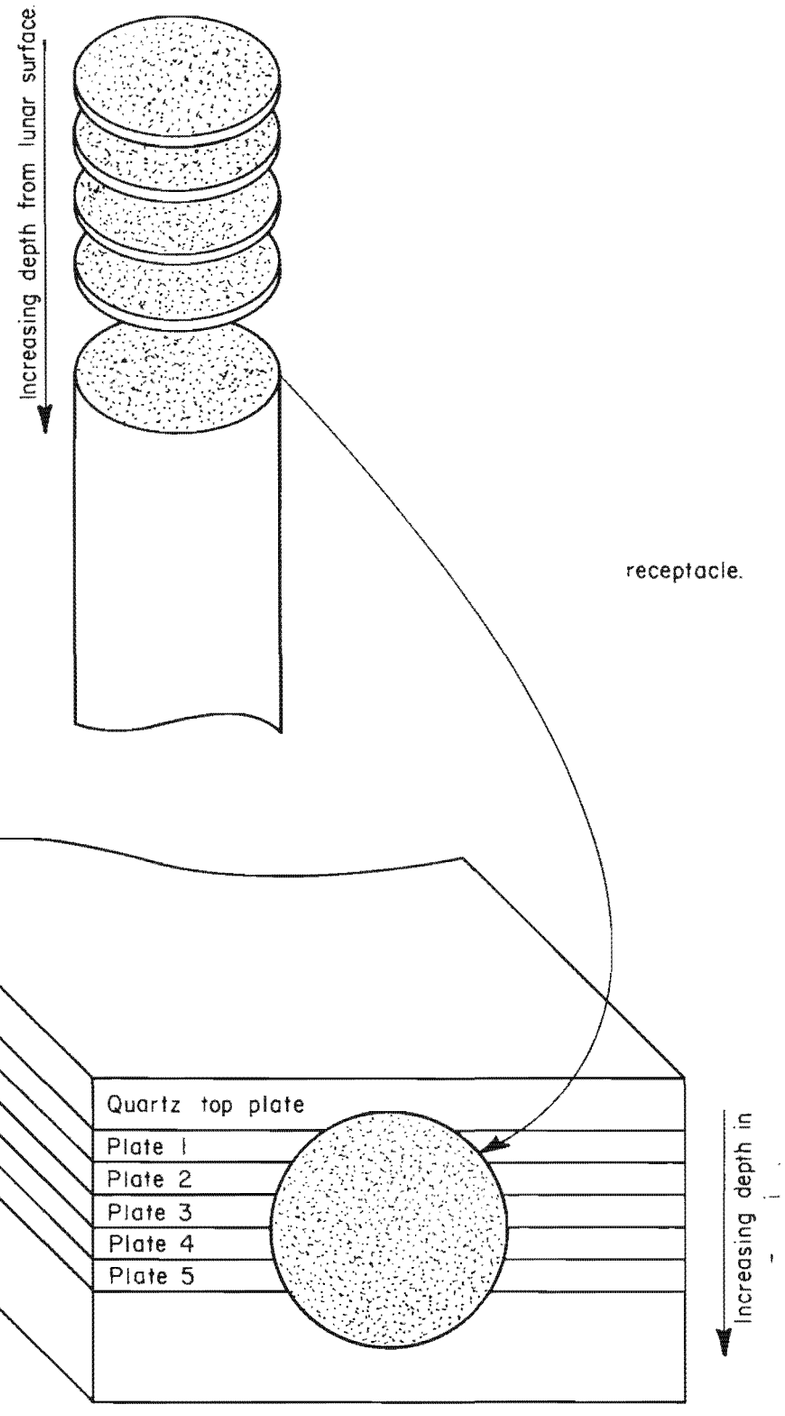

1. Vertical position of
and 60010 core se
removal of the soil
the top 5 mm.

receptacle.

3. The quartz top plate
removed for dissecti
The amount of materi
removed during a dis
pass depends on how
side plates are remov

Figure 2.2. This schematic drawing shows the two stages in which the soil column was removed from the core tube.

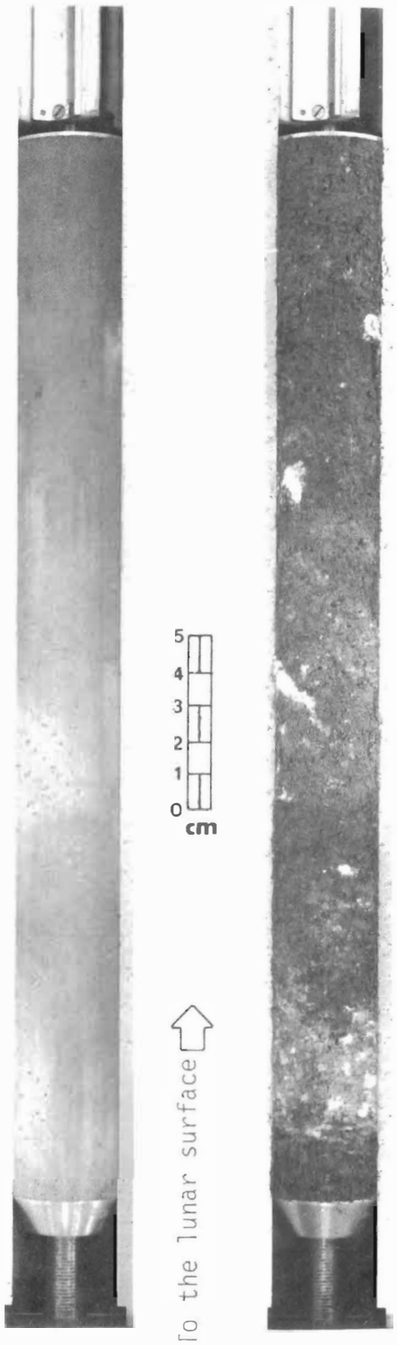

Figure 2.3. The 60009 soil column (left) immediately after extrusion shows little stratigraphy because of the smeared surface. Once the smeared material is removed to a depth of 1 to 2 mm (right), layers and heterogeneities are obvious.

2.2 METHODS OF DISSECTION

The method by which soil and particles are removed from a soil column as it rests in the aluminum receptacle is referred to as the core dissection. About 80% of the soil column is removed in a series of three or four passes along the length of the core. During a dissection pass a spatula is used to remove material from every 5 mm along the length, going completely across the exposed width, and dipping into the soil column approximately 1 cm (Figure 2.4). This "volume" is the standard dissection interval. What is removed amounts to a solid rectangle of soil about 5 mm by roughly 4 cm by 1 cm in size. As can be seen in Figure 2.2 the exposed diameter of the soil column changes as the aluminum side plates are removed. The amount of material removed in a standard dissection pass varies, depending on the exposed width and the number of side plates removed.

Before each dissection pass, the processor writes a dissection plan detailing any deviations from the standard dissection interval and any special samples that may need to be taken. Because the 60009 core was the first large diameter core to be dissected, four as opposed to two centimeters, a series of twelve samples were removed for track studies as an aid in developing a reasonable dissection plan. Appendix 1 shows the locations of the samples removed for the track work and presents the track data.

Except for "chemically-pure" dissection passes, material removed from a standard dissection interval is sieved through a 1 mm screen creating two subsamples from each interval: soil less-than-one millimeter and particles greater-than-one millimeter (Figure 2.5). The material is not vigorously sieved (to prevent breakage of fragile particles), and the larger particles tend to be heavily dust-covered (Figure 2.6). The greater-than-one millimeter material is divided into 1-2 mm, 2-4 mm, 4-10 mm, and greater-than-10 mm size fractions, based on their measured diameters. Each size fraction is separated into lithologic groups and photographed, as illustrated in Figure 2.6. The greater-than-one millimeter particles from each dissection interval are recombined and stored as one sample. During the chemically-pure dissection pass, every effort is made to keep chemical contamination to a minimum, and consequently the soil is not sieved. There were two chemically-pure dissection passes for 60009, but only one from the 60010 soil column.

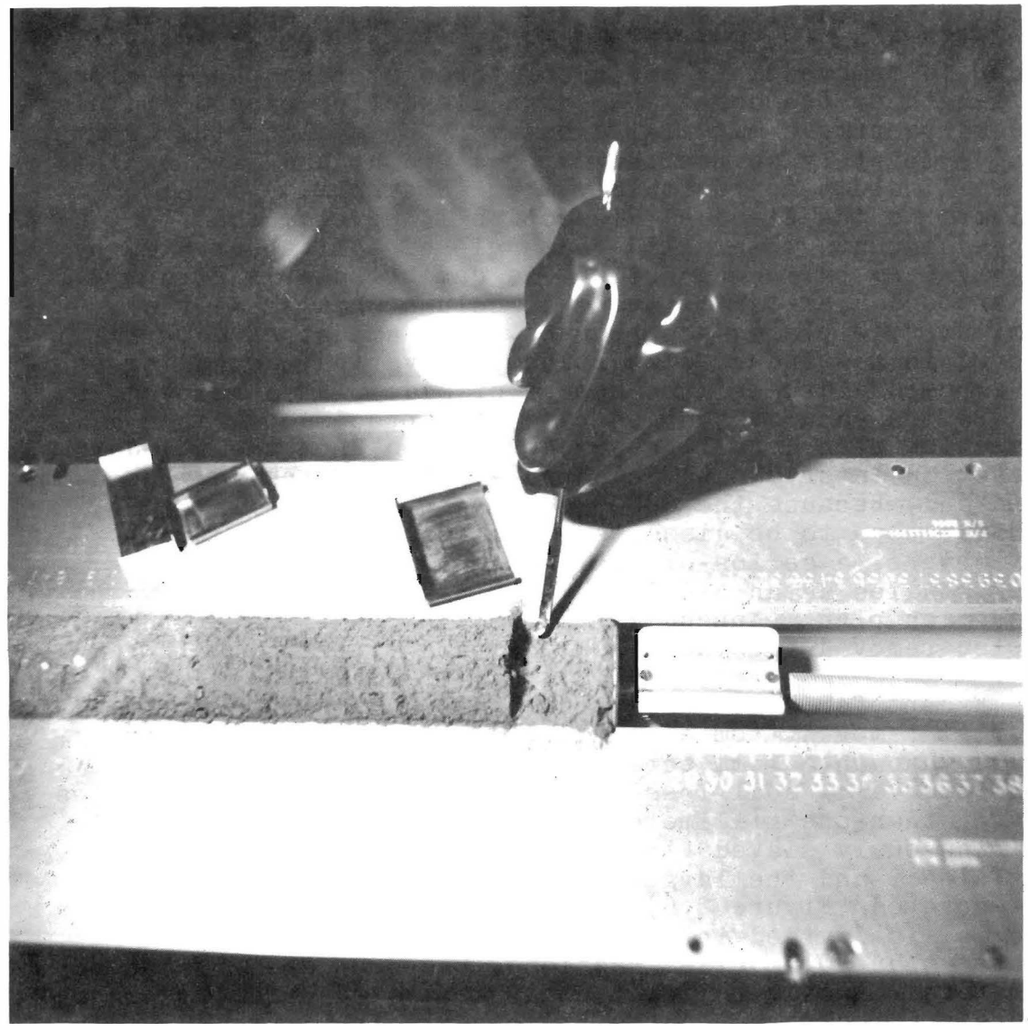

Figure 2.4. The entire extrusion and dissection process is accomplished in a nitrogen cabinet, hence the work is done in gloves. In the picture above, the core extruder plate holds the soil column in place on the right. The soil from a dissection interval is placed in an aluminum dish with a spatula. Here, the first dissection pass has proceeded about 3 cm from the bottom of soil column 15007. (NASA photo # S80-43512)

Figure 2.5. A one-millimeter sieve is used to separate individual particles from submillimeter "soil". (S-80-43506)

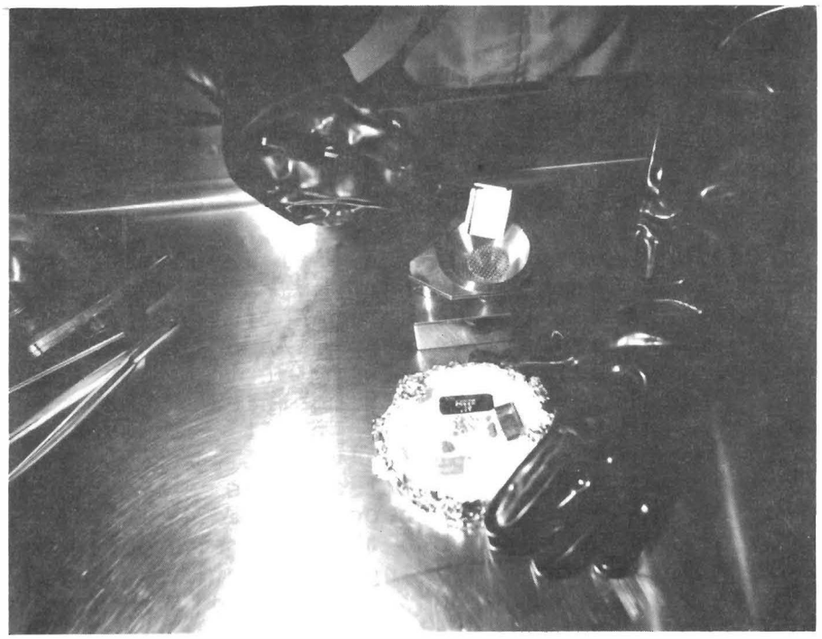

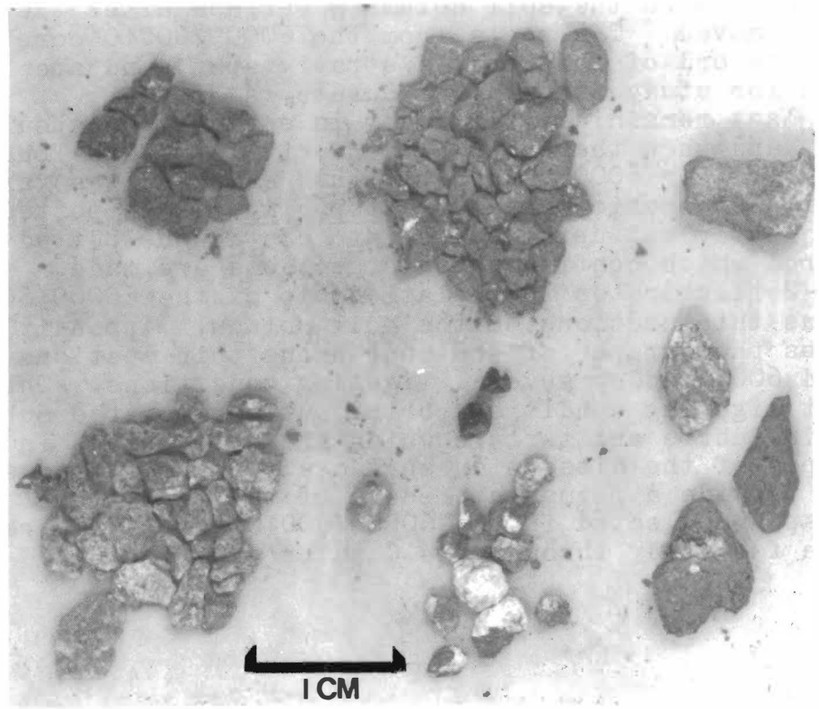

Figure 2.6. The 2-4 mm particles have been separated by size (using a scale) and grouped according to appearance. Some are heavily dust-coated. These particles are sample 60009,3105 from the 51.3-51.8 cm depth interval. (S-75-32796)

2.3 PEELS AND CONTINUOUS THIN SECTIONS: SAMPLES THAT RETAIN THE VERTICAL AND LATERAL RELATIONSHIPS

The processing procedure described above, relates a soil or suite of particles to a 0.5 cm interval of depth in the soil column. In situ relationships are destroyed by the scooping and sieving. To document the vertical and horizontal relationships for at least a portion of the soil column, peels and continuous polished thin sections are made from the last column of soil in the dissection cylinder (about 1 to 2 cm in diameter). Appendix 2 describes these procedures.

The procedure for obtaining a peel involves coating a plastic strip with cement and then laying it face down on the soil column. After the cement penetrates the core material, the plastic strip is removed and turned over to bring the adhering layer, the "peel", on top. On the average, the soil layer is about 1 mm thick. When the cement sets, the grains are held in position but can be removed with relative ease for individual study. The removal of the peel exposes a soil surface undisturbed by the scooping of the dissection process. Fine details of stratigraphy are visible on both the peel and core surfaces (Figure 2.7). The black-appearing globs on the right in Figure 2.7 are where the cement encountered a soil particle too large or heavy to be lifted by the peel; hence, the cement remained on the soil column's surface after the peel had been removed. The peels from the 60009/60010 core are a permanent record of that core's stratigraphy, and are available for study through the Curator's office.

The last remaining soil layer is entirely encapsulated in epoxy, and when the epoxy hardens, it forms one long potted butt. For 60009 and 60010 this extended the vertical length of each section minus the top 5 mm. Each potted butt is subsequently cut up and made into continuous potted butts, from which continuous thin sections are made. Appendix 2 illustrates the relationship of the 60009/60010 continuous thin sections to the soil column. Appendix 3 reproduces photographs of the continuous thin sections from 60009 and 60010 under several lighting conditions. The different lighting conditions bring out many of the subtle changes in fabric and texture which are not obvious in the photographs of the dissection surfaces. The continuous thin sections provide a permanent record of the regolith stratigraphy collected in the 60009/60010 core, and are available for study through the Curator's Office.

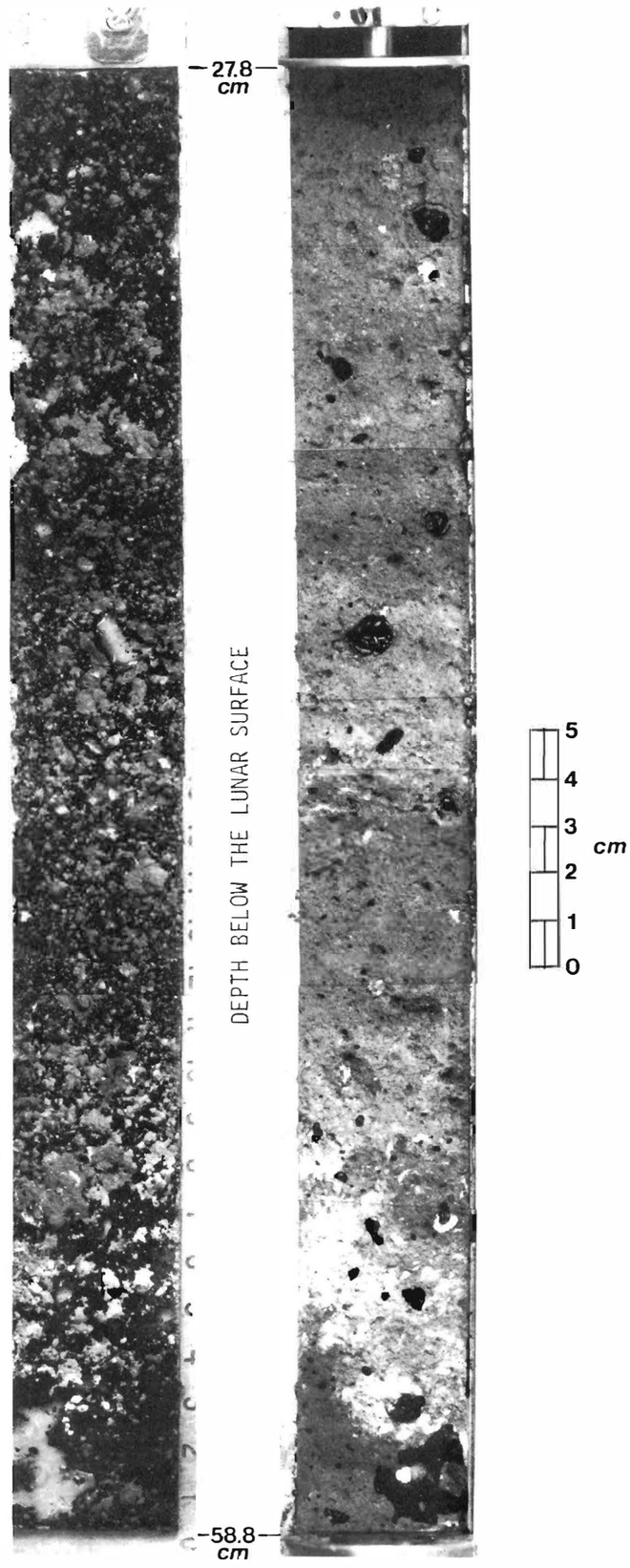

Figure 2.7. Peel (left) and post-peel soil surface (right) of 60009. The black globs are glue-coated particles too large or heavy to be lifted off by the peel.

2.4 PHOTOGRAPHY OF THE SOIL COLUMNS DURING SAMPLE REMOVAL

The lunar regolith is so heterogeneous, horizontally as well as vertically, that significant visual changes can be observed from one dissection pass to the next. Each dissection surface represents less than a 1 cm horizontal difference in distance. Because the 60009 portion was dissected in shallower increments than 60010, there were five dissection passes made for the former, and only four for the latter. Figure 2.8 shows the surfaces visible before each dissection pass was made for the 60009/60010 soil column. Post-peel photographs are included because they so beautifully illustrate the detailed stratigraphy that is preserved in the soil column.

Figure 2.8

60009 / 60010 Dissection Surfaces

Increasing depth in cross-section

60010, -

000-999 1000-1999 2000-2999 3000-3999 6000-6999

0.0
0.5

Increasing depth from lunar surface (cm scale)

27.3

60009, -

000-999 1000-1999 2000-2999 3000-3999 4000-4999 6000-6999

27.8

58.8

3.0 SAMPLES FROM THE 60009/10 CORE

3.1 STANDARD SAMPLES

The method by which a processor dissects a core has been described (Section 2.2). For each dissected column of soil that is sieved, there will be a minimum of two samples from every 0.5 cm along the length of the soil column: the submillimeter soil fraction and the supramillimeter fraction. The "chemically pure" dissections are not sieved to keep contamination to a minimum, so there is only the one (bulk) sample from each interval of a chemically pure pass.

The core samples are viewed primarily as soil samples, even though, like the surface soil samples, they contain a collection of lithic fragments. The standard soil samples from the 60009/60010 core are listed in Table 3.1. This table contains the standard samples from both the four dissected soil columns from 60010 and the five dissected soil columns from 60009. The submillimeter material is included in this table, as well as the unsieved bulk soil samples.

3.2 PARTICLES GREATER-THAN-ONE MILLIMETER

After being sieved at the 1 mm level, supramillimeter particles were separated into 1-2 mm, 2-4 mm, 4-10 mm, and greater-than-10 mm fractions to document grain size distributions above the one millimeter level. The particles were then physically recombined and are stored as one sample: the greater-than-one millimeter fraction. Table 3.2 lists these samples for each 0.5 millimeter interval. There are no such samples from the chemically-pure dissection passes. Any large fragments that may have been plucked from the soil during these passes are by definition, "special" samples.

3.3 SPECIAL SAMPLES

There are four categories of special samples. (1) Samples removed from a shorter or longer length than the 0.5 cm dissection interval are special. This is done to preserve similar-appearing material as an entity that does not follow the arbitrary length of the standard dissection interval. (2) Because no sampling is done across any obvious boundaries, samples that are not homogeneous across the exposed diameter, or width, of the soil column are kept separate. Marbled units are a good example of this: half of a dissection interval may be light-colored, the other half, darker. Each half of the dissection interval is sampled separately and considered a special sample. These

special samples may or may not encompass a standard length dissection interval. (3) Any unusual-appearing soil or particles are special samples. (4) Any material removed under different conditions to fulfill the requirements of an analytical study are considered special. The samples removed under red light illumination for fluorescence studies are an example of this.

The special samples are listed in Table 3.3. Special samples were collected from all dissected columns of soil, even the ones that were not subjected to sieving. Note that the intervals range in length and may even overlap for some special samples.

Table 3.1. Standard Samples from Core 60009/10.
(See Table 3.3 for special samples.)

Interval (cm)	FIRST COLUMN < 1mm		SECOND COLUMN (unsieved)		THIRD COLUMN < 1mm		FOURTH COLUMN < 1mm	
	Sample Number 60010,-	Original Weight(g)	Sample Number 60010,-	Original Weight(g)	Sample Number 60010,-	Original Weight(g)	Sample Number 60010,-	Original Weight(g)
0.0- 0.5	<See Table 3>							
0.5- 1.0	176	2.108	1066	1.055	2105	1.537	3105	2.869
1.0- 1.5	174	1.983	1065	1.389	2103	1.469	3103	2.747
1.5- 2.0	172	1.860	1064	1.149	2101	1.343	3101	2.333
2.0- 2.5	170	2.096	1063	1.192	2099	1.450	3099	2.087
2.5- 3.0	168	2.000	1061	1.400	2097	1.311	3097	1.878
3.0- 3.5	165	1.196	1059	1.300	2095	1.296	3095	2.660
3.5- 4.0	162	1.909	1058	1.635	2093	1.410	3093	2.316
4.0- 4.5	160	1.946	1056	1.116	2091	1.433	3091	2.276
4.5- 5.0	158	1.754	1055	1.267	2089	1.363	3089	2.173
5.0- 5.5	156	1.925	1054	1.020	2087	1.601	3087	2.682
5.5- 6.0	154	2.101	1053	1.020	2085	1.422	3085	2.717
6.0- 6.5	152	2.858	1052	1.664	2083	1.614	3083	2.455
6.5- 7.0	150	1.369	1051	1.137	2081	1.513	3081	2.521
7.0- 7.5	148	2.302	1050	0.972	2079	1.308	3079	2.791
7.5- 8.0	145	0.939	1048	0.622	2077	1.622	3077	2.320
8.0- 8.5	142	0.864	1047	1.308	2075	1.318	3075	2.992
8.5- 9.0	139	1.361	1046	1.121	2073	1.415	3073	2.266
9.0- 9.5	136	0.664	1045	1.250	2070	1.279	3071	2.481
9.5-10.0	134	1.885	1043	1.049	2069	0.998	3069	2.545
10.0-10.5	132	1.863	1041	1.039	2067	1.432	3067	2.526
10.5-11.0	130	2.058	1039	1.458	2065	1.308	3065	2.638
11.0-11.5	128	2.451	1038	1.330	2063	1.380	3063	2.929
11.5-12.0	126	2.203	1037	1.133	2061	1.614	3061	2.611
12.0-12.5	123	2.195	1035	0.759	2059	1.159	3059	3.848
12.5-13.0	121	2.281	1034	1.283	2057	1.299	3057	1.053
13.0-13.5	119	2.070	1033	1.314	2055	1.534	3055	2.695
13.5-14.0	116	2.508	1032	1.262	2053	1.895	3053	2.861
14.0-14.5	114	2.442	1031	1.151	2051	1.615	3051	2.790
14.5-15.0	112	2.051	1030	1.500	2049	1.532	3049	2.615
15.0-15.5	110	2.652	1029	1.302	2047	1.723	3047	2.637
15.5-16.0	108	2.463	1027	1.234	2045	1.580	3045	3.131
16.0-16.5	106	1.989	1026	1.532	2043	1.845	3043	2.686
16.5-17.0	104	2.126	1025	1.407	2041	1.342	3041	2.948
17.0-17.5	102	2.501	1024	1.066	2039	1.434	3039	2.777
17.5-18.0	100	2.195	1022	0.400	2037	1.463	3037	2.735
18.0-18.5	98	2.274	1021	0.515	2035	1.626	3035	2.978
18.5-19.0	96	1.989	1019	1.314	2033	1.743	3033	3.110
19.0-19.5	93	2.194	1018	1.306	2031	1.551	3031	2.627
19.5-20.0	91	2.399	1016	0.625	2029	1.274	3029	2.344
20.0-20.5	89	2.432	1015	1.412	2027	1.177	3027	2.706
20.5-21.0	87	2.161	1014	1.365	2025	1.345	3025	2.899
21.0-21.5	85	2.298	1012	0.895	2023	1.669	3023	2.676
21.5-22.0	81	2.305	1011	1.340	2021	1.527	3021	3.002
22.0-22.5	79	2.199	1009	1.458	2019	1.317	3019	2.260
22.5-23.0	76	2.260	1008	1.473	2017	1.360	3017	2.678
23.0-23.5	74	2.276	1007	1.781	2015	1.394	3014	1.539
23.5-24.0	72	2.330	1006	1.310	2013	.991	3012	1.291
24.0-24.5	70	2.399	1005	1.505	2011	1.250	3010	1.229
24.5-25.0	68	2.127	1004	1.630	2008	1.111	3008	2.727
25.5-25.5	66	2.481	1003	1.497	2006	1.263	3006	3.292
25.5-26.0	64	2.137	1002	1.537	2004	1.712	3004	2.347
26.0-26.6	62	3.004	1001	1.511	2002	1.686	3002	3.358
26.6-27.3	60	3.015	1000	2.476	2000	1.805	3000	4.416

Table 3.1. Standard Samples from Core 60009/10 (continued).

Interval (cm)	FIRST COLUMN < 1mm Sample Number	Original Weight(g)	SECOND COLUMN < 1mm Sample Number	Original Weight(g)	THIRD COLUMN < 1mm Sample Number	Original Weight(g)	FOURTH COLUMN (unsieved) Sample Number	Original Weight(g)	FIFTH COLUMN (unsieved) Sample Number	Original Weight(g)
	60009,-		60009,-		60009,-		60009,-		60009,-	
27.3-27.8	<----------				See Table 3					---------->
27.8-28.3	40	0.719	1000	0.941	2000	0.990	3000	2.990	4000	1.271
28.3-28.8	42	0.656	1002	0.874	2001	1.329	3002	2.730	4001	1.301
28.8-29.3	45	0.859	1004	1.059	2002	1.593	3005	2.310	4002	1.006
29.3-29.8	47	0.952	1006	1.176	2003	1.743	3007	2.909	4003	1.333
29.8-30.3	49	0.813	1008	1.027	2004	1.712	3009	2.464	4004	0.813
30.3-30.8	51	0.862	1010	0.948	2005	1.540	3011	2.867	4006	1.276
30.8-31.3	53	0.950	1012	1.126	2006	1.607	3015	1.263	4007	1.426
31.3-31.8	(See Table 3)		1016	0.909	2008	1.263	3017	2.343	4008	1.325
31.8-32.3	61	0.464	1019	0.990	2009	1.316	3019	2.690	4009	1.493
32.3-32.8	63	0.688	1021	0.968	2010	1.645	3021	2.624	4010	1.355
32.8-33.3	65	0.906	1024	0.941	2011	1.541	3023	2.704	4011	1.272
33.3-33.8	70	0.667	1028	0.946	2012	1.904	3025	2.767	4012	1.025
33.8-34.3	72	0.631	1030	0.908	2013	1.869	3028	3.024	4014	1.434
34.3-34.8	74	0.903	1032	1.101	2014	1.515	3030	2.820	4015	1.474
34.8-35.3	77	0.685	1035	0.922	2015	1.527	3032	2.745	4016	1.107
35.3-35.8	79	0.804	1037	1.235	2016	1.134	3034	2.667	4017	1.541
35.8-36.3	(See Table 3)		1039	1.320	2017	1.224	3036	2.683	4018	1.476
36.3-36.8	"		1041	1.229	2019	1.365	3038	2.062	4019	1.701
36.8-37.3	"		1044	0.991	2020	1.588	3041	2.665	4020	1.634
37.3-37.8	92	0.650	1046	0.794	2021	1.550	3044	3.047	4021	1.034
37.8-38.3	(See Table 3)		1048	1.556	2022	1.433	3046	2.973	4023	1.529
38.3-38.8	"		1052	1.117	2023	1.421	3048	2.779	4024	1.290
38.8-39.3	104	0.826	1054	0.796	2024	1.556	3050	2.325	4026	1.227
39.3-39.8	(See Table 3)		1059	0.368	2025	1.647	3052	2.727	4027	1.161
39.8-40.3	"		1063	1.122	2027	1.314	3056	2.453	4029	1.430
40.3-40.8	"		1063	1.122	2027	1.314	3056	2.453	4029	1.430
40.8-41.3	"		1065	1.229	2029	1.146	3058	2.330	4030	1.231
41.3-41.8	117	0.288	1067	1.285	2030	1.672	3060	2.556	4031	1.428
41.8-42.3	119	0.467	1069	0.801	2031	1.009	3062	2.223	4032	1.442
42.3-42.8	121	0.342	1071	1.146	2033	0.963	3065	2.413	4033	1.088
42.8-43.3	123	0.366	1074	0.883	2034	0.652	3067	2.651	4035	1.344
42.8-43.3	125	0.398	1076	0.787	2036	1.124	3070	3.245	4036	1.529
43.8-44.3	127	0.411	1078	1.818	2037	1.552	3072	3.104	4037	1.080
44.3-44.8	129	0.471	1080	1.245	(See Table 3)		3074	2.939	4038	1.277
44.8-45.3	131	0.405	1082	0.678	"		3076	2.948	4039	1.571
45.3-45.8	131	0.362	1084	0.585	"		3078	2.368	4040	1.383
45.8-46.3	135	0.319	1086	0.489	(See Table 3)		3080	1.463	4041	1.697
46.3-46.8	137	0.167	(See Table 3)		"		3082	1.831	4042	1.834
46.8-47.3	(See Table 3)		"		"		3085	2.194	4044	0.877
47.3-47.8	170	0.475	1093	0.440	2042	0.827	3087	2.611	4045	1.104
47.8-48.3	(See Table 3)		1095	0.827	2043	1.416	3089	3.018	4047	1.059
48.3-48.8	"		1097	1.057	2045	1.529	3091	2.592	4049	1.551
48.8-49.3	"		1099	0.959	2046	1.135	3093	3.089	4050	1.533
49.3-49.8	179	0.702	(See Table 3)		2047	0.766	3095	1.949	4051	1.375
49.8-50.3	183	0.591	1105	0.704	2048	0.990	3097	2.203	4052	1.788
50.3-50.8	186	0.841	1107	0.921	2049	0.773	3100	1.408	4053	1.635
50.8-51.3	(See Table 3)		(See Table 3)		2050	0.917	3102	1.471	4054	1.404
51.3-51.8	"		"		2051	1.435	3104	2.303	4055	1.451
51.8-52.3	"		"		2052	1.014	3106	1.353	4056	1.354
52.3-52.8	"		"		2053	1.352	3109	1.396	4057	1.335
52.8-53.3	206	0.436	"		2054	1.301	3112	3.279	4058	1.523
53.3-53.8	(See Table 3)		"		2055	1.272	3114	3.401	4060	1.398
53.8-54.3	212	0.806	1134	1.414	5056	1.415	3116	3.276	4061	1.295
54.3-54.8	215	0.651	1136	1.662	2057	1.257	3118	3.842	4062	1.285
54.8-55.3	217	0.485	1138	1.526	2058	1.342	3120	3.170	4063	1.371
55.3-55.8	222	0.515	1140	1.311	2059	1.397	3122	3.556	4064	1.309
55.8-56.3	226	0.316	1143	1.181	2060	1.870	3124	2.852	4065	1.734
56.3-56.8	(See Table 3)		(See Table 3)		2061	1.327	3126	3.027	4066	1.496
56.8-57.3	"		"		2062	1.384	3029	3.458	4067	0.897
57.3-57.8	242	0.769	1151	1.305	2063	1.408	3131	3.307	4069	1.471
57.8-58.3	244	1.194	1153	1.516	2064	1.555	3133	3.073	4070	1.452
58.3-58.8	246	1.100	1155	1.419	2065	1.402	3135	2.866	4071	1.473

TABLE 3.2. Greater than one millimeter particles from Core 60009/60010.
(See Table 3 for special samples.)

Interval (cm)	FIRST COLUMN Sample Original Number Weight(g) 60010,-	SECOND COLUMN Sample Original Number Weight(g) unsieved	THIRD COLUMN Sample Original Number Weight(g) 60010,-	FOURTH COLUMN Sample Original Number Weight(g) 60010,-
0.0- 0.5	<----------See Table 3---------->			
0.5- 1.0	177 0.146		2106 0.057	3106 .0274
1.0- 1.5	175 0.134		2104 0.065	3104 0.159
1.5- 2.0	173 0.144		2102 0.045	3102 0.160
2.0- 2.5	171 0.124		2100 0.046	3102 0.083
2.5- 3.0	169 0.298		2098 0.079	3098 0.115
3.0- 3.5	167 0.222		2096 0.048	3096 4.360
3.5- 4.0	164 0.191		2094 0.106	3094 0.077
4.0- 4.5	161 0.274		2092 0.026	3092 0.162
4.5- 5.0	159 0.972		2090 0.130	3090 0.757
5.0- 5.5	157 0.195		2088 0.104	3088 0.438
5.5- 6.0	155 0.184		2086 0.184	3086 0.411
6.0- 6.5	153 0.244		2084 0.168	3084 0.393
6.5- 7.0	151 0.231		2082 0.128	3082 0.517
7.0- 7.5	149 0.160		2080 0.852	3080 0.276
7.5- 8.0	147 0.232		2078 0.120	3078 0.208
8.0- 8.5	144 0.241		2076 0.074	3076 0.326
8.5- 9.0	141 0.667		2074 0.138	3074 0.241
9.0- 9.5	138 1.290		2072 0.106	3072 0.417
9.5-10.0	135 0.630		2070 0.158	3070 0.165
10.0-10.5	133 1.018		2068 0.695	3068 0.427
10.5-11.0	131 0.393		2066 0.324	3066 0.584
11.0-11.5	129 0.464		2064 0.212	3064 0.227
11.5-12.0	127 0.413		2062 0.333	3062 0.181
12.0-12.5	124 0.354		2060 0.143	3060 2.212
12.5-13.0	122 0.183		2058 0.141	3058 0.168
13.0-13.5	120 0.633		2056 0.293	3056 0.395
13.5-14.0	117 0.402		2054 0.577	3054 0.670
14.0-14.5	115 0.406		2052 0.299	3052 0.438
14.5-15.0	113 0.139		2050 0.220	3050 0.353
15.0-15.5	111 0.292		2048 0.279	3040 0.246
15.5-16.0	109 0.471		2046 0.145	3046 0.518
16.0-16.5	107 0.417		2044 0.360	3044 0.445
16.5-17.0	105 0.574		2042 0.343	3042 0.282
17.0-17.5	103 0.277		2040 0.220	3040 0.932
17.5-18.0	101 0.284		2038 0.123	3038 0.255
18.0-18.5	99 0.518		2036 0.256	3036 0.209
18.5-19.0	97 0.376		2034 0.287	3034 0.422
19.0-19.5	94 0.265		3032 0.310	3032 0.271
19.5-20.0	92 0.293		2030 0.558	3030 0.689
20.0-20.5	90 0.511		2028 0.286	3028 0.558
20.5-21.0	88 0.584		2026 0.424	3026 0.463
21.0-21.5	86 0.253		2024 0.853	3024 0.913
21.5-22.0	82 0.311		2022 0.480	3022 0.904
22.0-22.5	80 0.280		2020 0.649	3020 0.269
22.5-23.0	77 0.237		2018 0.212	3018 0.221
23.0-23.5	75 0.394		2016 0.124	3015 0.092
23.5-24.0	73 0.388		2014 0.066	3013 0.225
24.0-24.5	71 0.286		2012 0.153	3011 0.206
24.5-25.0	69 0.402		2009 0.161	3009 1.270
25.0-25.5	67 0.665		2007 0.216	3007 0.510
25.5-26.0	65 0.612		2005 0.449	3005 0.396
26.0-26.6	63 0.522		2003 0.314	3003 0.600
26.6-27.3	61 0.419		2001 0.110	3001 1.415

TABLE 3.2. Greater than one millimeter particles from Core 60009/60010
(See Table 3 for special samples.)
(continued)

Interval (cm)	FIRST COLUMN Sample Number	Original Weight(g)	SECOND COLUMN Sample Number	Original Weight(g)	THIRD COLUMN Sample Number	Original Weight(g)	FOURTH COLUMN Sample Number	Original Weight(g)	FIFTH COLUMN Sample Number	Original Weight(g)
	60009,-		60009,-		unsieved		60009,-		unsieved	
27.3-27.8	<--------				See Table 3					--------->
27.8-28.3	41	0.078	1001	0.068			3001	0.588		
28.3-28.8	43	0.041	1003	0.142			3003	0.937		
28.8-29.3	46	0.039	1005	0.109			3006	0.460		
29.3-29.8	48	0.136	1007	0.076			3008	0.421		
29.8-30.3	50	0.173	1009	0.151			3010	0.220		
30.3-30.8	52	0.107	1011	0.179			3012	0.444		
30.8-31.3	54	0.165	1013	0.170			3016	0.124		
31.3-31.8	(See Table 3)		1017	0.337			3018	0.202		
31.8-32.3	62	0.218	1020	0.124			3020	0.244		
32.3-32.8	64	0.201	1022	0.154			3022	1.004		
32.8-33.3	69	0.092	1025	0.155			3024	0.303		
33.3-33.8	71	0.155	1029	0.142			3026	0.179		
33.8-34.3	73	0.101	1031	0.256			3029	0.353		
34.3-34.8	75	0.169	1033	0.178			3031	0.273		
34.8-35.3	78	0.218	1036	0.057			3033	1.095		
35.3-35.8	80	0.121	1038	0.108			3035	0.479		
35.8-36.3	(See Table 3)		1040	0.161			3037	0.501		
36.3-36.8	"		1042	0.146			3039	0.160		
36.8-37.3	"		1045	0.072			3042	0.179		
37.3-37.8	93	0.036	1047	0.082			3045	0.332		
37.8-38.3	(See Table 3)		1049	0.091			3047	0.224		
38.3-38.8	"		1053	0.173			3049	0.293		
38.8-39.3	105	0.031	1055	0.044			3051	0.876		
39.3-39.8	(See Table 3)		1060	0.190			3053	1.100		
39.8-40.3	"		1062	0.091			3055	0.379		
40.3-40.8	"		1064	0.119			3057	0.308		
40.8-41.3	"		1066	0.210			3059	0.354		
41.3-41.8	118	0.021	1068	0.229			3059	0.270		
41.8-42.3	120	0.024	1070	1.289			3036	0.330		
42.3-42.8	122	0.051	1072	0.136			3066	0.507		
42.8-43.3	124	0.395	1075	0.216			3068	0.369		
43.3-43.8	126	0.138	1077	0.143			3071	0.610		
43.8-44.3	128	0.106	1079	0.105			3074	0.335		
44.3-44.8	130	0.202	1081	0.214			3075	0.211		
44.8-45.3	132	0.014	1083	0.070			3077	0.358		
45.3-45.8	134	0.036	1085	0.182			3079	0.643		
45.8-46.3	136	0.096	1087	0.068			3081	0.255		
46.3-46.8	138	0.096	(See Table 3)				3083	0.309		
46.8-47.3	(See Table 3)		"				3086	0.469		
47.3-47.6	171	0.209	1094	0.051			3088	0.296		
47.8-48.3	(See Table 3)		1096	0.288			3090	0.475		
48.3-48.6	"		1098	0.319			3092	0.735		
48.8-49.3	"		1100	0.123			3094	0.781		
49.3-49.8	182	0.073	1102	0.247			3096	0.082		
49.8-50.3	185	0.061	1106	0.151			3098	0.516		
50.3-50..6	187	0.251	1108	0.282			3101	0.635		
50.8-51.3	(See Table 3)		(See Table 3)				3103	0.913		
51.3-51.8	"		"				3103	0.913		
51.8-52.3	"		"				3108	0.543		
52.3-52.8	"		"				3111	0.542		
52.8-53.8	208	0.299	"				3113	0.545		
53.3-53.8	(See Table 3)		"				3115	0.363		
53.8-54.3	214	0.199	1135	0.109			3117	0.298		
54.3-54.8	216	0.147	1137	0.177			3119	0.241		
54.8-55.3	218	0.030	1139	0.080			3121	0.215		
55.3-55.8	225	0.127	1141	0.150			3123	0.372		
55.8-56.3	230	0.033	1144	0.196			3125	0.270		
56.3-56.8	(See Table 3)		(See Table 3)				3127	0.328		
56.8-57.3	"		"				3130	0.484		
57.3-57.8	243	0.295	1152	0.286			3132	0.504		
57.8-58.3	245	0.102	1154	0.156			3134	0.482		
58.3-58.7	247	0.178	1156	0.179			3136	0.117		

Table 3.3. Listing of Special Samples from Core 60009/60010.

Interval (cm)	FIRST COLUMN < 1mm # Wt.(g)	FIRST COLUMN > 1mm # Wt.(g)	SECOND COLUMN Soil Particles # Wt.(g)	THIRD COLUMN < 1mm # Wt.(g)	THIRD COLUMN > 1mm # Wt.(g)	FOURTH COLUMN < 1mm # Wt.(g)	FOURTH COLUMN > 1mm # Wt.(g)
	60010,-		60010,-	60010,-		60010,-	
0.0- 0.1	4 .883	,6 1.88					
0.0- 0.1	5 1.804		First 5mm were dissected across				
0.1- 0.2	7 1.410	,8 .075	entire cross section of the core				
0.2- 0.3	9 1.856	,10 .155	1mm at a time.				
0.3- 0.4	11 1.804	,12 .198					
0.4- 0.5	<----------		No Samples from this interval----------				>
0.5- 1.0							
1.0- 1.5							
1.5- 2.0							
2.0- 2.5							
2.5- 3.0							
2.5- 3.5			1062 0.003				
3.0-3.25	166 0.979						
3.5			1060 0.050				
3.5-3.75	163 0.762						
4.0- 4.5							
4.3			1057 0.005				
4.5- 5.0							
5.0- 5.5							
5.5- 6.0							
6.0- 6.5							
6.5- 7.0							
7.0- 7.5							
7.5-7.75	146 1.185						
7.5- 8.0			1049 1 158				
8.0-8.25	143 0.796						
8.5-8.75	140 0.843						
8.9- 9.2			1044 0.076				
9.0-9.25	137 1.025						
9.5-10.0							
9.6- 9.8			1042 0.015				
10.0-10.5							
10.3-10.7			1040 0.036				
10.5-11.0							
11.0-11.5							
11.5-12.0							
12.0-12.5			1036 0.843				
12.2-12.5	125 0.020		1036 0.843				
12.5-13.0							
13.0-13.5							
13.5		118 0.002					
13.5-14.0							
14.0-14.5							
14.5-15.0							
15.0-15.5							
15.5-16.0							
15.7			1028 0.040				
16.0-16.5							
16.5-17.0							
17.0-17.5							
17.5-18.0							
17.5-18.1			1023 1.104				
18.0-18.5							
18.5			1020 0.007				
18.5-19.0							
18.5-19.7		95 1.131					
19.0-19.5							
19.5-20.0			1017 0.932				
20.0-20.5							
20.5-21.0							
20.8-21.0			1013 0.502				
21.0-21.5							
21.2-22.3	83 0.456						
21.5-22.0							
21.5-22.1	84 0.094						
21.7-22.3			1010 0.113				
22.5-23.0							
23.0-23.5							
23.0-24.6							3016 11.64
23.5-24.0							
24.0-24.5							
24.5-25.0				2010 0.091			
25.0-25.5							
25.5-26.0							
26.0-26.5							
26.5-27.0							

Table 3.3. Listing of Special Samples from Core 60009/60010.
(continued)

Interval	FIRST COLUMN < 1mm # Wt.(g)	FIRST COLUMN > 1mm # Wt.(g)	SECOND COLUMN < 1mm # Wt.(g)	SECOND COLUMN > 1mm # Wt.(g)	THIRD COLUMN Soil Particles # Wt.(g)	THIRD COLUMN Soil Particles # Wt.(g)	FOURTH COLUMN < 1mm # Wt.(g)	FOURTH COLUMN > 1mm # Wt.(g)	FIFTH COLUMN < 1mm # Wt.(g)	FIFTH COLUMN > 1mm # Wt.(g)
	60009,-		60009,-		60009,-		60009,-		60009,-	
27.0-27.3										
27.3-27.4	4 1.915	3 0.156								
27.4-27.6	5 3.885	6 0.625								
27.6-27.8	7 3.890	8 0.427								
27.3-27.8										
27.8-28.3										
28.3-28.8										
28.3-28.9	44 0.015						3004 0.109			
28.8-29.3										
28.9-29.3							3005 2.310	3006 0.460		
29.3-29.8										
29.8-30.3										
30.3-30.8										
30.3-30.9							3011 2.867	3012 0.444		
30.8-31.3							3013 1.746	3014 0.198		
30.8-31.9						2007 0.548				
30.9-31.3							3015 1.263	3016 0.124		
31.3-31.8	55 0.588	56 0.041								
31.3-31.9			1014 0.504	1015 0.055						
31.5-31.8			1018 0.095							
31.8-32.3	59 0.225	60 0.005								
32.3-32.8										
32.6-33.1	66 0.034									
32.6-33.6				1026 1.062						
32.8-33.3										
32.8-33.8	67 0.140									
32.8-34.1	68 0.144									
33.0-34.1	68 0.144		1027 0.318					3027 0.533		
33.3-33.8										
33.8-34.3										
34.2-34.8	76 0.045									
34.3-34.8										
34.3-34.6				1034 0.038						
34.8-35.3										
35.3-35.8										
35.3-36.4						2018 0.256				
35.8-36.2	81 0.623	82 0.062								
35.8-36.3	83 0.519	84 0.072								
35.8-36.4			1039 1.320	1040 0.161						
36.3-36.9			1043 0.108							
36.3-37.0	85 0.386	86 0.026								
36.4-37.0	87 0.564	88 0.016								
36.7-37.1							3040 0.685			
36.8	89 0.041									
36.8-37.3										
36.8-37.4							3043 0.160			
37.0-37.3	90 0.684	91 0.048								
37.0-38.5	94 0.161									
37.0-38.5	95 0.490									
37.7-38.2			1051 0.164							

Table 3.3. Listing of Special Samples from Core 60009/60010. (continued)

37.9-38.3	96 0.655	97 0.039								
38.1				1050 0.015						
38.3-38.6	98 0.651	99 0.042								
38.3-38.8										4025 0.625
38.6-38.8	100 0.344	101 0.083	1054 0.796	1055 0.044						
38.8-39.3	108 0.204		1056 0.130							
38.8-39.5	102 0.164	103 0.017	1057 0.735	1058 0.097						
39.3-39.9	106 1.216	107 0.129								
39.5-40.3										4072 0.938
39.7-40.3	141 0.299	142 0.042								
39.8-40.9						2028 0.476				
40.1-41.0	109 0.170	110 0.239								
40.1-41.0	112 0.437	111 0.010								
40.1-41.0	113 0.027	114 0.070								
40.3-40.8	143 0.505	144 0.505								
40.8-41.3	145 0.462	146 0.067								
40.9-41.3						2035 5.043				
41.0-41.3	115 0.431	116 0.018								
41.3-41.8	147 0.424	148 0.162								
41.8-42.3	149 0.347	150 0.092								
41.9-42.5							3064 0.571			
42.1-43.1				1073 0.744						
42.3-42.8										
42.3-43.6						2032 0.274				
42.8-43.3	153 0.434	154 0.041								
42.8-43.8							3069 0.106			
42.8-44.3	157 0.084									
43.3-44.8	155 0.656	156 0.074								
43.8-44.8	158 0.444	159 0.053								
43.8-44.3										
44.3-44.8										
44.3-45.3					2038 1.732					
44.8-45.3	160 0.246	161 0.009								
45.3-45.8	162 0.171	163 0.092								
45.3-46.3					2039 1.101					
45.8-46.3	164 0.232	165 0.022								
46.0-46.9								3084 1.336		
46.3-46.8	166 0.091	167 0.009								
46.3-46.9			1088 0.762	1089 0.077	2040 0.936					
46.3-46.9			1090 0.217							
46.3-47.1										4043 1 505
46.8-47.4	139 0.165	140 0.031								
46.8-47.4	168 0.341	169 0.023								
46.9-47.3			1091 0.658	1092 0.089	2041 0.866					
47.3-47.8										
47.7-48.3						2044 0.554				
47.8-48.3										4048 1 946
47.8-48.4	172 0.653	173 0.135								
48.4-49.0	174 0.781	175 0.189								
49.0-49.3	176 0.858	178 0.212								
49.0	177 0.060									
49.1-49.8			1101 0.824	1102 0.247						
49.1-51.6								3099 15.072		
49.3-49.8	180 0.064									
49.3-50.4				1104 0.528						
49.4-50.0	181 0.222									
49.4-49.8				1103 0.326						
49.7-50.9				1109 1.327						
49.8-50.3	184 0.050									
50.3-50.8										

Table 3.3. Listing of Special Samples from Core 60009/60010. (continued)

50.8-51.3	188 0.281	189 0.025	1110 0.628	1111 0.357						
50.8-51.3	190 0.440	191 0.179	1112 0.302	1113 0.037						
51.3-51.8	192 0.282	193 0.060	1114 0.519	1115 0.485						
51.3-51.8	194 0.498	195 0.102	1116 0.415	1117 0.047						
51.8-52.3	196 0.320	197 0.061	1118 0.382	1119 0.142			3106 1.353	3108 0.543		
51.8-52.3	198 0.457	199 0.210					3107 1.581			
51.8-52.4			1120 0.612	1121 0.073						
52.3-52.8	200 0.477	201 0.042	1122 0.863	1123 0.090			3109 1.396			
52.3-52.8	202 0.340	203 0.104	1124 0.621	1125 0.125			3110 2.031			
52.8-53.2	204 0.434	205 0.040								
52.8-53.3			1126 0.673	1127 0.181						
52.8-53.3	207 0.055		1128 0.589	1129 0.132						
53.3-53.8	209 0.748	211 0.158	1130 1.200	1130 0.162						
53.3-53.8	210 0.209		1132 0.392	1133 0.016						
53.8-54.3	213 0.093									
54.3-54.8										
54.6-55.3	220 0.505	221 0.049								
54.8-55.3	219 0.029									
55.2-55.8			1142 0.370							
55.3-55.8	224 0.210									
55.6		223 0.031								
55.8-56.3	231 0.277	227 0.016	1145 0.229							
55.8-56.3		228 0.101								
55.8-56.3		229 0.212								
56.0-56.6	234 0.201									
56.0-56.6	233 0.030									
56.2-56.6							3128 0.283			
56.3-56.6	232 0.397	233 0.030								
56.3-56.7			1146 0.260							
56.3-56.7			1147 1.335	1148 0.076						
56.6-56.8	236 0.722	237 0.093								
56.7-57.3			1149 1.109	1150 0.094						
56.8-57.1	238 0.214	239 0.038								
57.1-57.3	240 0.935	241 0.053								
57.3-57.8										
57.8-58.3										
58.3-58.8										

4.0 STRATIGRAPHIC DESCRIPTIONS BY CORE PROCESSORS

4.1 INTRODUCTION

None of the opened Apollo cores were observed to be homogeneous over their entire length; the 60009/60010 core contained many interesting changes from top to bottom. This vertical heterogeneity could reflect stratification produced by multiple events or complex single event deposits. Except for the peels and encapsulated samples, about 3/4ths by volume of each core is removed by scooping, obliterating the intergrain relationships that the soil had when it was still a part of the lunar regolith.

The visual observations of the core processors are an integral part of the characterization of the soil columns. Each processor has brought different perceptions, skills and biases to the effort. Some have made observations and collected data with little to no interpretive attempts, not even wanting to define units (or strata). Others have been keenly interested in the interpretations of their observations, and have defined units on the basis of changes in color, grain size, and/or other features. J.S. Nagle was the processor of soil column 60009/60010. The following are based on his definitions, observations, and compilations.

4.2 BASIS FOR DISTINGUISHING UNITS

In general, visually-discernable zones in the 60009/60010 core were characterized on the basis of (1) color, (2) texture, (3) fabric and structure, and (4) lithologies of the greater-than-one millimeter particles. Texture includes grain-size distribution, sorting, rounding, (of particles greater-than-one millimeter), and packing. Fabric, a measure of grain alignment and distribution, is included when observed. Structure is considered, first in terms of what may be artifacts of sampling or handling, and after that, in terms of sedimentary structures, such as massive units versus marbled units. An attempt is made to determine general lithologic categories of supramillimeter material based on binocular microscope observations of the often dust-covered, particles. Because only binocular microscopes are available to the core processors, lithologies cannot be accurately determined in many cases. In addition to this, lithologic descriptions themselves are subjective: what one processor may call an agglutinate, another processor may call a glass-coated soil breccia. Accordingly, the nomenclature each processor used will be defined for each core (Figure 4.2).

A convention used by the processors is to treat the soil column as if it were a breccia. The homogeneous

appearing material within a visually-distinct unit is referred to as the "matrix". Any heterogeneities within the unit judged to be significantly different from the matrix are called "clasts". These "clasts" may be individual lithic particles or simply light-colored soil clods with little or no internal cohesion in a darker matrix (or vice versa).

4.2.1 Color

Color is determined by comparing bulk soil to color chips from a book of standard colors (Munsell, 1968) under consistent lighting conditions. Color standards are now being included in the color photography of the cores. This will allow much more consistency and reliability in the color prints produced. Color is one of the most obvious visual criteria that can be used to distinguish stratigraphic units.

4.2.2 Texture

Texture includes grain size distribution, sorting, modality, rounding and sphericity, and packing.

Grain size distribution is the basic parameter used to characterize terrestrial sedimentary rocks and soils. It is derived by comparing amounts (usually weight percents) of material in different size fractions of the soil, measured on a mm-scale geometric progression. Folk (1968) provides a review of the techniques and statistical parameters of grain size distributions. For all lunar surface soils, and for most of the cores, sieving has been done at the one millimeter interval to provide "fines" of less-than-one millimeter grain size, and particles greater-than-one millimeter (for surface soils these are referred to as the "coarse fines", although the terminology has been used for convenience rather than for accuracy). The terms submillimeter material (or soil) and particles greater-than-one millimeter (>1 mm) will be used in this catalog.

The particles >1 mm from surface soils have been sieved at the 1 mm, 2 mm, 4 mm, and 10 mm intervals to provide grain size distributions. The greater-than-one millimeter particles have not been sieved for the core samples. Instead, the processor manually has separated these particles into the 1 to 2 mm, 2 to 4 mm, 4 to 10 mm and greater than 10 mm intervals by comparing the median particle diameter with a scale. The actual dimensions measured by estimating with a scale versus sieving are somewhat different. Also, measured grain size distributions will be different from mechanically sieved samples because friable clasts will be preserved and counted in the former, but not in the latter.

The grain size distributions for the greater-than-one millimeter particles from each depth interval in the 60009/60010 core are presented in Table 4.1. The data from each dissection pass that was sieved has been combined.

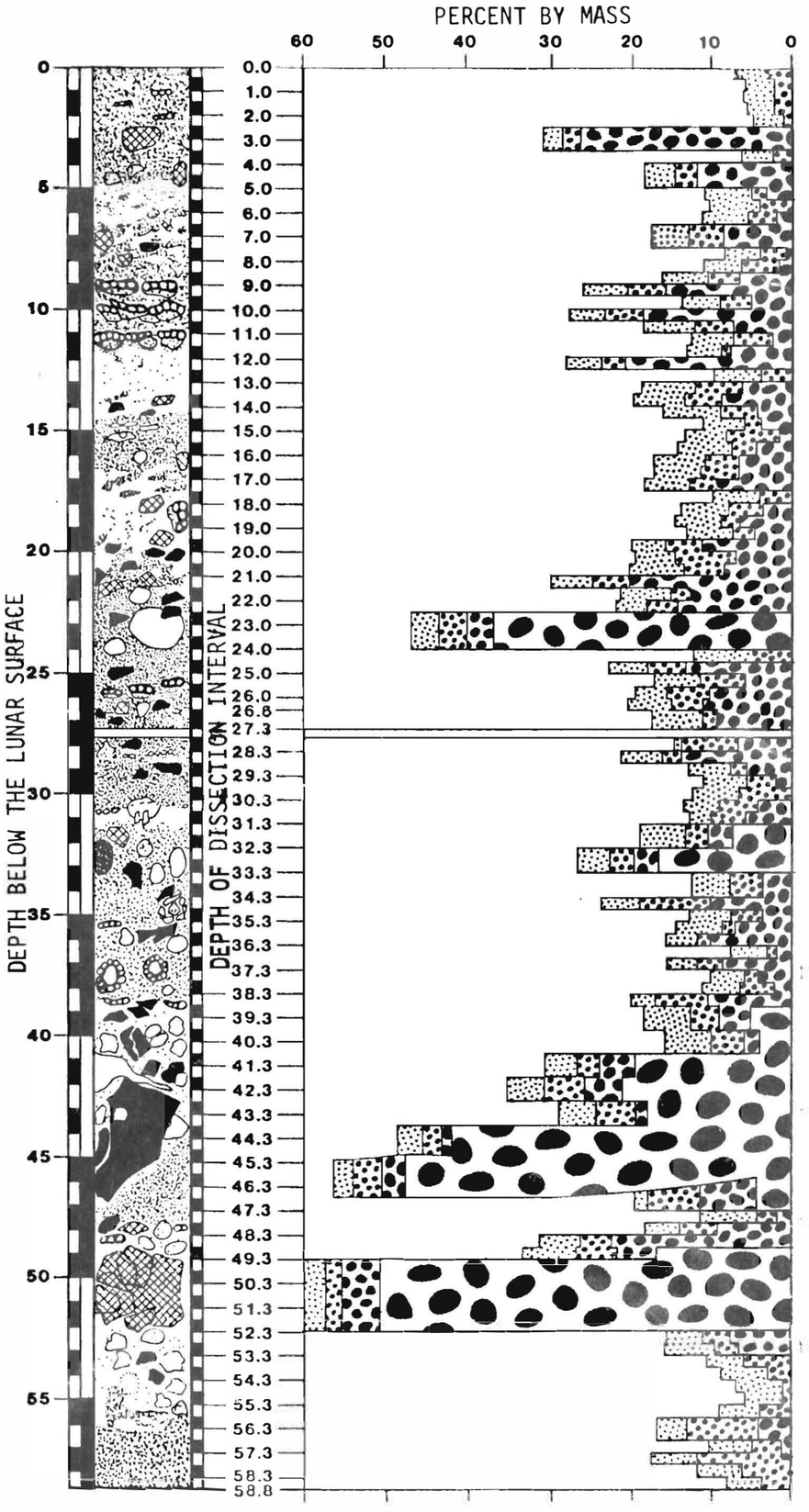

FIGURE 4.1. Grain size distributions based on measured particles greater than one millimeter. This includes data only from those dissection passes where the soil material was put through a one millimeter seive.

Table 4.1. Grain size distributions for subsamples from the 60009/60010 core. The weights are given in grams.

Interval	<1mm	1-2mm	2-4mm	4-10mm	>10mm
0.5- 1.0	6.614	0.254	0.142	-0-	-0-
1.0- 1.5	6.199	0.242	0.143	-0-	-0-
1.5- 2.0	5.546	0.213	0.114	-0-	-0-
2.0- 2.5	5.633	0.205	0.044	-0-	-0-
2.5- 3.5	11.310	0.461	0.317	-0-	4.345
3.5- 4.0	6.373	0.265	0.136	-0-	-0-
4.0- 5.0	10.945	0.499	0.344	0.072	1.444
5.0- 5.5	6.208	0.409	0.107	0.241	-0-
5.5- 6.0	6.300	0.457	0.297	-0-	-0-
6.0- 6.5	6.927	0.460	0.277	0.142	-0-
6.5- 7.5	11.638	0.627	0.610	1.210	-0-
7.5- 8.0	6.061	0.309	0.202	0.073	-0-
8.0- 8.5	5.939	0.317	0.311	0.091	-0-
8.5- 9.0	5.885	0.390	0.304	0.436	-0-
9.0- 9.5	5.318	0.400	0.375	0.605	0.473
9.5-10.0	5.430	0.425	0.218	0.340	-0-
10.0-10.5	5.821	0.379	0.374	0.975	0.468
10.5-11.0	6.076	0.447	0.362	0.522	-0-
11.0-11.5	6.760	0.410	0.380	0.159	-0-
11.5-12.0	6.410	0.331	0.079	0.559	-0-
12.0-12.5	7.174	0.340	0.360	0.931	1.129
12.5-13.0	4.613	0.312	0.192	-0-	-0-
13.0-13.5	6.252	0.497	0.448	0.438	-0-
13.5-14.0	7.211	0.556	0.419	0.712	-0-
14.0-14.5	6.811	0.562	0.378	0.269	-0-
14.5-15.0	6.153	0.358	0.162	0.244	-0-
15.0-15.5	6.627	0.380	0.463	0.097	-0-
15.5-16.0	7.111	0.552	0.257	0.375	-0-
16.0-16.5	6.481	0.433	0.350	0.478	-0-
16.5-17.0	6.355	0.434	0.364	0.462	-0-
17.0-17.5	6.681	0.446	0.267	0.748	-0-
17.5-18.0	6.559	0.409	0.284	-0-	-0-
18.0-18.5	6.823	0.437	0.380	0.221	-0-
18.5-19.0	6.818	0.432	0.152	0.525	-0-
19.0-19.5	6.539	0.360	0.149	0.303	-0-
19.5-20.0	6.024	0.378	0.343	0.812	-0-
20.0-20.5	6.190	0.384	0.579	0.517	-0-
20.5-21.0	6.325	0.518	0.377	0.656	-0-
21.0-21.5	8.864	0.696	0.567	2.441	-0-
21.5-22.0	6.195	0.487	0.195	0.949	-0-
22.0-22.5	3.503	0.171	0.164	0.607	-0-
22.5-24.0	16.047	1.020	0.903	0.327	11.640
24.0-24.5	4.850	0.391	0.282	-0-	-0-
24.5-25.0	6.607	0.401	0.333	1.017	-0-
25.0-25.5	7.027	0.449	0.442	0.509	-0-
25.5-26.0	6.175	0.295	0.279	0.904	-0-
26.0-26.6	7.558	0.521	0.344	1.061	-0-
26.6-27.3	9.380	0.601	0.211	1.078	-0-

Table 4.1. Grain size distributions for subsamples from the 60009/60010 core. The weights are given in grams.
(continued)

27.8-28.3	4.659	0.326	0.079	0.342	-0-
28.3-28.8	4.260	0.261	0.075	0.071	0.731
28.8-29.3	4.228	0.253	0.090	0.294	-0-
29.3-29.8	5.037	0.299	0.224	0.107	-0-
29.8-30.3	4.304	0.283	0.302	-0-	-0-
30.3-30.8	4.677	0.228	0.267	0.215	-0-
30.8-31.3	3.822	0.317	0.236	-0-	-0-
31.3-32.3	1.317	0.063	0.043	-0-	-0-
32.3-32.8	4.854	0.281	0.191	0.437	-0-
32.8-33.3	8.424	0.378	0.403	0.430	0.767
33.3-33.8	8.881	0.514	0.417	0.328	1.996
33.8-34.8	9.387	0.477	0.467	0.391	-0-
34.8-35.3	4.352	0.298	0.472	0.606	-0-
35.3-35.8	5.329	0.297	0.201	0.246	-0-
35.8-36.3	6.137	0.380	0.135	0.504	-0-
36.3-37.3	8.195	0.405	0.117	0.373	0.623
37.3-38.3	4.491	0.218	0.183	0.054	0.406
38.3-38.8	5.343	0.287	0.263	0.130	-0-
38.8-39.3	4.230	0.158	0.385	0.553	-0-
39.3-40.3	8.526	0.572	0.344	0.446	0.536
40.3-41.3	8.969	0.579	0.397	0.215	0.464
41.3-42.3	8.391	0.417	0.394	0.530	2.385
42.3-43.3	8.625	0.645	0.660	0.648	2.843
43.3-44.3	9.829	0.638	0.668	0.228	2.577
44.3-upper 1/2	10.494	0.734	0.511	0.223	8.884
47.3 lower 1/2	8.886	0.551	0.761	0.626	10.215
47.3 upper portion	2.669	0.083	0.229	0.245	0.129
upper portion	3.704	0.231	0.179	0.074	-0-
upper portion	5.683	0.315	0.319	0.641	-0-
mid portion	5.845	0.426	0.345	1.934	-0-
mid portion	5.305	0.546	0.392	0.386	1.327
51.8 lower portion	12.763	1.753	1.483	1.750	22.089
51.8-52.8	2.894	0.149	0.119	0.256	-0-
52.8-53.3	3.970	0.267	0.152	0.304	-0-
53.3-53.8	4.601	0.259	0.289	-0-	-0-
53.8-54.3	4.690	0.285	0.149	-0-	-0-
54.3-54.8	5.504	0.348	0.062	-0-	-0-
54.8-55.3	4.696	0.245	0.054	-0-	-0-
55.3-55.8	5.382	0.304	0.396	0.210	-0-
55.8-56.8	10.674	0.479	0.527	0.613	0.533
56.8-57.3	5.502	0.339	0.213	0.079	-0-
57.3-57.8	5.381	0.339	0.476	0.311	-0-
57.8-58.3	5.783	0.340	0.215	0.219	-0-
58.3-58.8	5.385	0.228	0.260	-0-	-0-

Weights are in grams. The size intervals for which weights are given are: <1 mm, 1-2 mm, 2-4 mm, 4-10 mm and >10 mm. The total weight of the sieved soil from each interval, (excluding the unsieved samples and the encapsulated samples) can be determined by adding the weights in each size interval together. Figure 4.1 is a graphical presentation of the changes in the grain size distribution of >1 mm material through the soil column.

Sorting is derived from size distribution, and is a measure of the spread of grain sizes within a sample. A rough estimate of sorting can be gained during the initial processing of core material from how much material is in the greater-than-one millimeter fraction compared with the amount in the submillimeter fraction.

Modality is determined by comparing mass distribution of the different size fractions, most easily by inspection of a histogram. One peak indicates a unimodal soil, but two or more indicate a bimodal or polymodal soil. Because the entire soil must be sieved to determine if there is one mode, it is obviously not possible to state that a core soil sieved only at 1 mm is unimodal or not.

Rounding and sphericity can be estimated by the method outlined in Pettijohn (1957). Clasts and particles are judged to be rounded, sharply angular, or subrounded to subangular. Rounded particles, as considered here, are particles which have all edges rounded, whereas angular particles have all edges sharply angular. Subrounded to subangular particles show some edges rounded or angular, or all or some edges slightly rounded.

Packing is a measure of the abundance and degree of contact of the >1 mm fraction in the submillimeter matrix of the soil column. Terminology follows Folk (1964), with material being predominantly fine-grained and sparsely packed; or tightly packed, with framework configurations. Sparsely-packed supramillimeter particles indicate the particles are separated by matrix. Tightly-packed means the matrix occurs interstitially to the coarser-grained framework (particles or clasts). A form of packing commonly observed in the lunar regolith core samples, but seldom observed in terrestrial deposits, is a crenulate and interpenetrating contact between friable clasts and matrix.

4.2.3 Fabric and Structure

In the case of lunar core samples, much fabric is caused by sampling disruption. For example, some soil columns were observed to have, with respect to the lunar surface, horizontally-aligned grains in the center of the soil column, but parallel alignments next to the side of the drive tube. Chaotic disarray also can be caused by sampling, as in the case of the 60009/60010 core. Figure 1.4 shows dents on the bit and scratches on the outside of the core tube. Dissection uncovered one large and numerous

Figure 4.2. presents a graphic illustration of the features and stratigraphy observed during dissection of the 60009/60010 soil column. This is followed by graphic presentations of the ranges in abundances of the major lithologies of the supramillimeter particles. Below are the definitions of these lithologies, described by the core processor during dissection.

DEFINITIONS	ABBREVIATIONS	KEY
Clear or white crystals (show planar faces)	W Xl	
Light grey colored crystalline fragments	LG Xl Fg	
Chalky or sugary-white fragments: light colored or transparent but not obviously crystalline	W bx	
Dark aphanitic fragments	B Fg	
Soil breccia fragments and heavily soil-coated fragments	So bx	
Discrete glassy particles and discrete glass chips	Gl Cps	
Unfragmented glassy aggregates	UFGA	

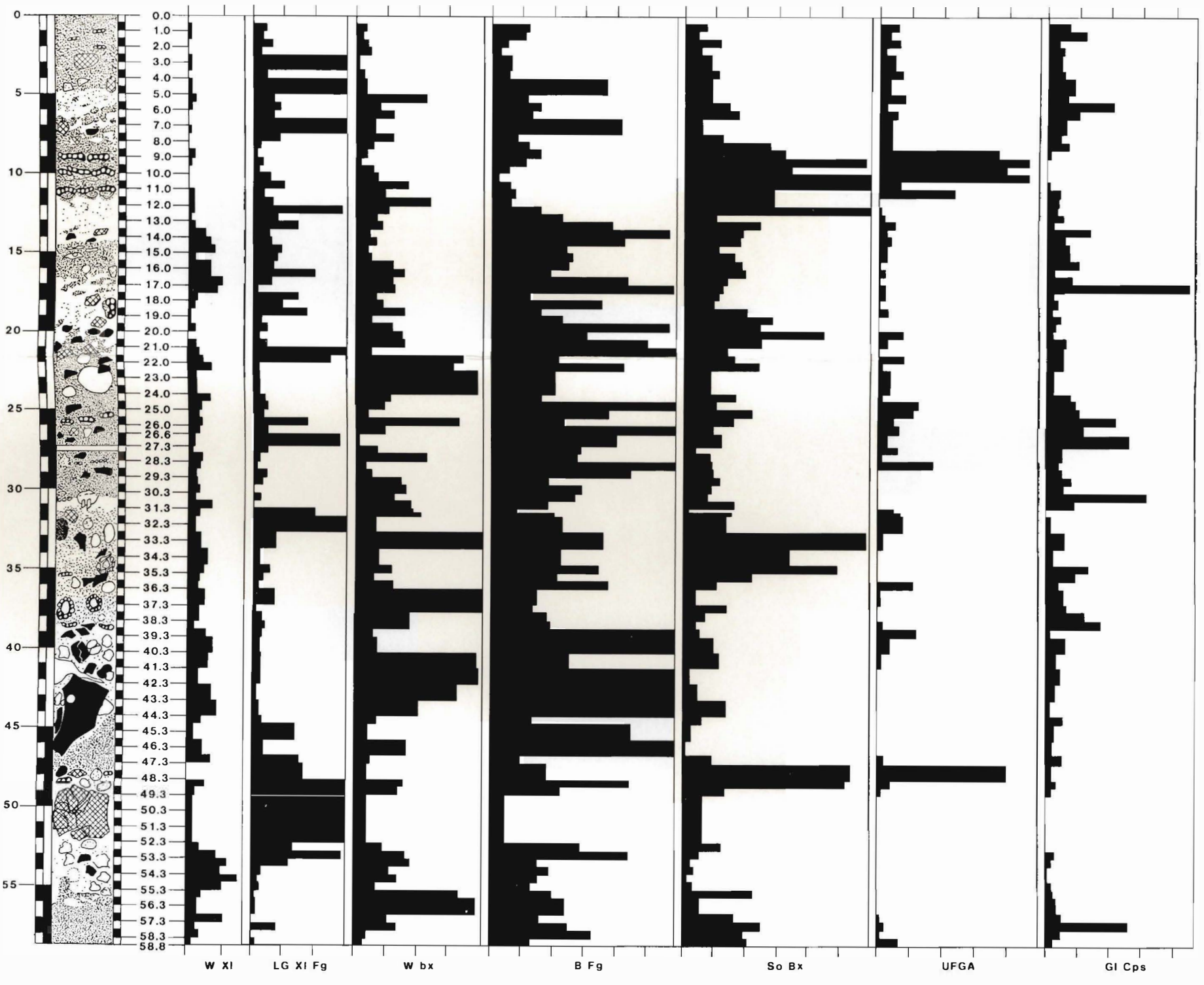

smaller, freshly-broken rock fragments within the soil column. The scratches inside and outside the core tube extended up to the area of the rock fragments. The long axis of the large fragment (60009,2069) was parallel to the drive tube wall; numerous splinters of the rock were found next to its fractured side. The boundary of the stratigraphic unit in which the broken rock fragments occurred was 3 cm lower immediately adjacent to the large rock, than on the other side of the soil column. J. Young noted the difficulty in driving the core into the ground at a depth roughly corresponding to the depth the rock was found in the soil column. All this evidence indicates the rock was broken and upended during sampling. This is what apparently caused disruption of the fabric and structure in the lower portion of the 60009 soil column.

Four types of fabric have been observed in lunar cores: (1) horizontal or laminar; (2) chaotic; (3) swirled; and (4) massive. The first three are self-explanatory, but the fourth type of fabric refers to places where there are all equant grains and no elongate grains to show any kind of orientation trend.

Structure has been exhibited primarily in the form of layering. It has been observed in nearly all lunar cores. Individual layers may be internally massive, graded, or contain heterogeneities, such as clasts. Marbled layers exist which consist of irregular domains of light-colored soil or crushed, friable clasts which give a marble appearance to the unit.

4.2.4 Lithologies of the Greater-Than-One Millimeter Particles

Because all rock fragments were measured, weighed and photographed, it is possible to retrieve specific particles and determine lithology, composition, and location in the soil column for nearly every particle greater-than-one millimeter. Figure 4.2 contains a list of the lithologies or particle types identified during the dissection of 60009/60010.

Glassy and lithified soils seem to reflect a spectrum of particle types ranging from pure dark glass (Gl Cps), through particles that contain glass and soil (UGA), to particles that appear to be only lithified soil (SoBx). Their shapes range from spherical and/or vesicular droplets, to compact glass and soil masses, to very irregular glassy networks with attached soil and/or soil breccia. Petrographic studies are needed to thoroughly understand the nature of these particles. Because thin sections were not made during core dissection, these complex particles were classified based on observable surface properties: broken versus unbroken glass; and relative abundance and mode of occurrence of glass and soil.

Figure 4.2 graphically presents the lithologic distributions through the soil column.

4.3 STRATIGRAPHIC DESCRIPTION OF THE CORE

4.3.1 Introduction

The stratigraphy of the 60009/60010 soil column is summarized here. In general, it consists of a succession of light-colored marbled zones alternating with darker, massive units. Within some zones are complex features and textures. These units are graphically illustrated in Figures 4.1 and 4.2, and are readily apparent in the photos in Figure 2.8. The marbled units appear to be composed of light-colored clasts in a darker matrix. Some light-colored clasts appear to grade into the darker matrix; others have an irregular contact with the matrix. White or light-colored clast sizes range from the limit of the core tube diameter (4 centimeters) downward to the limit of vision (about 1/2 millimeter). Massive strata are always darker than the marbled layers, although even the former may contain light-colored clasts. Massive layers tend to have irregular or gradational-appearing lower boundaries, but distinct upper boundaries.

4.3.2 Description of Visual Stratigraphic Units

The top of the soil column extends from the lunar surface to 4.5 cm. It is dark, massive and contains a zone of black vesicular glass (shiny on top, soil-coated on the bottom). Most of the >1 mm particles are unfragmented. Only 6% by weight is greater than 1 mm, making the unit fine-grained.

The next visual unit lies between 4.5 and 7.5 cm and is light-colored and marbled. Friable soil clasts make up approximately 30% of the unit. Soil clasts at the base of the unit are approximately 1 cm in diameter, but grade to smaller, approximately 2 mm in diameter at the top. The base of the unit is inclined upward, which translates to the lunar southeast (Figure 4.3). Dark aphanitic breccias, white crystalline rock fragments and soil breccias are the common >1 mm fragments.

A dark, but coarse-grained soil occupies the interval between 7.5 and 12.5 cm. As much as 50% of some dissection intervals in this unit consist of particles >1 mm. Most of the coarse particles consist of fused or lithified soil. These occur in a well-defined stratigraphic succession. At the top is a concentration of dark, vesicular glass that is dust-free on the upper side, but consists of dark, densely lithified soil breccia on the underside. This soil breccia contains mm-sized white clasts. The soil breccia is less strongly lithified, contains smaller white clasts away from the glass coating. The weakly lithified soil breccia grades into cohesionless dark soil that contains approximately 5 mm very irregular, filamentous (not crenulate) patches of light soil.

Between 12.5 and 14-15 cm of 60010 is a light-colored unit with structure that varies from top to bottom. Larger

Figure 4.3. Where lunar surface orientation of a core tube is known, compass directions of the soil column within the core can be determined. Lunar surface photograph AS16-115-18557 shows that the core was taken with the numbers on 60009 facing southwest and the numbers on 60010 northeast. Every core is extruded with the numbers facing upward. All dissections take a longitudinal planar slice of soil, approximately parallel to the numbers which can be seen on the outside of the core tube. In 60010/09, this plane lies in a northwest-southeast direction.

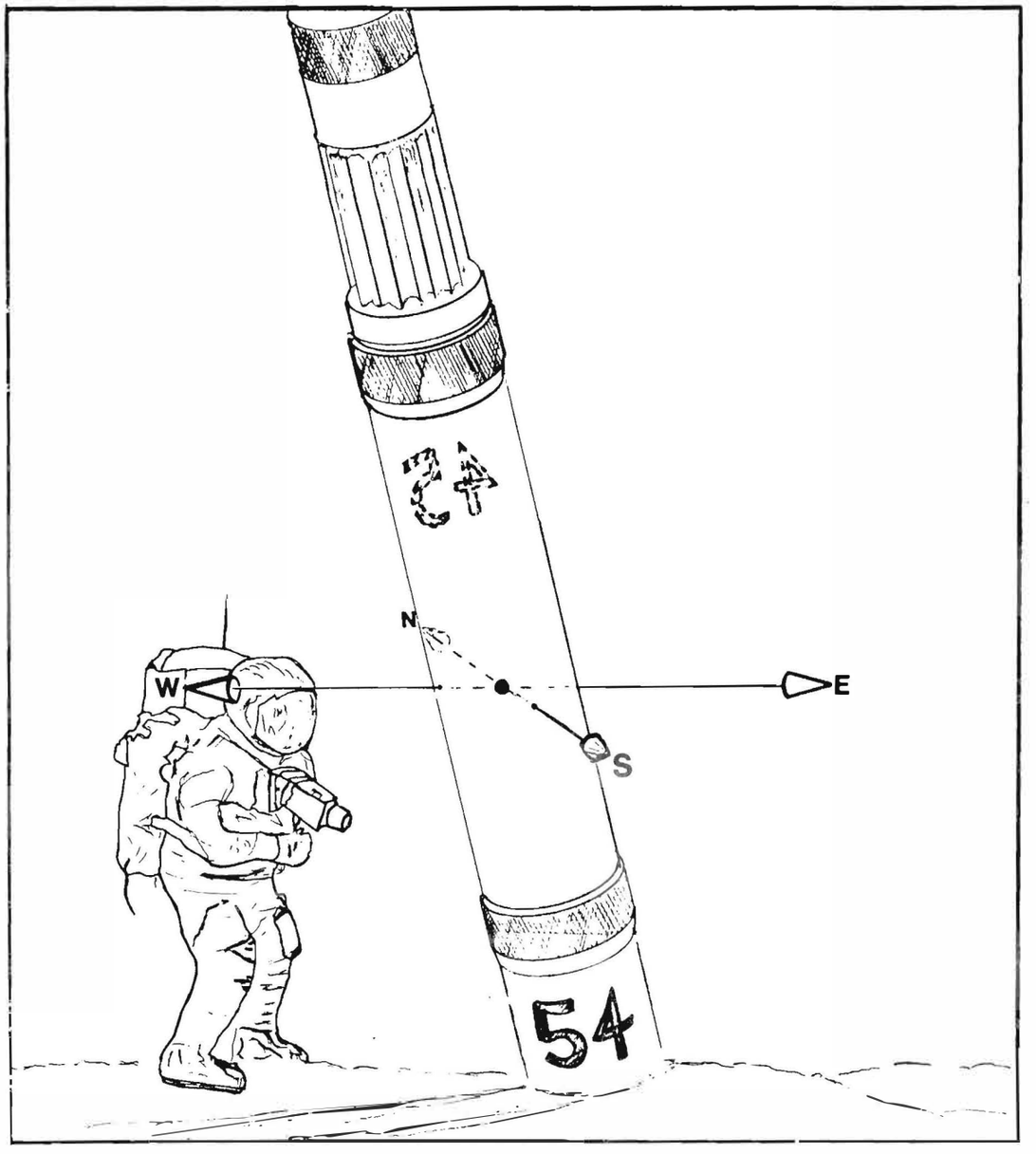

clasts occur at the top that are 5 mm across; these clasts show chaotic arrangement and crenulate, interfingering margins. At the base of the unit are light-colored soil clasts which are mm-sized and horizontally aligned. Rock fragments comprise approximately 15% of the total. Most are dark aphanitic breccias, soil breccias, chalky white rocks and the same mafic-bearing white crystalline fragments seen in the next two units.

A gradational boundary leads to the next unit between 14-15 and 18 cm. It is a relatively dark, massive, fine-grained soil with approximately 10% >1 mm. A well-defined horizontal fabric is clearly shown by flat-lying white clasts. The supramillimeter fraction contains dark aphanitic breccias, soil breccias, chalky white rocks, and white crystalline fragments which appear to contain about 1/3 mafics by volume.

A light-colored, marbled soil occurs between 17.5 and 22 cm; it is packed with 5 mm-to cm-sized irregular interfingering clasts of light soil in a moderately dark matrix. Although soil clasts are very common, lithified rock fragments are not and make up only 20% of the unit. These rock fragments are predominantly soil breccias, dark aphanitic breccias, chalky white fragments, and white crystalline rock fragments with approximately 1/3 mafics. The latter was not found below this unit. Light soil clasts are much flatter in the uppermost cm of this unit than in the remainder of the unit. At the upper surface of the unit is a white rock fragment that has a glass-lined impact pit on the upper surface (S-76-23993, Figure 4.4, top). The lower portion is transitional with the next unit.

Between 22 and 32 cm, which spans the lower section of 60010 and the top of 60009, is a dark, massive, relatively fine-grained unit. Although it averages 10% >1 mm, coarse particles occur in zones, not randomly, especially in 60010. Except for some distinctive, horizontally-lying, pancake-shaped dusty, unfragmented aggregates within the unit, aphanitic dark breccia fragments, chalky white rocks and soil breccias are the most common lithic types. There is a slight decrease in average grain size, from 22 to about 25 cm, which reflects a decrease in abundance of dark aphanitic fragments and chalky white rocks. At the 25 cm depth there is a concentration of oriented, unfragmented aggregates with glass on top and soil underneath.

In the 32-36 cm interval, sandwiched between two dark soils, is a light-colored soil with a marbled appearance. It contains 5 mm-to cm-sized, irregular, interfingering clasts of light-colored soil in a moderately light matrix. Although relatively large clasts appear to make up the bulk of this unit, the clasts are uncohesive soil and only 20% of the material in the unit was retained on the 1 mm sieve. This coarse fraction is similar to that of the underlying units, containing dark aphanitic breccias, chalky white rocks, white or clear crystal (plagioclase) fragments, and

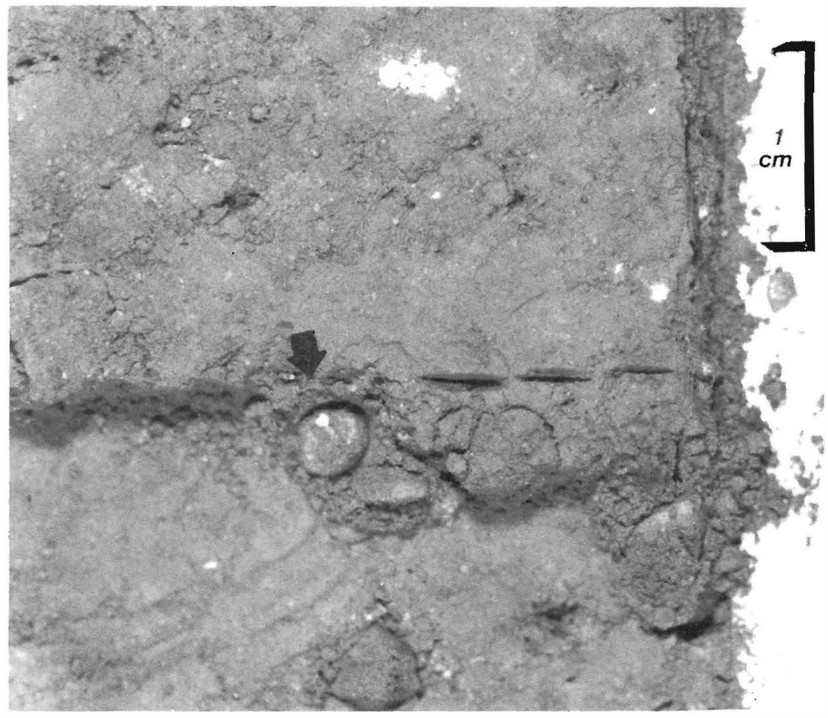

Figure 4.4. Above: Arrow points to a rounded, light-colored fragment with an impact pit on its upper surface. (S-76-23993)

Below: The dashed line indicates an irregular boundary based on color. The arrow points to a glass-coated white fragment with splintery plagioclase pointing down. (S-75-24777)

soil breccias. Features at the top of the unit are distinctive. Some white clasts with rounded bottoms have flat tops that appear to be truncated and coated with clear glass (Figure 4.4, bottom). Plagioclase "splinters" penetrate through the rounded bottom of one clast into the underlying soil, and there is a fine layer of white powder and white crystal fragments (plagioclase) surrounding the flattened top of one clast. Unfragmented aggregates with vesicular glass on top, soil below, occur only at the top of the unit; elsewhere in the unit vesicular glass is fragmented and randomly oriented.

Between 36 and 39 cm is a dark, relatively massive soil with very unusual friable clasts. This unit contains 14% >1 mm. Most of the coarse particles are dark aphanitic breccias or chalky white rocks, but the larger rock fragments are horizontally rather than randomly aligned. The friable clasts are among the most distinctive observed. This unit contains both white soil clasts and dark brown soil clasts. They are both oval to subspherical and well-rounded. The unit also contains a few clasts of light-colored soil that are coated on all sides with dust-free, dark vesicular glass. Although these clasts did not survive handling, one is reconstructed in Figure 4.5.

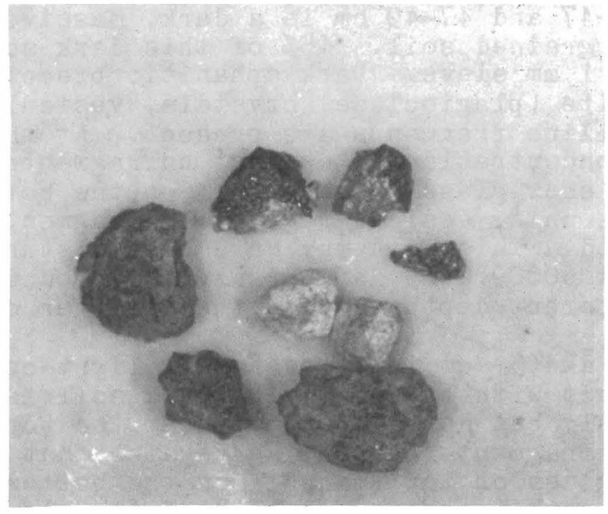

Figure 4.5 shows a glass-coated lithic fragment (sample number 60009,3043), which was so fragile that it broke apart during dissection. The glass appeared to completely encase the lighter colored interior lithology, which was so fragile that it broke into two pieces also. (S-75-32258)

A light-grey soil is between 39 and 44-47 cm. The top of the unit is distinct, but the boundary is uneven. The basal contact of this unit is fairly flat and sharp, and marked by flattened white clasts. Part of the lower contact has been disturbed by the large rock discussed below. This light grey soil is much coarser-grained than the underlying dark massive soil; approximately 1/3 of its mass was retained on the 1 mm sieve. Two lithologies dominate the coarse fraction: mm-to cm-sized chalky white clasts and dark angular to splintery aphanitic breccia fragments. There are unfragmented glass-coated aggregates with glass-side up preferred orientations. Cones of dark soil penetrate downward into the top of this light-colored unit. The conical depressions at the top of the unit are reminiscent of the "raindrop pattern" of impact pits seen on the present-day lunar surface. This unit was severely distorted during sampling by rock 60009,2069, which was fragmented and upended. Linear elongation of friable clasts next to the rock (see the 60009 photography prior to the first dissection in Figure 2.8) and a three centimeter difference in the occurrence of the base of the unit across the diameter of the soil column are attributed to the disturbance when the rock was being forced into and upwards in the drive tube. A sharp contact marks the next unit.

Between 44-47 and 47-49 cm is a dark, massive, relatively fine grained soil. 15% of this dark soil was retained on the 1 mm sieve. Dark aphanitic breccias, chalky white rocks, white (plagioclase) crystals, vesicular glass and grey crystalline fragments are present. At the base of the unit is a concentration of compact unfragmented glassy aggregates that show glass on top, soil on the bottom; elsewhere in the unit, vesicular glass is fragmented and randomly oriented. This unit may have been disturbed by movement of rock 60009,2069 during sampling; boundaries occurred at different depths across the diameter of the core.

Between 49 and 51 cm is a moderately light-colored soil. The contact with the overlying dark soil is irregular and subhorizontal, but not distinct. Near the top of the unit are many unfragmented glassy aggregates that show dust-free vesicular glass on top and soil on the bottom. There is a variety of rock fragments, but the fragments appear rounded, and sparsely rather than densely packed. In common with the next lower unit, parts of the matrix seem to be light-colored with irregularly-shaped soil clasts. There are grey dust-free crystalline rock fragments, which are smaller and more rounded than in the next unit. This unit contains, in decreasing order of abundance, dark aphanitic breccia fragments, soil breccias, chalky white rocks and plagioclase fragments. Discrete, friable and rounded soil clasts range from 1-5 mm, and many have a thin white coating.

Between 50 and 54 cm is the unit with the coarsest grain size in 60009/10, and one of the coarsest units in any lunar core. The matrix is relatively light-colored, and appears to consist of very irregularly-shaped two-centimeter-diameter areas of light and dark soil. These areas appear to be equidimensional, but with interfingering, crenulate margins. The most distinctive characteristic of the interval is the concentration of rock fragments, which make up over 75% of the mass of the unit, and are so abundant that they form a packed, framework texture. This unit can be described as a gravel deposit with interstitial soil. Most of the rock fragments readily shed dust, and are tough, grey, fine-grained crystalline rocks. White (plagioclase) crystals also occur and are up to one cm in diameter.

The lightest colored unit in the soil column is from about 54 to about 56.8 cm. Light and dark soil patches interfinger giving a mottled appearance to the unit. It is fine-grained with only 10% greater than 1 mm. The coarse fragments are mainly chalky white rocks and white (plagioclase) crystals, with a few dark, aphanitic fragments. The upper and lower boundaries appear transitional. Very friable 1 to 5 mm white clasts were observed prior to dissection.

The succeeding 1-2 cm (56-57 cm depth) is a transition zone between the dark soil at the base of the core and the very light soils of the overlying interval. Sedimentary structures in this transitional unit are unique and distinctive. The interval consists almost entirely of light-and dark-colored, non-cohesive, but discrete cm-sized patches of soil with crenulate and interfingering margins. Approximately 35% of the interval is whitish, chalky to powdery material, 25% is dark soil, and the remaining 40% is a light-grey soil (matrix). After sieving, 17% of the mass was retained on the 1 mm sieve. These coarse-grained particles consist mostly of tough (non-friable) dark aphanitic fragmental breccias and friable white rock fragments, with soil breccias and white (plagioclase) fragments also present. The most distinctive aspect of this unit is the structure. Prior to the first dissection, the unit appeared to contain white and dark laminations, but during subsequent dissection passes, the laminations appeared to thickened to the North (see Figure 4.3 for determination of compass direction) and merged with friable white clasts that were flattened on the bottom. In the last dissection pass, the light-colored clasts of this unit appeared surrounded by pods of dark soil continuous with the basal unit.

The lowest soil, from 57 to 59 cm, is a generally dark-colored and fine-grained unit. Only 10% is greater than 1 mm. There are oriented unfragmented glassy fragments with shiny vesicular glass tops over soil breccias

5.0 LUNAR SAMPLE INVESTIGATOR STUDIES

5.1 INTRODUCTION

Studies of the lunar cores are unique in that the data can be related to a depth in the soil column, and therefore to a depth in the regolith. All investigators' analyses can be related to the depth interval from which their samples came. This depth interval is reported here, whether the investigator used it or not (some researcher's publish their results in g/cm^3, for example).

The 60009/60010 soil column was dissected and ready for distribution to principal investigators and their teams by the middle of 1976. (Studies already had been done in several characterization areas such as grain size distribution, petrography, FMR analysis and particle track distributions). This section presents the available data and makes correlations among the data sets. In some cases the "raw" data will be presented, in either the text or as appendices. This will only be done for some data sets. References for all analyses and studies to date will be given at the end of this catalog. For this core there are eight categories of data: (1) grain size distribution, associated with petrography; (2) FMR and magnetic studies; (3) petrography, associated with chemistry; (4) chemical studies; (5) isotopic studies; (6) nuclear fission particle tracks; (7) physical properties; and (8) miscellaneous.

5.2 GRAIN SIZE DISTRIBUTION

The only reported grain size studies on samples that were sieved are those of McKay et al (1976, 1977). Half gram aliquots of submillimeter material were sieved into 8 size fractions between 10 and 1000 μm. The aliquots were from the major stratigraphic units observed during dissection, and from both sides of major boundaries defined by the FMR profiles of Morris and Gose (1976). Appendix 4 presents the sieved size data and includes the parent and subsample numbers, depth intervals from which the samples came, and the weights in grams collected in each size fraction. It also includes the measured grain size data from 1 to 10 mm provided by the Curator's Office. As reported in Section 4.2.2, the size fractions in the 1 to 10 mm range were determined by measuring intermediate axes on individual grains. Measured and sieved data are comparable, but not in a quantitative sense.

The standard grain size parameters determined by McKay et al (1976, 1977) are M_z, the graphic mean grain size and σ_I, the graphic inclusive standard deviation. For a discussion of the derivation these parameters, see Folk (1968).

Figure 5.1 presents M_z and σ_I, determined both with and without the subcentimeter size data. The parameters are given in terms of phi (ϕ). This can be converted to millimeters by the relationship: $mm = e^{-\phi \ln 2}$.

Histograms constructed from the cumulative curves are given in Figure 5.2. From these it is readily seen that bimodal distributions occur at 20 to 20.5 cm and 53.3 to 53.8 cm intervals. This is typical for immature to submature soils. Figure 5.3 (far right) presents a plot of M_z (subcentimeter data included) versus depth. A slight systematic variation occurs with depth. Two soils nearest the top of the soil column are very fine-grained; beneath them there is a trend towards increasing grain size with depth. Two notable exceptions are the coarest-grained soil, near the bottom, and the finest-grained soil beneath it.

Aliquots of the same samples listed in Figure 5.1 were magnetically separated using the method of Rhodes et al. (1975). The weight percents of the magnetic fractions is shown in Figure 5.4 from McKay et al. (1976, 1977). The magnetic fraction is at a minimum about 90 μm, and generally increases in the larger and smaller fractions.

Agglutinates contain fine-grained metal and, for the 60009/60010 core samples studied, agglutinatic abundance parallels the magnetic fraction, although the former is not equivalent to the latter as can be seen in Figure 5.3. Agglutinates represent only a portion of the total magnetic fraction. Lunar and meteoritic metal are also components of the magnetic fraction. Agglutinates and grain size distributions are maturity indices and, in the case of this core, at least, so is the magnetic fraction. A maturity index is a parameter which reflects the amount of residence time (in at least a relative sense) that a soil has spent on the lunar surface. Discussions of the compositions and interpretations of the magnetic and non-magnetic soil fractions are given in Adams et al. (1975), Charette and Adams (1975), Rhodes et al. (1975, 1976), Via and Taylor (1976), Hu and Taylor (1977) and McKay et al. (1977).

Figure 5.1. Grain size parameters: M_z is the graphic mean grain size; σ_I is the graphic inclusive standard deviation. These two parameters have been determined separately for the submillimeter size data and the subcentimeter size data, as indicated. The parameters are given in units of ϕ, and can be converted to millimeters by the relationship: $mm = e^{-\phi \ln 2}$.

INTERVAL (cm)	SUBCENTIMETER DATA Mz (ϕ)	σ_I (ϕ)	SUBMILLIMETER DATA Mz (ϕ)	σ_I (ϕ)
0.5 - 1.0	3.53	2.31	3.80	2.16
3.5 - 4.0	3.67	2.30	3.94	2.10
11.0 - 11.5	3.31	2.80	3.92	2.37
14.0 - 14.5	3.06	2.81	3.79	2.33
20.0 - 20.5	3.26	3.34	4.54	2.30
24.5 - 25.0	3.23	2.60	3.70	2.32
28.8 - 29.3	3.26	2.84	3.90	2.17
42.8 - 43.3	2.69	3.04	3.65	2.40
48.4 - 49.0	3.16	3.36	4.24	2.26
53.3 - 53.8	2.52	3.10	3.76	2.15
58.3 - 58.8	3.90	2.60	4.28	2.20

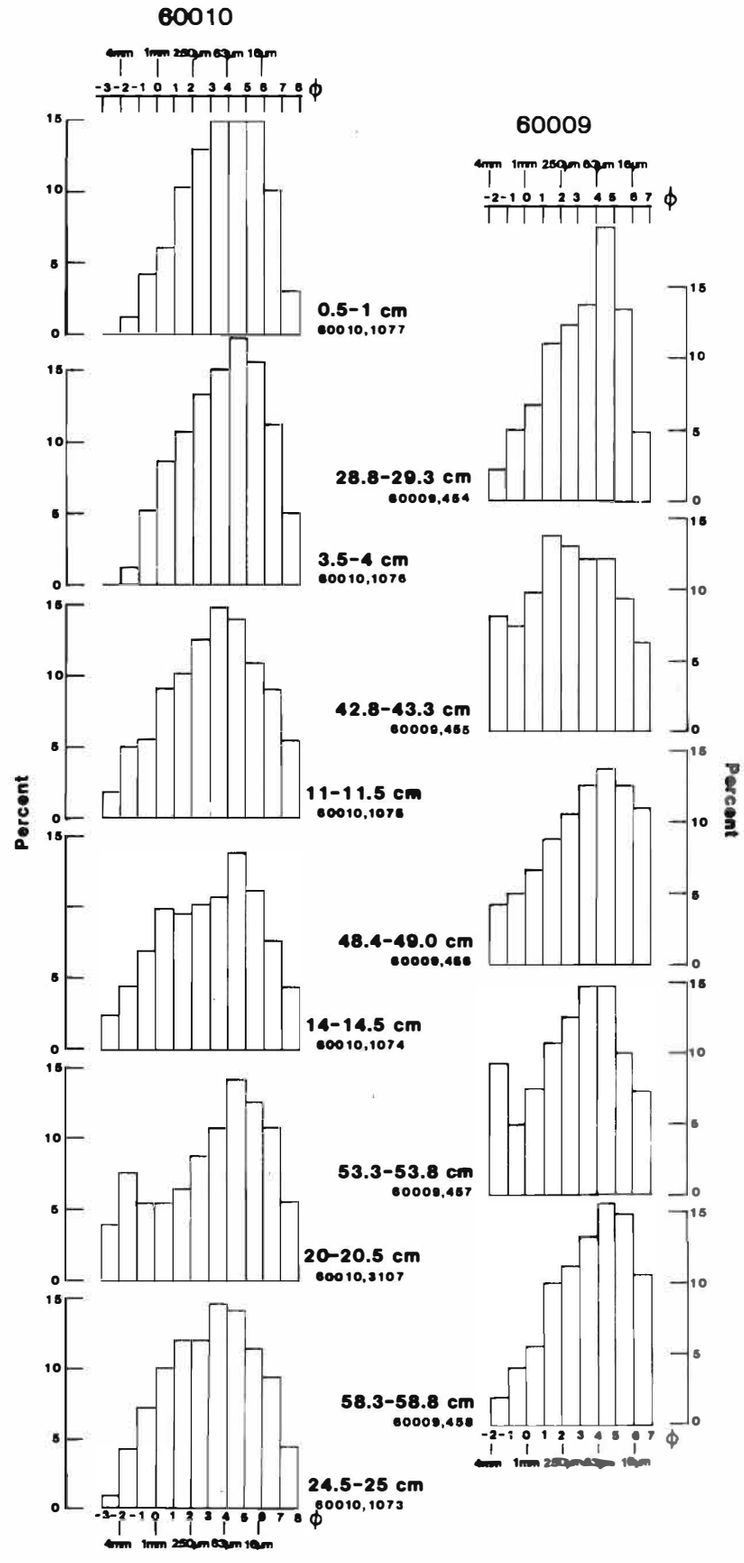

Figure 5.2. Histograms of grain size distribution comparing intervals of 60010 (McKay et al., 1977) and 60009 (McKay et al., 1976).

These histograms were constructed from cumulative curves made from the data in Figure 5.1.

Figure 5.3 compares several different data sets and how they vary through the length of the soil column. On the far right is the mean grain size (M_z) represented by the closed circles (•); to its left is the percent magnetic fraction from the 90-150 μm size interval represented by the crossed circles (⊗); further left is the number percent of agglutinates in the 250-500 μm size fraction represented by the dotted circles (⊙). These three data sets are based on analyses of submillimeter alliquots from the eleven intervals in the core studied and reported by McKay et al. (1976, 1977). Arrows at the right indicate sample depths.

On the far left, the stable component of natural remnant magnetism (NRM), normalized for variations in iron content (Fe^0), is plotted. These measurements were made on the two plastic-encapsulated sections from the 60009/60010 core (the amount of cross sectional material encapsulated is roughly 1 x 1 x 2 cm). This work was done by Banerjee et al. (1977).

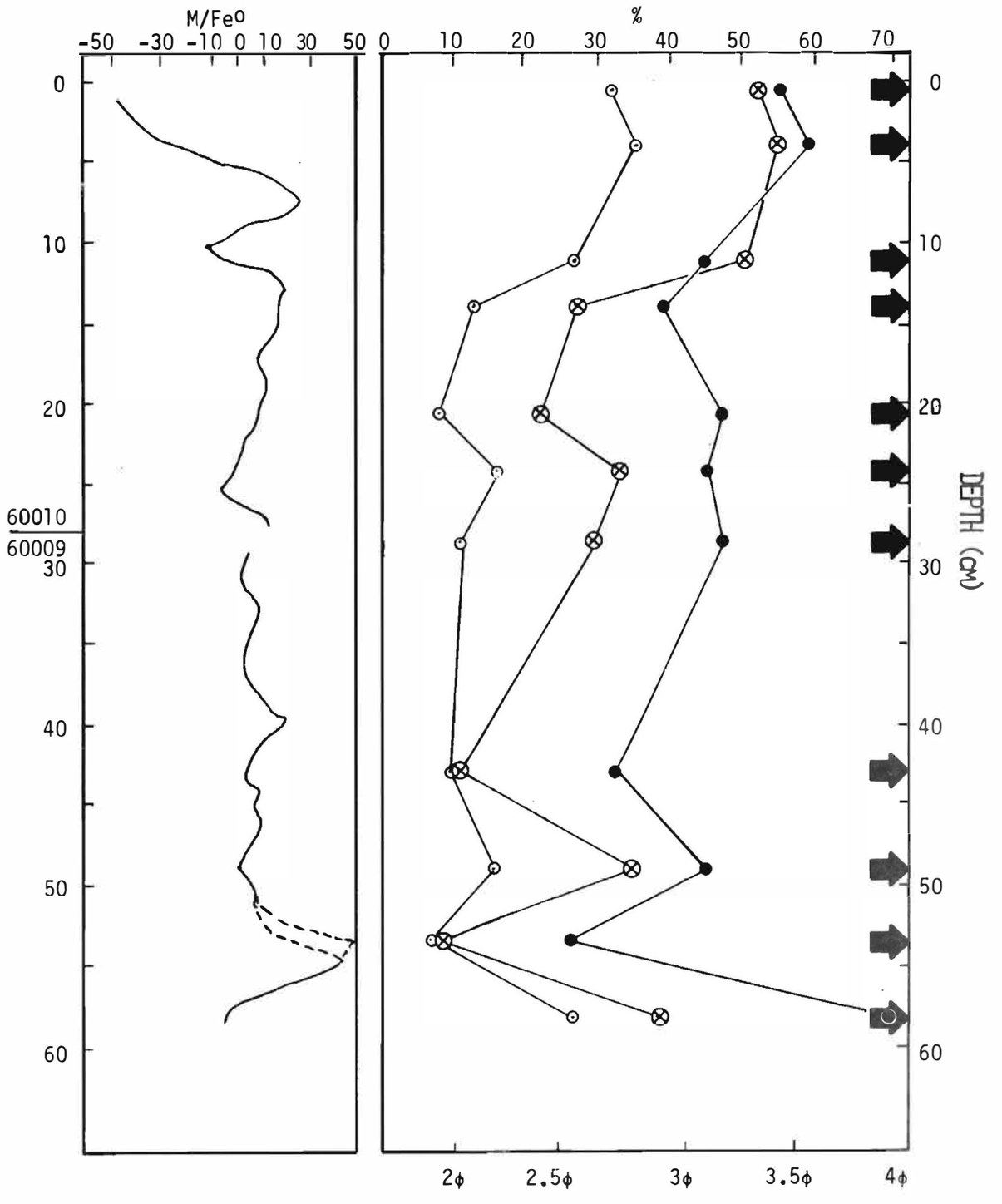
M/Fe°
-50 -30 -10 0 10 30 50
%
0 10 20 30 40 50 60 70
0
10
20
60010
60009
30
40
50
60
DEPTH (CM)
2ϕ 2.5ϕ 3ϕ 3.5ϕ 4ϕ

Figure 5.4 presents the magnetic fraction in weight percent as determined by the method of Rhodes et al. (1975) for the grain size fractions of McKay et al. (1976, 1977).

	0 5 - 1 cm 60010,1077	3.5 - 4 cm 60010,1076	11 - 11.5 cm 60010,1075	14 - 14.5 cm 60010,1074	20 - 20.5 cm 60010,3107	24.4 - 25 cm 60010.1073	28.8 - 29.3 cm 60009,454	42.8 - 43.3 cm 60009,455	48.4 - 49 cm 60009,456	53.3 - 53.8 cm 60009,457	58.3 - 58.8 cm 60009,458
>1000 µm	69.8	50.8	59.3	28.5	28.5	29.2	40.0	19.9	54.2	11.8	62.6
250 - 500 µm	49.7	52.9	47.1	24.8	31.9	26.6	32.3	20.5	36.4	8.5	36.0
150 - 250 µm	50.7	46.1	40.2	22.3	26.9	24.1	29.1	17.0	31.9	5.4	33.5
90 - 150 µm	52.1	53.9	50.5	27.1	22.9	29.8	27.9	13.4	31.6	4.1	37.3
45 - 75 µm	69.1	58.4	57.8	55.6	31.1	34.4	35.1	20.6	36.5	8.3	39.0
<20 µm	36.6	57.5	61.7	62.5	58.7	49.0	46.1	35.3	46.7	26.2	53.9

5.3 MAGNETIC STUDIES

5.3.1 Ferromagnetic Resonance

Morris and Gose (1976) have measured values of I_s/FeO, and Fe^o for virtually every 0.5 cm dissection interval of the core. The parameter I_s/FeO is the ferromagnetic resonance (FMR) maturity (i.e., surface exposure) index (Morris, 1976, 1978). I_s is the relative concentration of metallic iron produced by the exposure-induced reduction of FeO in silicate and oxide phases; normalization of I_s to FeO (I_s/FeO) thus produces a parameter proportional to the length of surface exposure. Only iron grains smaller than about 300 Å contribute to I_s.

The static magnetic technique measures saturation magnetization and the paramagnetic susceptiblity. In lunar samples the former is a measure of the magnetic mineral content. Only grains larger than 100 Å in diameter are detected. The dominant magnetic phase in soils is Fe^o, but other minerals such as kamacite (about 7% Ni) contribute. According to Pearce et al. (1974), a conservative estimate of the error in Fe^o content is about 10% by this method. The paramagnetic susceptibility, on the other hand, is nearly exclusively from the Fe^{++} content, expressed by Gose and Morris (1977) as FeO. Comparison of their values with chemically-determined FeO suggests an accuracy of about 5% by the static magnetic technique.

The results from both the static magnetic technique and the FMR experiments are presented for 131 samples from the 60009/60010 core in Figure 5.5 (Morris and Gose, 1976). One feature of this profile is the decrease in I_s/FeO from the lunar surface to a depth of about 12.5 cm. A similar decrease, although to different depths, is observed in the Apollo 15 and 17 deep drill cores and in the 74001/74002 core. A discussion of the concept of a moon-wide "in situ" reworking of the regolith is given by Morris (1978).

Housley et al. (1976) analyzed aliquots from every half centimeter of the 60009 core, using the FMR technique. (Morris' I_s and Housley's Fe^o are essentially the same measurement). There is general agreement between the results obtained by these groups (Figure 5.5). The only difference between the set of samples each group analyzed is about a one centimeter lateral difference. Both investigators show the FMR data to be particularly sensitive in reflecting stratigraphic units. Morris and Gose (1976) found all major breaks in the FeO and I_s/FeO values correspond to boundaries between the stratigraphic units observed during dissection. Not all stratigraphic units observed during dissection appear in the FMR data, however. The average values of FeO, I_s/FeO, Fe^o and log (I_s/Fe^o) for the stratigraphic units of Duke and Nagle (1974) are given in Figure 5.6 (from Morris and Gose, 1976).

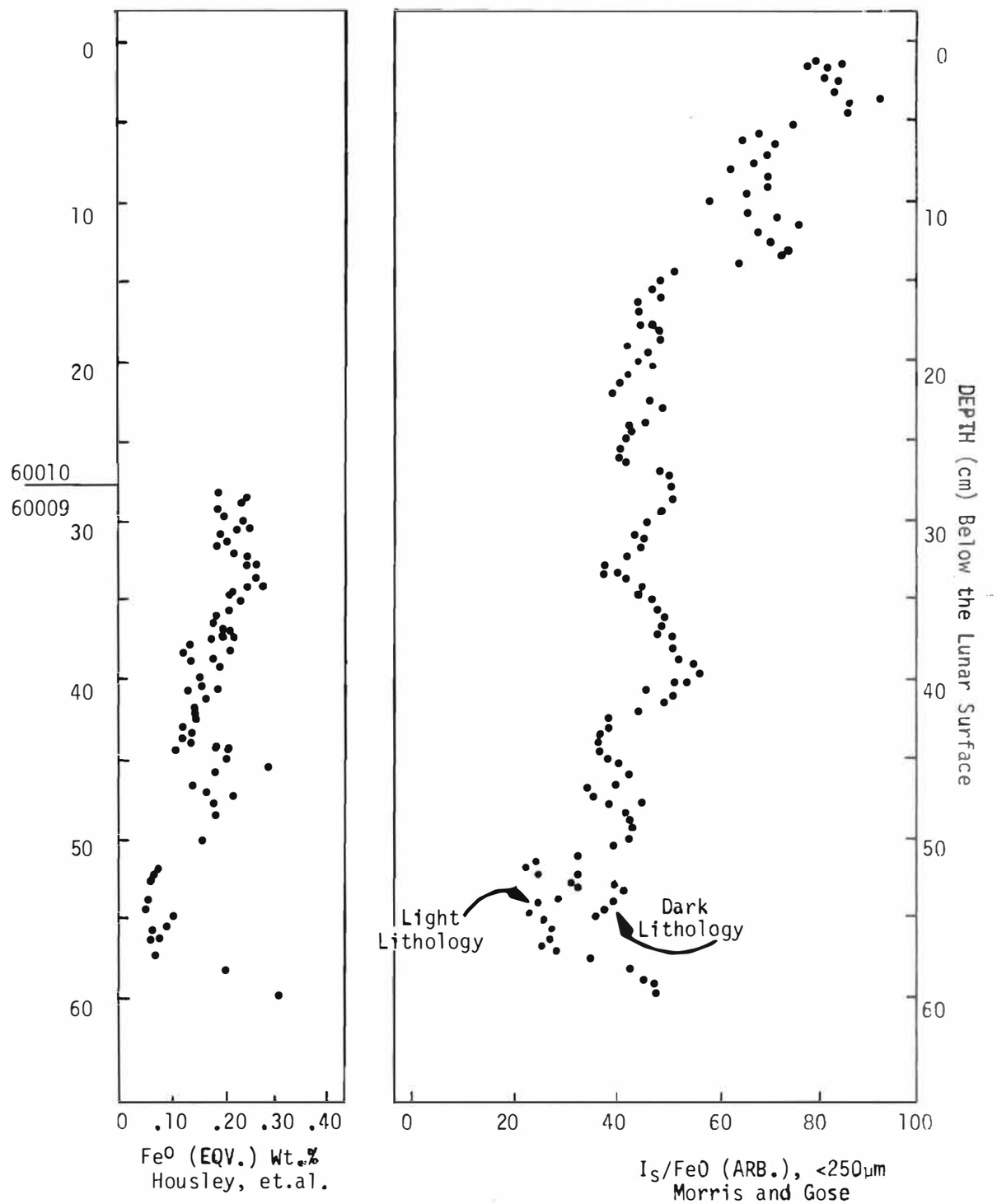

Figure 5.5 on the far right shows the I_S/FeO profile based on 131 samples analyzed by Morris and Gose (1976). The units in which the I_S/FeO data is presented are arbitrary. On the left is data for the 60009 section only, from Housley et.al., (1976). This data is presented as equivalent Fe^0 in weight percent (wt.%), and is essentially the same measurement as the I_S/FeO.

Figure 5.6 presents the average values of FeO, I_s/FeO, Fe^0, and log (I_s/Fe^0) for the stratigraphic units of Duke and Nagle (1974). This data is from Morris and Gose (1976).

Unit	Depth interval (cm)	FeO (wt.%)	I_s/FeO (ARB), <250 μm	Fe° (wt.%)	log (I_s/Fe°)
60010					
7	0–3.0	5.3 ± .6	86 ± 11	0.57 ± .08	2.91 ± .06
6	3.0–7.0	5.5 ± .6	71 ± 11	0.51 ± .15	2.90 ± .11
5	7.0–11.5	5.6 ± .7	70 ± 11	0.51 ± .10	2.88 ± .06
4	11.5–14.5	4.9 ± .4	62 ± 16	0.52 ± .15	2.78 ± .08
3	14.5–18.5	5.3 ± .8	48 ± 3	0.45 ± .07	2.76 ± .07
2	18.5–23.0	4.8 ± .9	47 ± 8	0.44 ± .16	2.72 ± .14
1	23.0–27.8	4.6 ± .3	46 ± 6	0.38 ± .04	2.74 ± .05
60009					
10	27.8–30.8	5.6 ± .5	47 ± 5	0.52 ± .19	2.72 ± .14
9	30.8–36.2	5.2 ± .6	45 ± 6	0.50 ± .10	2.67 ± .08
8	36.2–39.8	4.2 ± .3	52 ± 6	0.36 ± .03	2.78 ± .07
7	39.8–47.3	3.7 ± .7	41 ± 9	0.41 ± .25	2.62 ± .21
6	47.3–48.2	5.0 ± .2	43 ± 0	0.44 ± .04	2.68 ± .06
5	48.2–49.6	5.5 ± .4	44 ± 2	0.46 ± .18	2.74 ± .11
4	49.6–52.8	4.2 ± .1	41 ± 6	0.34 ± .04	2.70 ± .10
		4.0 ± .7	29 ± 8	0.50 ± .22	2.37 ± .23
3	52.8–56.8	3.6 ± 1.2	39 ± 3	0.31 ± .02	2.64 ± .11
		1.9 ± .2	26 ± 3	0.30 ± .56	2.51 ± .46
2	56.8–57.8	3.7 ±	41 ± 5	0.30 ± .10	2.72 ± .01
1	.9 57.8–59.5 .1	5.7 ±	49 ± 2	0.48 ± .04	2.76 ± .05

5.3.2 Natural Remanent Magnetism

Another approach to magnetic studies of lunar cores is reported in Banerjee et al. (1977). This group suggests that there is a record of fluctuations in the stable component of natural remanent magnetization (NMR) of soil versus depth in encapsulated core sections of 60009/60010. The encapsulated soil columns were first magnetically-cleaned by removing secondary magnetizations acquired during and after transport to the Earth. Each was then scanned passively for NRM fluctuations. The resolution of the NRM measurements is on the order of 2 centimeters. The results are presented in Figure 5.3 (far left), so they can be compared with the magnetic fraction of McKay et al. (1977). The curves at the top and the bottom of the NRM results are due to edge effects (Banerjee et al., 1977). The magnetization fluctuations have been normalized to the measured I_s values from Morris and Gose (1976). The remaining peaks and troughs are inferred to represent ambient lunar field fluctuations in the last 1-2 billion years (Banerjee et al., 1977).

5.4 PETROGRAPHY

Petrographic studies have been performed mainly by two groups using two different approaches. The Stony Brook group studied continuous thin sections made from the encapsulated portion of the soil column. Their primary focus was the petrologic and chemical information related to the geologic provenance at the Apollo 16 site, and, to a lesser extent, regolith processes and in situ grain relationships. The major lithic components reported in Simon et al. (1978) are (1) a few exotic fragments of mare basalts; (2) anorthosites-norites-trocotolites (ANT suite), poorly represented as lithic fragments; (3) light matrix breccias (LMB's), chemically equivalent to the ANT suite; (4) feldspathic basalts, rare in this soil column; (5) pyroxene poikilitic rocks (POIK's); (6) recrystallized noritic breccias, chemically-equivalent to POIK's; and (7) a fused soil component including agglutinates and dark matrix breccias. Mineral fragments, primarily plagioclase, with fewer pyroxene and olivine fragments, and glass fragments were other components reported by Simon et al. (1978). Photomicrographs of a POIK rock, a troctolitic/feldspathic basalt, a feldspathic basalt, a cumulate-textured ANT rock, and two mare basalt fragments are shown in Figure 5.7 (from Simon et al., 1978). The tables with all their modal analyses are presented in Appendix 5.

Vaniman et al. (1978) report electron microprobe analyses of glasses, minerals and lithic fragments greater than 0.02 mm in size. Figure 5.8 presents analyses of POIK pyroxenes and several individual pyroxene fragments from the

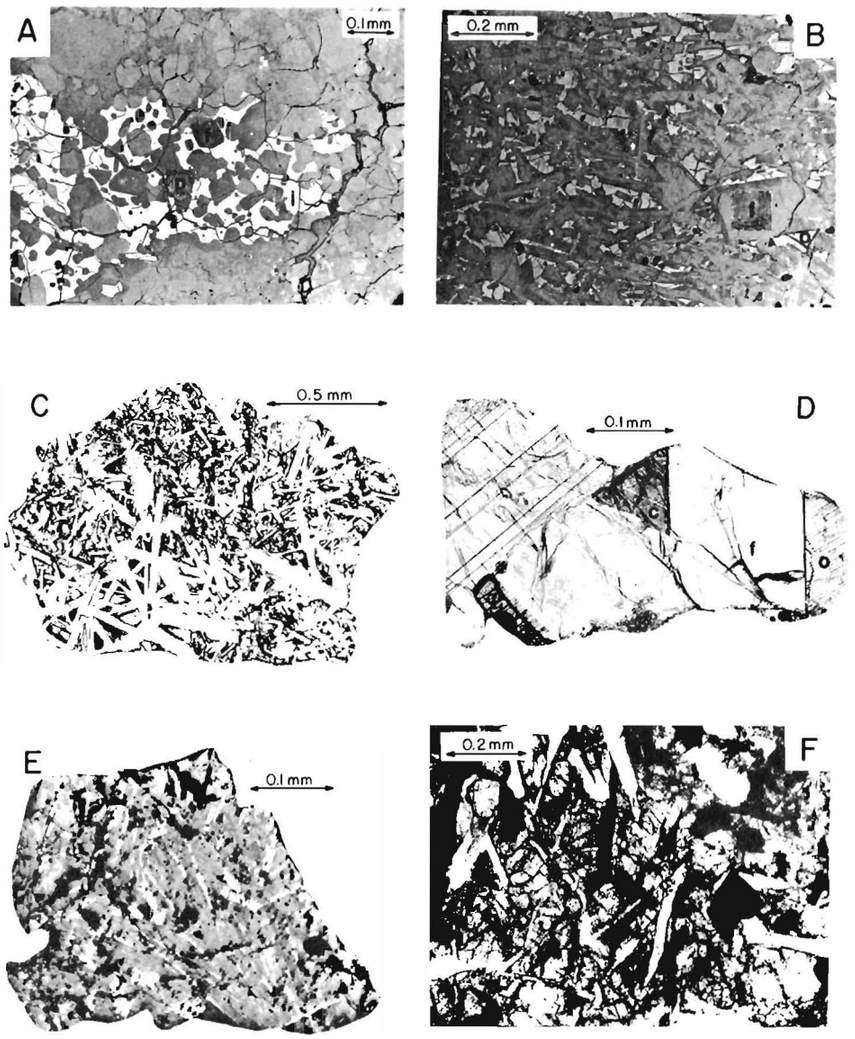

Figure 5.7. Photomicrographs from Vaniman et.al.(1978), of igneous rocks in 60009/60010.

(A) Poikilitic rock representative of lithology contributing to the two pyroxene cluster (see POIK rock 21, Figure 5.8, for analysis). Symbols: i = poikilitic ilmenite; p = pyroxene; f = feldspar.
(B) Troctolitic-feldspathic basalt (see Basalt 66, Figure 5.9, for analysis). Symbols: f = blocky feldspar; o = intergranular olivine.
(C) Feldspathic basalt with laths of feldspar and intergranular pyroxene (see basalt 70, Figure 5.9, for analysis).
(D) Cumulate-textural two pyroxene ANT rock. Symbols: o = orthopyroxene; c = clinopyroxene; f = feldspar.
(E) Mare fragment similar to Apollo 17 olivine porphyritic ilmenite basalts.
(F) Mare fragment similar to Apollo 12 ilmenite basalts.

(A), (B), and (E) were taken in reflected light; the others in plane-polarized light.

Figure 5.8 Two-pyroxene cluster: In POIK lithic fragments of 60009/60010 and in mineral fragments from 60009/60019 (from Vaniman et al., 1978).

	POIK Lithic		Mineral Fragments 60010	
	1	2	3	4
SiO_2	53.2	50.4	53.2	51.0
Al_2O_3	1.34	2.80	1.73	2.71
TiO_2	1.03	2.13	0.92	2.16
FeO	16.4	8.6	16.5	8.5
MnO	0.19	0.17	0.15	0.06
MgO	25.4	16.0	25.7	16.5
CaO	2.25	18.9	2.15	18.8
Cr_2O_3	0.34	0.68	0.33	0.68
Σ	100.15	99.68	100.68	100.41
Si	1.936	1.876	1.926	1.880
Al^{IV}	0.058	0.123	0.074	0.118
$\Sigma_{tet.}$	1.994	1.999	2.000	1.998
Al^{VI}	0.000	0.000	0.000	0.000
Ti	0.028	0.060	0.025	0.060
Fe	0.499	0.268	0.498	0.264
Mn	0.006	0.005	0.004	0.002
Mg	1.376	0.886	1.386	0.906
Ca	0.087	0.753	0.083	0.742
Cr	0.010	0.020	0.009	0.020
$\Sigma_{oct.}$	2.006	1.992	2.005	1.994
$\Sigma_{cations}$	4.000	3.991	4.005	3.992
Wo	4.4	39.4	4.2	38.8
En	69.9	46.3	70.3	47.3
Fs	25.7	14.3	25.5	13.9

All analyses normalized to 6 oxygens. Columns 1 and 2: Pyroxenes of POIK lithic fragment 21 (60010,6025); Columns 3 and 4: Pyroxene fragments of level 3, 60010, 6 cm depth.

Figure 5.9 Analyses of three >1.5 mm melt rock fragments determined by combined modal and microprobe analysis (from Vaniman et al., 1978).

	Basalt 70	Basalt 61	Troctolitic Basalt 66
SiO_2	45.4	46.4	43.0
TiO_2	1.07	0.20	0.17
Al_2O_3	26.5	27.1	24.2
FeO	5.4	3.4	6.4
MnO	0.06	0.05	0.06
MgO	5.2	6.2	12.4
CaO	16.0	15.0	13.8
Na_2O	0.35	0.65	0.36
K_2O	0.03	0.20	0.03
Cr_2O_3	0.13	0.08	0.20
Σ	100.1	99.3	100.6
Mg/(Mg + Fe)	0.63	0.76	0.78
CaO/Al_2O_3	0.60	0.55	0.57
Qz	21.7	27.3	6.8
An	52.4	52.4	49.8
Ol	20.7	19.9	41.6
Wo	5.2	0.4	1.8

Analytical method described in Vaniman and Papike (1977a); the four component norm is determined following the method of Walker et al. (1972), modified by T.L. Grove.

soil column. This data illustrates the two-pyroxene cluster (a high calcium and a low calcium pyroxene) found in this core (and the deep drill core), and demonstrates that the source for the two-pyroxene cluster is the POIK's (and RNB's). The compositions of three feldspathic basalts (melt rock fragments) are given in Figure 5.9: two are anorthositic gabbros and one is troctolitic. Vaniman et al. (1978) propose that these basalts, along with mare basalts, may be the primary rock type in the Apollo 16 soils that contribute Fe-rich pyroxenes to the regolith.

Figure 5.7D is a rare example of a noritic rock with cumulate texture that is probably an example of the source of the large, unshocked plagioclase crystals characteristic of this core. The two pyroxenes in this norite correspond to the two-pyroxene-cluster found in this core. Figure 5.10 lists the compositions of a low-Ca and a high-Ca pyroxene found about 43 cm beneath the surface in the soil column, associated with the distinctive feldspar component.

Light matrix breccias are abundant to moderately-abundant from bottom to top in this core. They are not homogeneous as a group, but they are considered chemically-equivalent to the ANT suite based on pyroxene compositions (Vaniman et al., 1978). A major component of this soil column is ANT-type plagioclase with compositions between An_{96} and An_{97} at all levels. A coarse-grained layer of this plagioclase occurs at 52 to 57 cm in the core. The plagioclase in this zone is homogeneous, and LMB's are associated with the plagioclase (Vaniman et al., 1978).

Only two mare basalt fragments were large enough in the continuous thin sections to permit an accurate petrographic description (Figure 5.7E and F). Figure 5.11 presents the modal data for the two fragments. One is similar to Apollo 17 olivine porphyritic ilmenite basalts (Papike et al., 1974). This is also similar to one of two mare fragment types found by Delano (1975) at the Apollo 16 site. The other is a third type of mare basalt, emphasizing the heterogeneity of the mare basalt component at Apollo 16.

Vaniman et al. (1978) combine the core components, modal proportions, and chemistry to calculate the major element soil chemistry by a modal recombination technique (agglutinates are ignored). Using the bulk soil chemistries they obtain, they describe the change from the lower, coarse-grained anorthositic layer to the upper, more fine-grained and mafic layers as a modal exchange of POIK's, pyroxene, olivine and clear glass for the coarse plagioclase and ANT suite components of the anorthositic layer. This is graphically presented in Figure 5.12. The grain size distribution for the 0.2 to 2 mm size range is shown on the far left and illustrates grain size distribution throughout the soil column. The next column presents the agglutinate abundances for the size interval 0.02 to 2 mm. The last two columns present the single crystal plagioclase and POIK distributions respectively for the 0.02 to 2.0 mm size

Figure 5.10 Columns 1 and 2 are low-Ca and high-Ca end members of pyroxenes normalized to six oxygens; Column 3 is a representative olivine (Fo_{62-63} cluster) normalized to four oxygens. (60009,6024 from Vaniman et al., 1978)

	1	2	3
SiO_2	53.3	49.9	36.7
Al_2O_3	0.55	2.88	0.14
TiO_2	0.46	2.22	0.00
FeO	22.0	8.5	32.6
MnO	0.31	0.09	0.33
MgO	22.3	16.1	30.9
CaO	1.18	18.7	0.24
Cr_2O_3	0.07	0.77	0.00
Σ	100.17	99.16	100.96
Si	1.979	1.867	0.995
Al^{IV}	0.024	0.128	0.004
$\Sigma_{tet.}$	2.000	1.995	0.999
Al^{VI}	0.003	0.000	0.000
Ti	0.013	0.062	0.000
Fe	0.684	0.265	0.738
Mn	0.010	0.003	0.007
Mg	1.237	0.899	1.250
Ca	0.047	0.748	0.006
Cr	0.002	0.023	0.000
$\Sigma_{oct.}$	1.996	2.000	2.001
$\Sigma_{cations}$	3.996	3.995	3.000
Wo	2.4	39.1	—
En(Fo)	62.5	46.9	62.6
Fs(Fa)	35.1	14.0	37.4

Figure 5.11 Model data for mare basalt fragments. Fragment A is similar to Apollo 17 olivine porphyritic ilmenite basalts. Fragment B is similar to Apollo 12 ilmenite basalts. From Vaniman et al. (1978).

	Fragment A	Fragment B
pyroxene	40.6	58.4
plagioclase	25.9	26.7
olivine	5.8	—
ilmenite	16.2	8.1
glass	11.5	6.7
FeS	—	0.1

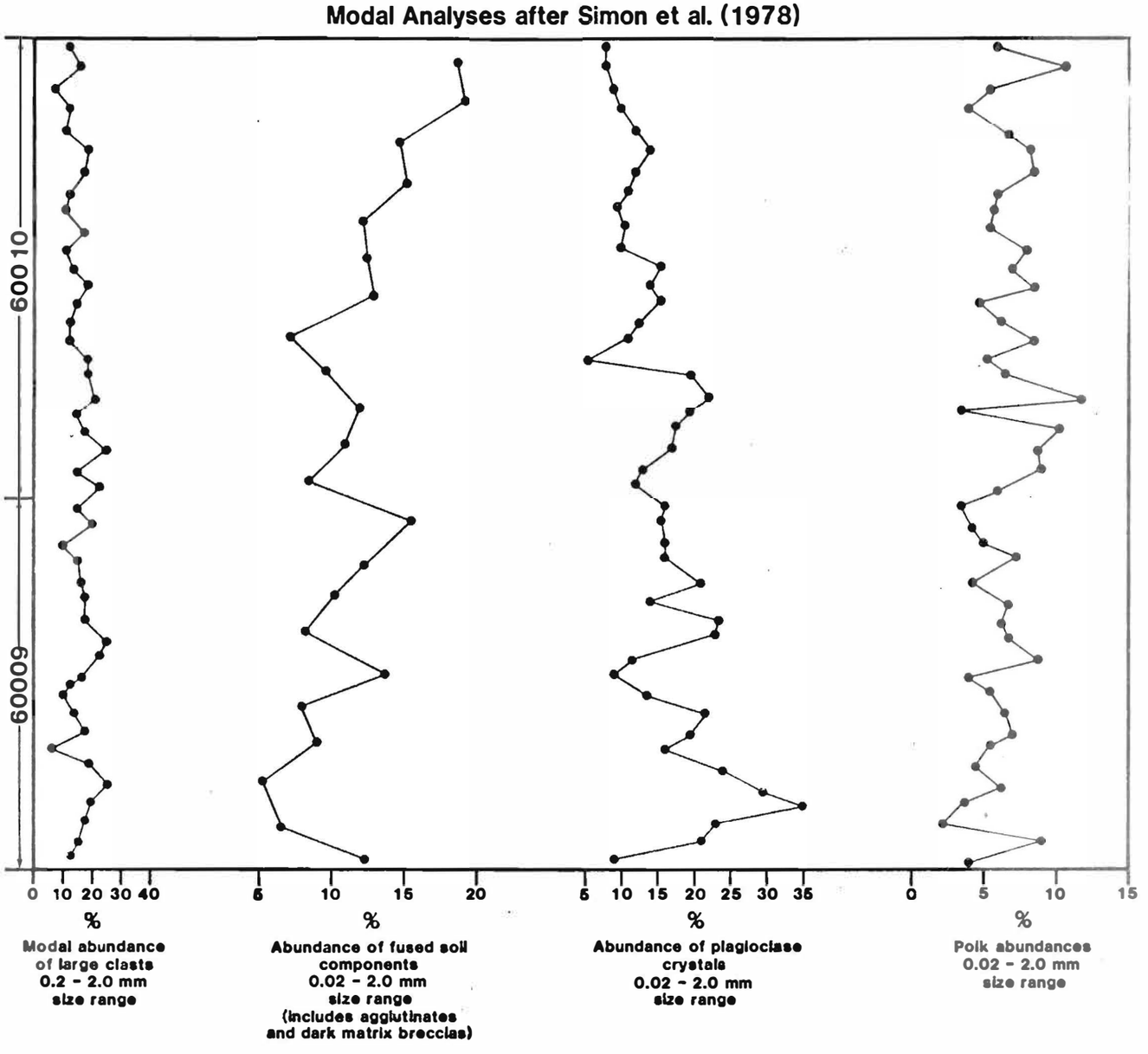

Figure 5.12. The plagioclase and POIK trends illustrate that the plagioclase and ANT content decreases towards the lunar surface; the POIK's and more mafic components do not. The abundance of large clasts decreases and fused soil components increase towards the surface, indicating that the more mature soils are towards the top.

range. Decreasing grain size parallels increasing agglutinate content. This indicates the more mature soils are towards the top (a notable exception being the lowest interval in the soil column, reported by McKay et al., 1976). The plagioclase content significantly decreases upward in the soil column; the POIK's do not.

The other major petrographic study was by McKay et al. (1976, 1977) who analyzed sieved size fractions of submillimeter soils from eleven selected intervals in the soil column. The primary focus of this work was regolith processes and relative importance of mixing versus in situ reworking. The major petrographic types of McKay et al. (1976, 1977) are: (1) agglutinates; (2) poikilitic rocks; (3) metamorphosed breccias, chemically equivalent to the recrystallized ANT suite and LMB's of Simon et al. (1978; (4) light matrix breccia which is polymict, unrecrystallized and consists of crushed plagioclase and associated mafic phases; (5) crushed ANT suite fragments, similar to (4) above but not polymict; and (6) brown matrix breccias, equivalent to the "vitric matrix breccia" of Warner et al. (1973) and Phinney et al. (1976). A range in glass components and mineral fragments, mainly plagioclase with lesser amounts of olivine and pyroxene, are the only other significant components. A complete listing of modal compositions by McKay et al. (1976, 1977) are given in Appendix 6.

The agglutinate content parallels three other maturity indices: mean grain size (see Section 5.1), I_s/FeO (see Section 5.2) and the magnetic fraction, which for this core at least, is a maturity indicator. In the 60009 part of the soil column there are significant differences in maturity parameters, but none appear systematic: the unit with the highest abundance of plagioclase crystals is bracketed by samples containing the least; agglutinate abundances are just the opposite. The 60009 part of the soil column shows a large range in petrology, chemical composition and maturity. None of the samples are mature, and most are submature and immature according to the definitions based on agglutinate content (McKay et al., 1974) and FMR intensity (Morris, 1976). McKay et al. (1976, 1977) plotted various components against each other to see which were related, and to determine whether in situ reworking or mixing was the dominant process. Figure 5.13 shows the percent of metamorphosed breccias (Vaniman et al., 1978: recrystallized ANT suite) plotted against agglutinates for the 150-250 μm size fraction; a good positive correlation is obvious. The least-squares fit line goes through the origin. This indicates that samples in this series without agglutinates should contain no metamorphosed breccias. McKay et al. (1976) interpret this to mean that a major component of these soils is one that contains both metamorphosed breccias and agglutinates, and that this component is present in different intervals in variable proportions.

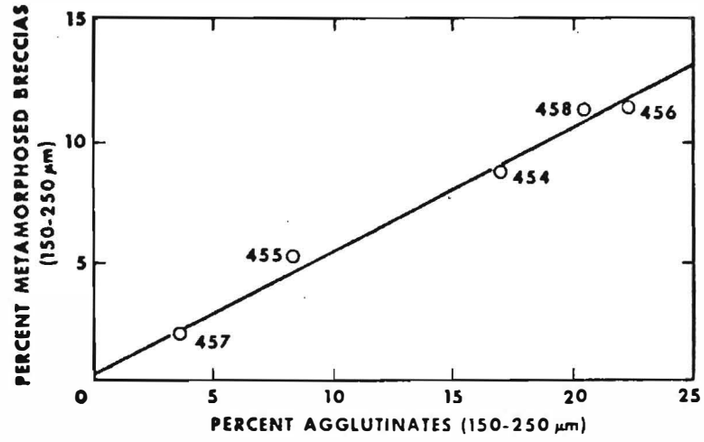

Figure 5.13. This figure shows the pronounced positive correlation between the metamorphosed breccia fragments and agglutinate content for the 150-250 μm size fraction from 60009 samples. The line shown is a least squares fit. Correlation coefficient for these data is 0.99. (From McKay et al., 1976.)

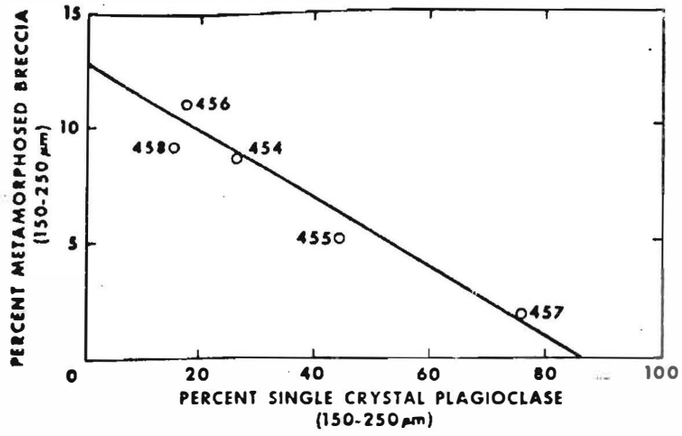

Figure 5.14. This figure shows the inverse correlation of metamorphosed breccia fragments and single crystal plagioclase for the 150-250 μm size fraction in 60009 samples. The least squares line is shown. Correlation coefficient for these points is 0.98. (From McKay et al., 1976.)

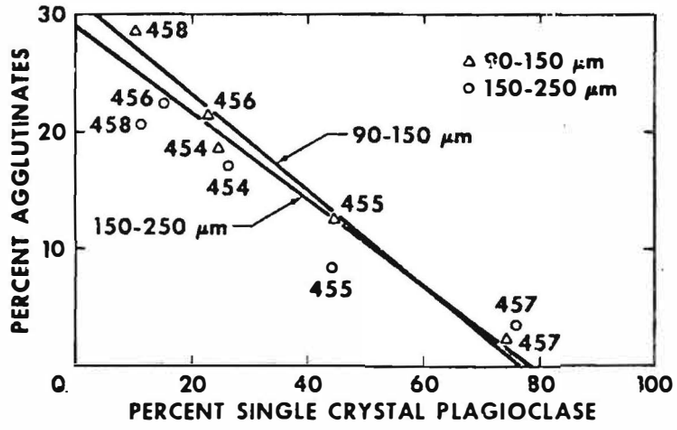

Figure 5.15. The inverse correlation between agglutinates and single crystal plagioclase grains is shown here for 2 size fractions. Correlation coefficient for the 90-150 μm fraction is 0.98 and for the 150-250 μm fraction is 0.94. (From McKay et al., 1976.)

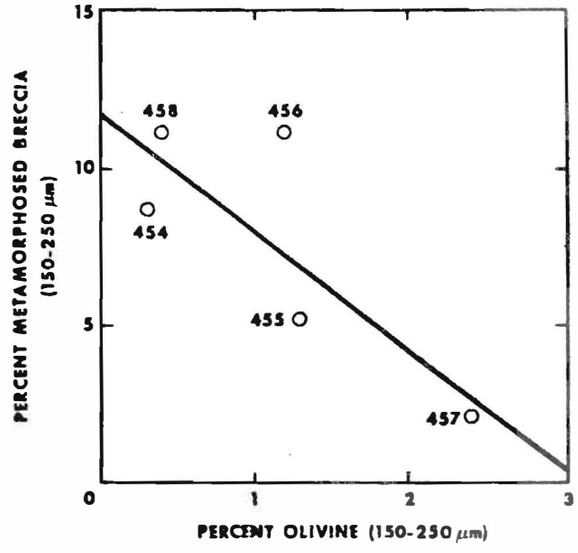

Figure 5.16. The inverse correlation between metamorphosed breccia and olivine crystals in the 150-250 μm size fraction is shown. This correlation while not particularly strong (correlation coefficient 0.79) implies that olivine correlates positively with single crystal plagioclase. (McKay et al., 1976)

Figure 5.14 shows a negative correlation between metamorphosed breccia and single crystal plagioclase, for the 150-250 μm size fraction. Figure 5.15 shows a negative correlation between agglutinate abundances and single-crystal plagioclase abundances for two size fractions. McKay et al. (1976) interpret this to mean that the other major component of the 60009 soil column is the plagioclase-rich soil. Furthermore, the plagioclase-rich soil cannot simply be an immature version of the other soils because plagioclase crystals will not be turned into the metamorphic breccias and POIK's by reworking processes. Figure 5.16 from McKay et al. (1976) suggest to these investigators that the large olivine crystals, although not abundant, may be associated with the plagioclase-rich soil type. This is in agreement with the results of Simon et al. (1978) and Vaniman et al. (1978).

Correlations between soil components and maturity indices are also reported in McKay et al. (1976) for the 60009 portion of the soil column. Figures 5.17 and 5.18 plot mean grain size M_z versus metamorphosed breccia and agglutinate content, respectively. The more mature soil component is the more mafic one; the plagioclase-rich soils are very immature. Because it is not possible to make a mature soil rich in lithic fragments from an immature soil rich in plagioclase crystals, McKay et al. (1976) conclude the following: the variations observed can be explained by mixing of two end member soils. One is very immature and consists primarily of large single plagioclase crystals of plutonic affinity, (the same conclusion reached by Vaniman et al., 1978), possibly olivine, but few if any agglutinates, metamorphosed breccias, brown matrix breccias or POIK's. The other end member is of intermediate maturity with a moderate abundance of agglutinates along with a variety of lithic fragments of a more mafic composition.

In McKay et al. (1977), the upper part of the soil column is described as the result of mixing of three end member soils and in situ reworking. All of the maturity indices including grain size, I_s/FeO, magnetic data, and agglutinate content, point to systematic in situ reworking for the uppermost 12.5 centimeters of the 60010 soil column. The major end member soils are shown in a triangular diagram in Figure 5.19. The three components are single crystal plagioclase, POIK, and metamorphosed breccia (Simon et al., 1978: equivalent LMB/recrystallized ANT). The soils from both the 60009 and 60010 sections are plotted. The lower triangle, Figure 5.20, shows the same relationships, but for a different grain size fraction.

It is beyond the scope of this catalog to devise a single petrologic classification scheme and then apply the two groups' results to it. One difficulty is the different size ranges for which each group present their modal analyses. For example, the magnetic fraction, of which an important soil component, agglutinates, is a major part,

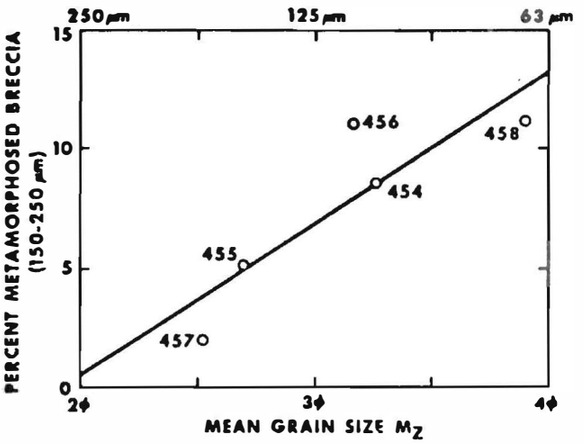

Figure 5.17 shows that for the 60009 samples, the metamorphosed breccia component in the 150-250 μm size fraction has a positive correlation with mean grain size of the bulk soil. Correlation coefficient is 0.87. (McKay et al., 1976)

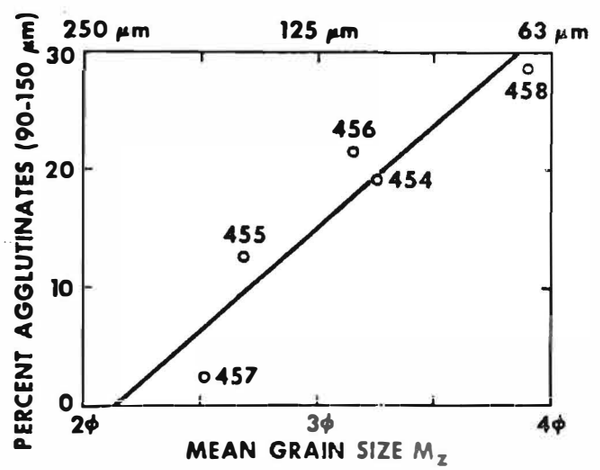

Figure 5.18 shows for 60009 samples, the strong correlation between agglutinates in the 90-150 μm grain size fraction and mean grain size of the bulk soil. Samples containing the highest agglutinates are the finest grained. Correlation coefficient for these data is 0.94. From McKay et al. (1976)

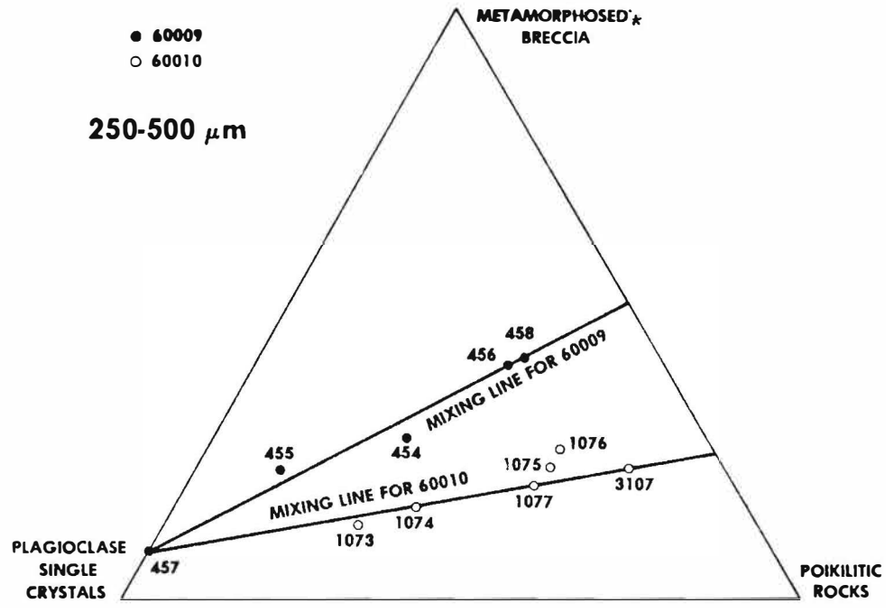

Figure 5.19 Three of the major components in 60009/10 plotted on a triangular diagram after normalization to 100 %. The data for the 250-500 μm size fractions indicates two mixing trends having respective end members 457 to 3107 and 457 to 458. The 60010 soils lie mostly along the 457-3107 line and the 60009 soils lie mostly along the 457-458 line. (* LMB/Recrystallized ANT suite). From McKay et al. (1976).

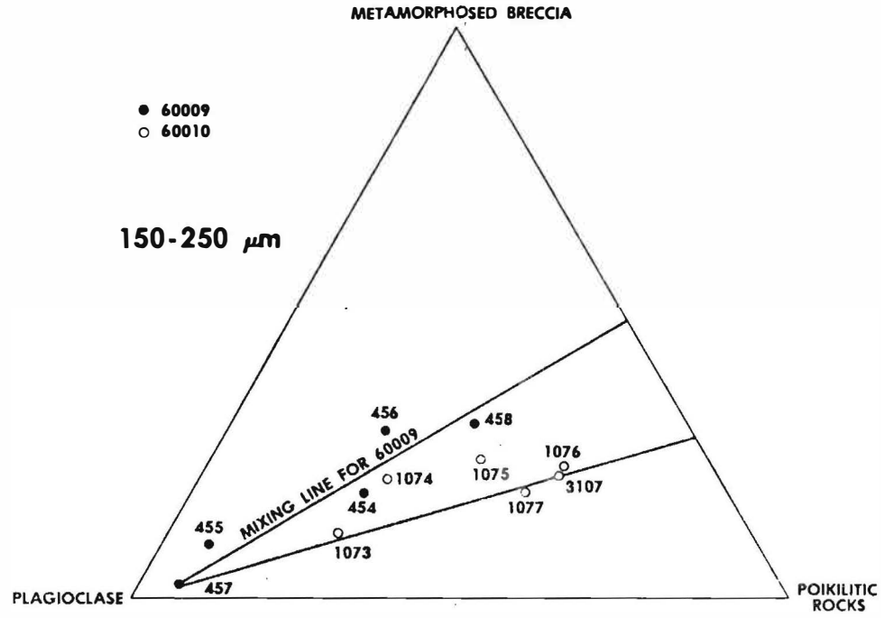

Figure 5.20. A three component plot for the 150-250 μm size fraction of 60009/10 samples illustrating the same mixing trends shown in Figure 5.19. From McKay et al. (1976).

shows a pronounced and systematic range in abundance depending on the size fraction studied (McKay et al., 1976, 1977). For modal studies, not only did each group use different size fractions, but the distributions were determined by different techniques: by measuring, in the case of Simon et al. (1978); and by sieving for McKay et al. (1976, 1977). In Simon et al. (1978), essentially the entire soil column was considered; in McKay et al. (1976, 1977) polished grain mounts of sieved submillimeter soil from eleven selected intervals were studied. The soil column in Simon et al. (1978) was treated as a breccia for modal classification: matrix, less than 0.02 mm; small clasts, 0.02 to 0.2 mm; large clasts, 0.2 to 2.0 mm; and extra large clasts (not included in percentages), greater than 2 mm. Because of all these complicating differences, the modal percentages will not be compared in detail. Instead, both groups' modal percentages are included in Appendices 5 and 6.

Significantly, the two groups' results are in general agreement. The POIK melt-rock is a major contributor of lithic and mineral fragments in 60009/60010. POIK, plagioclase, and LMB/ANT are the three most abundant lithic components found by Simon et al. (1978) in the soil column. Their studies also showed that glass (of anorthositic gabbro composition), pyroxene and olivine are primary soil components, which contribute significantly to the total chemical variation in the soil column when a bulk soil composition is calculated from modal data. McKay et al. (1976, 1977) distinguish two mixing trends involving the same three major components in the double drive tube. The lower soils can be described as mixtures of plagioclase fragments and a 4:1 ratio of POIK: metamorphosed breccia (ANT suite). The upper soils are mixtures of the same plagioclase-fragment composition with an end-member of 1:1 POIK: metamorphosed breccia. Both groups were in agreement concerning maturation effects, but McKay et al. (1976, 1977) presents more data related to in situ reworking processes.

5.5 CHEMICAL COMPOSITION

Chemical studies were performed by two groups, and both found essentially the same trends. Ali and Ehmann (1976, 1977) determined 27 major, minor and trace element abundances in twenty-seven submillimeter size fractions from 60009, and 28 elemental abundances in nine submillimeter samples from 60010 by instrumental neutron activation analysis. Blanchard et al. (1976) and Blanchard and Brannon (1977) studied subsamples of McKay et al. (1976, 1977). Appendix 7 gives Ali and Ehmann's (1976, 1977) results. Their data provide the best vertically continuous suite of analyses. Appendix 8 presents the analytical results of

Blanchard et al. (1976) and Blanchard and Brannon (1977), which can be correlated with the grain size and petrographic studies of McKay et al. (1976, 1977).

On the basis of Ca, Al, and ferromagnesian element abundances, five chemically-distinguishable units occur in the 60009 part of the soil column (Ali and Ehmann, 1976). In sharp contrast to this, very little variation in bulk chemical composition was found in the 60010 part of the core (Ali and Ehmann, 1977) except in the siderophilic elements Fe, Co, and Ni, which are indicative of a meteoritic component. Figure 5.21 from Ali and Ehmann (1976, 1977) compares their chemical units, CU, with the stratigraphic units, SU, of Duke and Nagle, (1976). For the 60009 section, the chemical unit boundaries agree with the stratigraphic unit boundaries, although only five chemical units are defined compared with ten stratigraphic units. For the upper core, with little chemical variation, the chemical units selected were, in fact, influenced by the stratigraphic units, although boundary locations were not always the same. The compositional variations are briefly summarized here. Note that for the 60009 section, Ali and Ehmann (1976) have numbered their chemical units from the top down; but from the bottom to the surface of the 60010 section in their 1977 paper.

Chemical unit (CU) 1, from 27.8 to 38.8 cm at the top of the 60009 section, is characterized by low Ca and Al abundances increasing towards the base, and high ferromagnesian element abundances. CU 2, from 38.8 to 47.1 cm, is richer in Ca and Al, poorer in ferromagnesian elements, and much more uniform. CU 3, from 47.1 to 53.0 cm is very similar to Unit 1 and may have been derived from the same source. CU 4, from 53 to 56.9 cm, has the highest Ca and Al abundances of all the CU units and the lowest ferromagnesian elements, which decrease in abundance towards the lower boundary. This unit has a positive Eu anomaly. CU 5, from 56.9 to 58.8 cm, has the lowest Ca and Al abundances and highest ferromagnesian abundances of all the units.

The basal unit of 60010 from 26.6 to 27.3 cm is the first CU unit in the upper half of the soil column (Ali and Ehmann, 1977). It is higher in Al and Ca; mafic elements show a slight decrease, and sharp differences exist for Ce, Nd, V, Ta and Th, compared with the 60009 CU 1. This unit is chemically quite distinct from the top unit in 60009, even though the two were not distinguished during dissection (Duke and Nagle, 1976). CU 2, from 23 to 26.6 cm, has high Ca and Al abundances, mafic mineral elements exhibit the lowest abundances in the 60010 section, and so do the trace elements except for Co, Ni and Sc. CU 3 from 14.5 to 23 cm shows an increase in mafics and decrease in Al and Ca, compared with the underlying unit. CU 4, from 11.5 to 14.5 cm, shows an increase in mafics (Mg, Fe, Ti, and Mn), in Sc, Co, Ba, Nd, Eu, and Ni compared with adjacent units. It

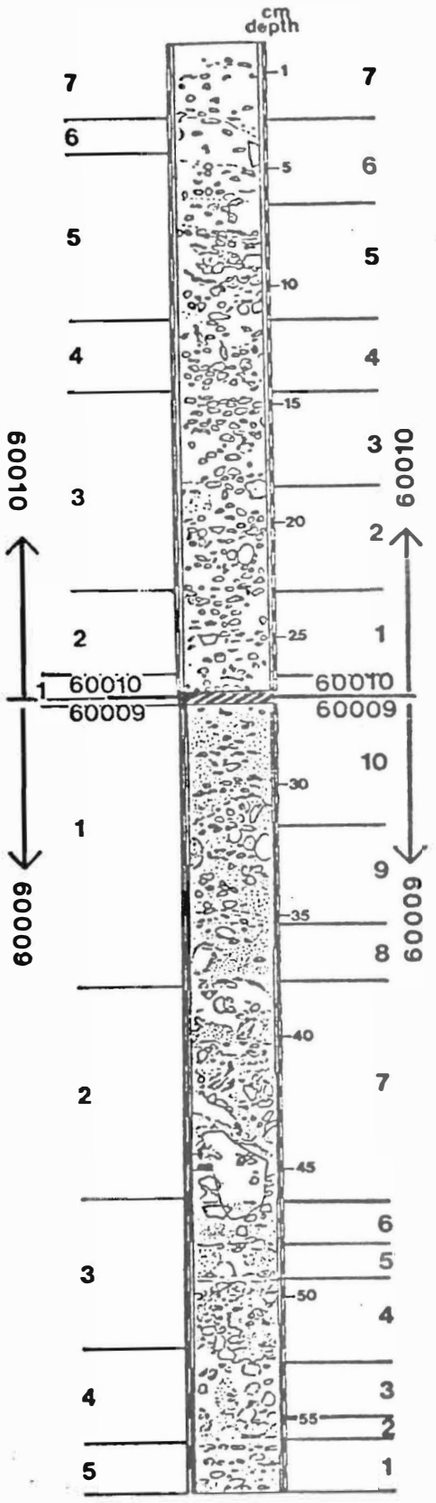

Figure 5.21 compares the stratigraphic units from Duke and Nagle (1976), with chemical units from the Ali and Ehmann (1976, 1977).

shows little variation in Ca and Al. CU 5, from 4.5 to 11.5 cm, contains slightly higher abundances of Si, Ti, Cr, Mn, and Ni, and includes SU 5 and the lower portion of SU 6 (Duke and Nagle, 1976). CU 6 extends from 3.0 to 4.5 cm. It corresponds to the upper SU 6. SU 6 cannot be considered a single chemical unit because the differences are simply too great. Compared to CU 5, CU 6 has higher abundances of Ca, Al and Si and almost twice as much Fe. Except for Nd and Yb, all the trace elements exhibit their highest abundances. CU 7 goes from the surface to 3 cm. Chemically it is typical of Apollo surface soils, Figure 5.22 and 5.23. The other soil column samples are included in this table as well, for comparison.

Figure 5.24 graphically presents the composition profiles for diagnostic elements in the soil column. It is

Element	Range for core 60010	Range for surface soils*
O%	41.1–44.8	43.3–47.2
Si	20.2–22.6	19.5–22.2
Al	14.2–15.8	13.5–16.6
Ca	11.1–12.9	9.1–13.4
Mg	3.1–3.9	2.38–4.40
Fe	3.1–6.4	2.30–5.8
Na	0.296–0.331	0.18–0.47
Ti	0.269–0.486	0.16–0.42
K	0.076–0.095	0.04–0.21
Cr	0.066–0.088	0.04–0.10
Mn	0.054–0.069	0.03–0.06
Ni ppm	200.–10,600.	46.–740.
Ba	100.–180.	57.–190.
Co	22.7–142	7.40–59.0
Ce	21.–36.	8.80–41.5
V	15.4–35.5	6.50–30.0
Nd	11.–20.	8.–23.
La	9.8–13.0	2.70–15.7
Sc	6.96–9.54	4.7–12.0
Sm	4.3–6.2	2.1–7.7
Th	0.8–1.7	0.5–3.2
Hf	2.8–4.1	1.0–5.3
Dy	2.6–4.8	2.2–10.1
Yb	2.21–3.23	1.20–4.95
Eu	1.05–1.23	0.99–1.51
Tb	0.67–1.44	0.24–1.30
Lu	0.48–0.64	0.21–0.83
Ta	0.37–0.70	0.14–0.88

Figure 5.22 is a comparision of the ranges in chemical compositions in the 60010 core samples with the Apollo 16 surface soils and is from Ali and Ehmann (1977). The data under "Range for surface soils" is from Wanke et al. (1975); Rose et al. (1975); Taylor et al. (1973); Boynton et al. (1975, 1976); Bansal et al. (1972); Wasson et al. (1975); Janghorbani et al. (1973); and Ehmann et al. (1974).

obvious that the upper unit of 60009 and lowermost unit of 60010 are compositionally different, that the second and fifth analyses from the top of the soil column have high meteoritic components, and that the intermediate 60010 units (except for the meteoritic components) are very similar. The effects of in situ reworking of the soil appear to dominate the effects of physical mixing in the 60010 section. Figure 5.25, from Ali and Ehmann (1977), shows the composition profiles for Co and Ni, meteorite indicator elements in the soil column. Interelement relationships as seen in these two figures show a strong inverse correlation of elements characteristic of mafic minerals (Fe, Sc) and elements characteristic of an anorthositic component (Ca and Al). The strong positive correlation between Fe and Mn seen in core section 60009 (Ali and Ehmann, 1976) is not so

	Range for core	Unit 1	Unit 2	Unit 3	Unit 4	Unit 5	Range for surface soils*
O(%)	42.1–45.4	43.7	43.9	44.8	45.1	45.4	44.1–45.3
Si	19.7–22.5	21.7	21.4	21.2	20.7	22.5	19.7–21.4
Al	14.1–18.0	14.7	15.6	14.9	17.3	14.1	13.5–16.6
Ca	10.1–14.3	11.6	12.4	12.5	13.0	11.1	10.8–13.4
Mg	2.21–4.76	4.29	3.58	4.19	2.38	4.53	2.38–3.97
Fe	1.33–4.18	3.61	2.95	3.38	1.65	4.18	2.30–4.80
Ti	0.184–0.511	0.380	0.299	0.380	0.238	0.432	0.16–0.42
Na	0.27–0.32	0.30	0.30	0.30	0.29	0.32	0.18–0.47
K	0.026–0.122	0.095	0.055	0.094	0.035	0.122	0.04–0.21
Cr	0.018–0.093	0.077	0.048	0.074	0.026	0.093	0.04–0.10
Mn	0.026–0.068	0.059	0.047	0.055	0.030	0.068	0.03–0.06
Sc(ppm)	2.5–8.6	7.24	5.93	6.72	3.04	8.60	4.7–12.0
Co	6.90–27.1	23.4	19.4	19.9	8.74	27.1	7.40–59.0
Ba	46–196	133	156	101	60	124	57–190
La	3.5–13.8	12.2	11.3	10.8	4.8	13.8	2.70–15.70
Ce	6.4–34.3	30.3	26.8	27.6	11.3	40.2	8.80–41.5
Nd	3.8–30.7	22.7	12.8	21.0	6.8	28.6	8–23
Sm	1.3–5.5	4.5	4.0	4.2	1.7	5.5	2.1–7.7
Eu	0.80–1.28	1.12	1.18	1.18	0.97	1.24	0.99–1.51
Tb	0.22–1.00	0.84	0.74	0.73	0.32	1.00	0.24–1.30
Yb	1.26–4.27	3.75	3.34	3.21	1.59	4.27	1.20–4.95
Lu	0.14–0.50	0.42	0.40	0.37	0.16	0.50	0.21–0.83
Hf	0.96–4.2	2.65	2.90	2.50	0.96	2.33	1.0–5.3
Th	0.46–2.40	1.72	1.23	1.46	0.60	2.40	0.5–3.2
V	6.3–38.0	23.8	23.0	22.0	12.0	38.0	6.50–30.0
Cl	23–500	191	247	101	204	32	15–260
Ta	0.15–0.74	0.61	0.50	0.46	0.17	0.60	0.14–0.88

Figure 5.23 is a comparison of elemental abundances in the 60009 samples with Apollo 16 surface soils and is from Ali and Ehmann (1976). Data in the column "Range for surface soils" is from Wanke et al. (1975); Rose et al. (1975); Taylor et al. (1973); Boynton et al. (1975, 1976); and Bansal et al. (1972).

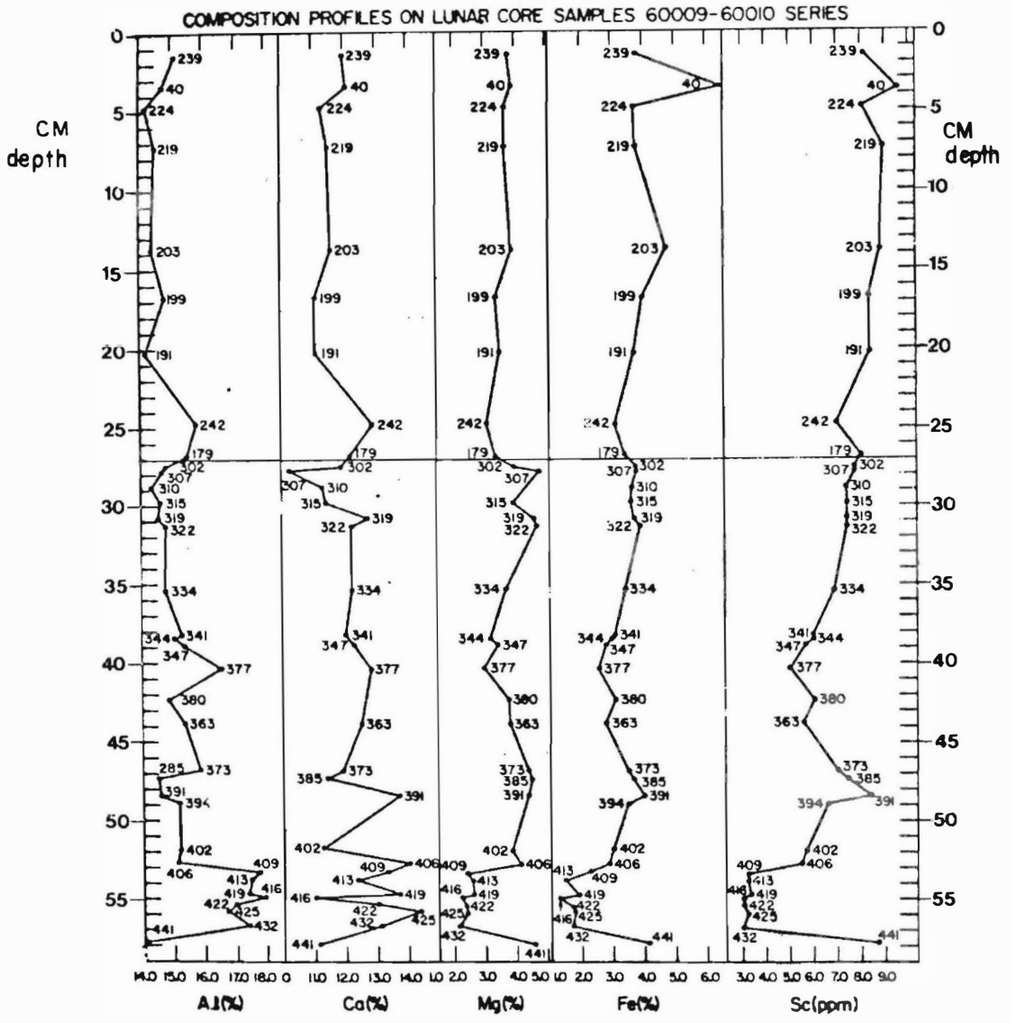

Figure 5.24. Composition profiles for diagnostic elements in cores 60009/60010. From Ali and Ehmann (1977).

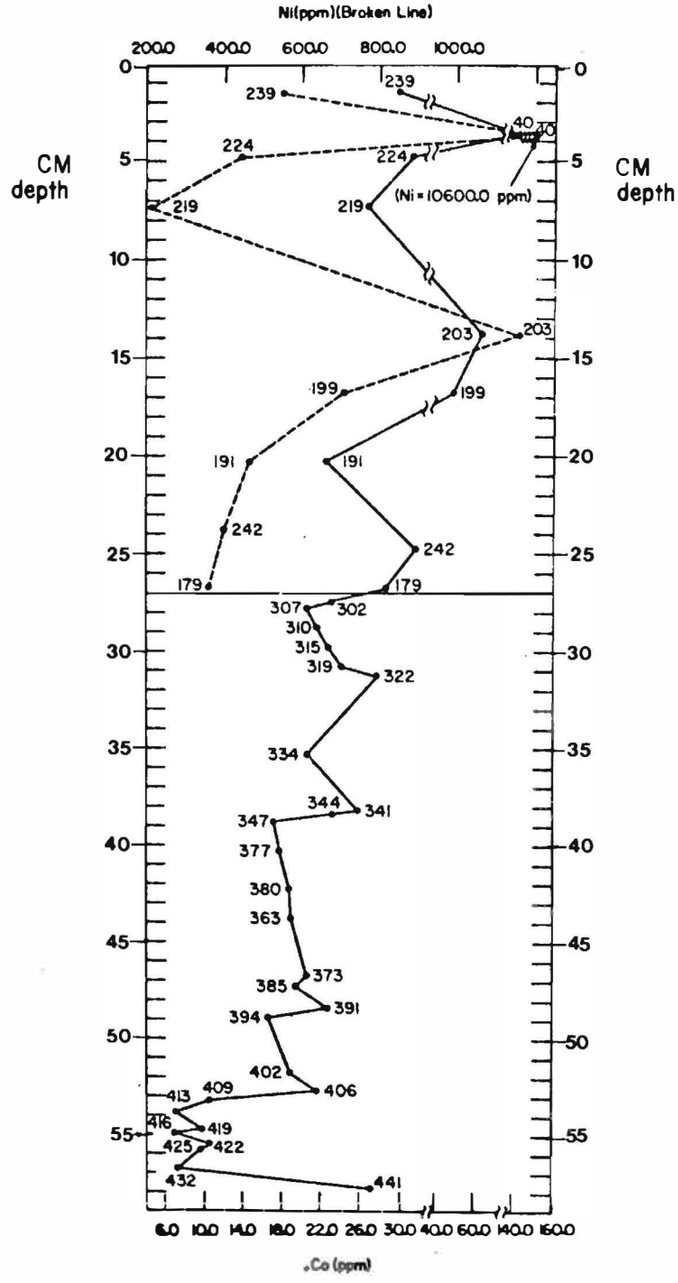

Figure 5.25. Composition profiles for meteorite indicator elements in cores 60009/60010. From Ali and Ehmann (1977).

evident in section 60010 (Ali and Ehmann, 1977). Both sections show a strong negative correlation between K and Al.

Ali and Ehmann (1977) subsamples 242, 179, 239 and 199 (Figure 5.26) show Fe-Al trends that define a regression line similar to the non-mare trend of Hubbard et al. (1973). Subsamples 191, 219 and 224 are depleted in Al with respect to Fe, and define a second trend (mare glass-brown glass breccia-KREEP). These samples may contain a KREEP component similar to the one in the 60009 section (Ali and Ehmann, 1976). However, Blanchard et al. (1976) suggest the "KREEP" component of Ali and Ehmann is supplied by the ferromagnesian component.

Based on their chemical studies, Ali and Ehmann (1977) suggest the 60009 section is a mechanical mixture of three end members: (1) anorthositic rocks which supply the Eu; (2) a major component (rich in agglutinates) which supplies most of the ferromagnesian minerals; (3) minor amounts of a KREEP-like component which supplies the REE, except for Eu. However, the KREEP-like component is not abundant in the top section of the soil column, and Ali and Ehmann (1977) favor the suggestion of Blanchard et al. (1976) that REE are carried largely in the ferromagnesian component. The chemical data support in situ reworking as the dominant

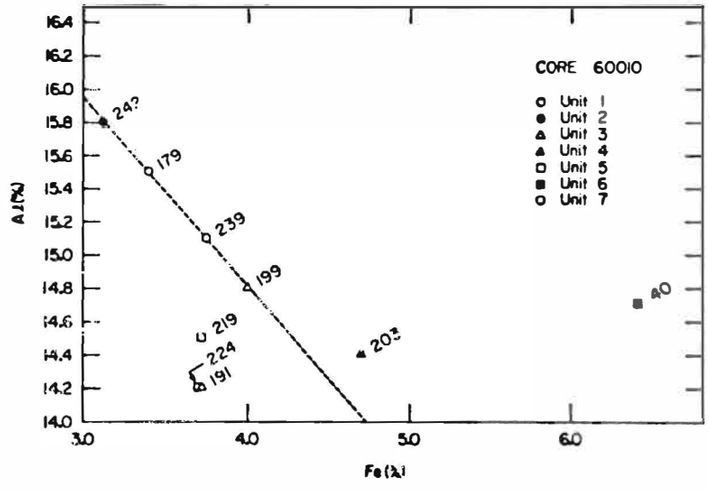

Figure 5.26. Correlation of Fe and Al in core 60010. The lines in the correlation plots are not mathematically fitted. From Ali and Ehmann (1977).

-

Sample	Depth range (cm)	Ave. depth g/cm²†	^{26}Al	^{22}Na
60010,19	0–0.1	0.05	180 ± 15	142 ± 42
60010,26	0.1–0.2	0.25	207 ± 18	169 ± 50
60010,33,34	0.2–0.4	0.5	179 ± 15	78 ± 37
60010,241*	0.5–1.0	1.2	199 ± 12	62 ± 30
60010,238*	1.0–1.5	2.2	156 ± 16	79 ± 47
60010,233,235*	1.5–2.5	3.4	83 ± 9	62 ± 25
60010,231*	2.5–3.0	5.0	135 ± 14	43 ± 30
60010,227,239*	3.5–4.5	7.2	116 ± 7	57 ± 18
60010,223,225*	4.5–5.5	9.1	75 ± 5	48 ± 16
60010,213,215 216,217*	8.0–9.5	16.1	63 ± 7	—
60010,143,144,145, 196,198	17.0–19.5	34	79 ± 4	58 ± 12
60010,180,181,182, 184,186*	24.5–26.6	48	71 ± 7	78 ± 21
60009,1016,1019,1021, 1024,1028,1032	31.3–34.8	61	72 ± 5	—
60009,1067,1069,1071, 1074,1076,1078	41.8–44.3	81	66 ± 5	42 ± 12
60009,1116,1120,1124, 1128,1132,1134*	55.0–58.0	106	65 ± 6	63 ± 15

*New measurements.
†Ave. density = 1.9 g/cm³ for 60009-60010

Figure 5.27. ^{26}Al and ^{22}Na in Apollo 16 double drive tube 60009-60010. From Fruchter et al. (1977).

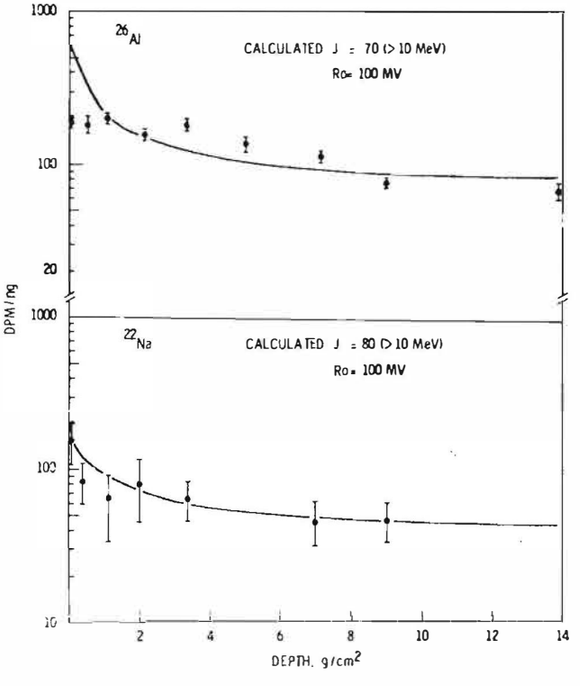

Figure 5.28. Comparison of calculated and measured ^{22}Na and ^{26}Al concentration gradients in the top portion of Apollo 16 drive tube 60010. From Fruchter et al. (1977).

process in the (upper 12.5 cm) 60010 section, and mixing as the dominant process in the 60009 section. Overall the soil column is not like typical highlands surface soils, but is generally enriched in Al and Ca and depleted in elements characteristic of mafic minerals.

5.6 COSMOGENIC RADIONUCLIDES: ^{22}Na, ^{26}Al and ^{53}Mn

Radionuclides produced by solar and galactic cosmic rays are useful for studying depositional histories of lunar soil columns. This section presents the analyses of ^{22}Na ($t_{1/2}$ =2.6 years), which reflects processes during the past 0-10 years; ^{26}Al ($t_{1/2}$= 0.73 my), which covers the time span over 0-3 my; and ^{53}Mn ($t_{1/2}$= 3.7 my), which provides information through the past 10 my.

The ^{22}Na analyses by Fruchter et al. (1976, 1977) indicate that the soil column has not been significantly disturbed (by loss of material or mixing) during the collection and subsequent handling prior to analyses. The ^{26}Al analyses produce a profile or gradient (when plotted against depth in the soil column as g/cm^3) that suggests gardening in the upper 2 or 3 cm over a time span comparable to the half life of ^{26}Al. Figure 5.27 presents their tabulated analyses and Figure 5.28 is a graphical presentation of their data for these two isotopes.

Nishiizumi et al. (1979) have provided complementary analyses for this soil column by analyzing for ^{53}Mn in submillimeter soil aliquots of about 150 mg each. In the upper centimeters of the regolith, ^{53}Mn is produced by solar cosmic rays (SCR). ^{53}Mn is produced by the higher energy galactic cosmic rays (GCR) to depths of several meters. Their results for ^{53}Mn are graphically presented in Figure 5.29. Figure 5.30 correlates their samples with depth. The measured profile is higher in roughly the upper centimeters than theory would indicate it should be. The depth integrated ^{26}Al activity is also higher. In addition, both the ^{26}Al and ^{53}Mn profiles show a decrease (disturbance) in the upper few centimeters at about the same depths. Nishiizumi et al. (1979) suggest that this may have a statistical significance because other cores display similar trends; there may be a correlation between this surface decrease and the size and frequency of the cratering events which dominate present day regolith gardening. This could also have been caused by a disturbance that occurred during core collection.

5.7 NOBLE GAS STUDIES

Isotopic abundances of the noble gases have been determined in grain size separates of the same eleven soils studied by McKay et al. (1976, 1977) by Bogard and Hirsch

(1976, 1977). Noble gas abundances also were determined in magnetic and plagioclase separates from several of these soils. In addition, as part of the preliminary examination, four samples from the top 4 mm of the 60010 section were analyzed for noble gas abundances and studied by FMR techniques. The extensive results are given in Appendix 9. (Except for the top 5-mm samples, all the samples analyzed by Bogard and Hirsch (1976, 1977) were split from the same samples studied by McKay et al. (1976, 1977)).

Noble gas isotopic analyses were made mass spectrometrically by standard techniques (Bogard et al., 1973). The results for the 60010 samples are presented in Tables 1 - 3 in Appendix 9; results for the 60009 and top 5 mm samples from 60010 are presented in Tables 5 - 7 in Appendix 9. Grain size data were subjected to ordinate

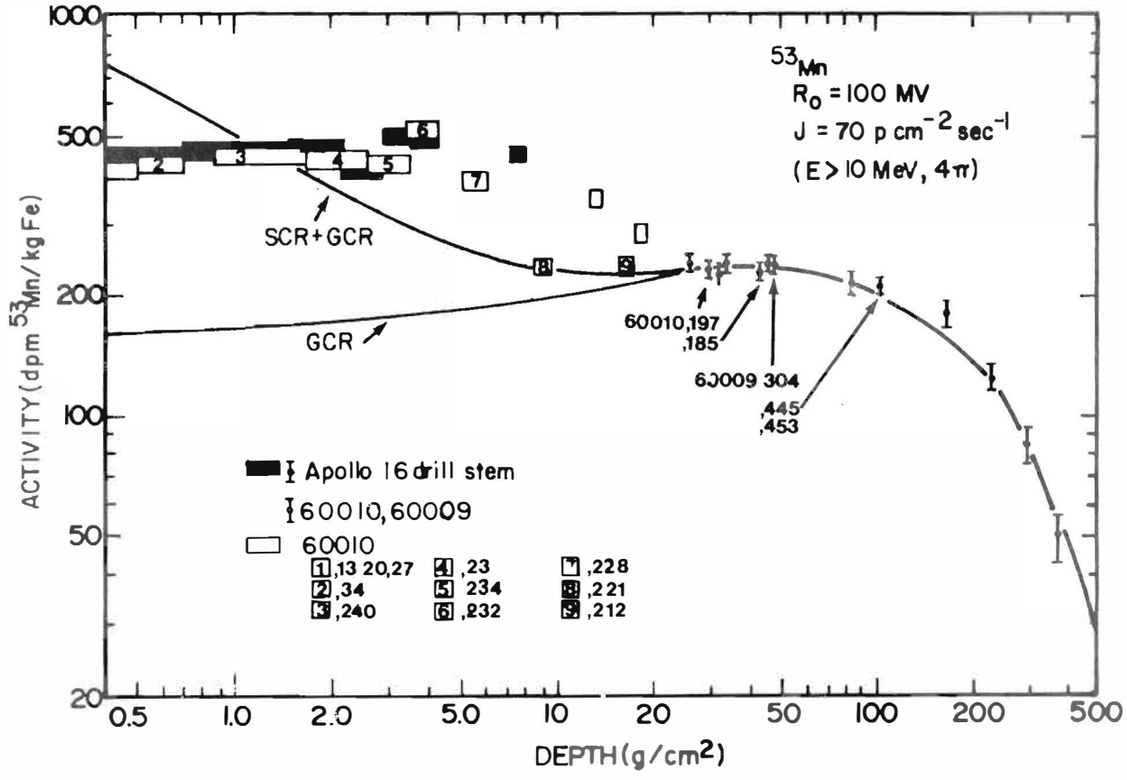

Figure 5.29. ^{53}Mn data measured to date in Apollo 16 lunar cores from Nishiizumi et al. (1979). The theoretical curves were calculated using the Reedy-Arnold model. The GCR curve was normalized to the data points in the 20- to 100 g/cm^2 region as described in Nishiizumi et al. (1979).

intercept analyses (Eberhardt et al., 1970; Pepin et al., 1974) to determine the surface-correlated component (mainly solar wind-implanted) and the volume-correlated component (mainly cosmic ray-produced, or ^{4}He and ^{40}Ar from radioactive decay). The results of these ordinate-intercept analyses are listed in Tables 4 and 8 respectively for the 60010 and 60009 samples, in Appendix 9.

5.7.1 Surface-Correlated Noble Gases

The isotopic compositions of surface-correlated solar wind gases are similar to one another and similar throughout the length of the soil column. There is a trend for He/Ne and Ne/Ar ratios to increase with decreasing grain size. This correlation is probably due to the fact that finer grain sizes contain more mafics (Blanchard et al., 1976),

Sample Number	Depth (g/cm^2)	Depth from lunar surface (cm)
60010,13	0.0-0.2	0.0-0.1
60010,20	0.2-0.3	0.1-0.2
60010,27	0.3-0.5	0.5-0.7
60010,34	0.5-0.7	0.3-0.4
60010,240	0.9-1.7	0.5-1.0
60010,237	1.7-2.6	1.0-1.5
60010,234	2.6-3.5	1.5-2.0
60010,232	3.5-4.3	2.0-2.5
60010,228	5.2-6.1	3.0-3.5
60010,221	8.7-9.6	5.0-5.5
60010,212	16.5-17.4	9.5-10.0
60010,197	29.5-30.4	17.0-17.5
60010,185	42.6-43.4	24.5-25.0
60009,304	47.4-48.3	27.4-27.6
60009,445,453	103.2-104.1	58.3-58.8

Figure 5.30. Subsamples with their calculated depth as g/cm^2 compared with their actual depth from the lunar surface. Nishiizumi et al. (1979)

which are more retentive of the lighter noble gases than felsic minerals (Signer et al., 1976; Walton et al., 1973). The noble gas concentrations vary widely for a given grain size from one depth to another, but the variation is always proportional to differences in soil maturity indices such as those measured by McKay et al. (1976, 1977). Figure 5.31 shows two such correlations: petrographic agglutinates (top) and the magnetic fraction (bottom) separated by McKay et al. (1976) versus ^{36}Ar in two size fractions and ^{4}He in one size fraction respectively.

When the ^{36}Ar is plotted against I_s/FeO, the relationship is still linear, but the trend does not go through the origin (Figure 5.32) for either the 60009 or 60010 samples. Bogard and Hirsch (1976) consider that the five 60009 soils they analyzed are composed of varying mixtures of a mature soil with an immature soil, and that the trend represents a mixing line rather than reworking, or soil evolution. The six 60010 samples plotted in Figure 5.32 (open diamonds) yield a trend that is quite different: although the lowest two 60010 soils (60010,3107 and ,1073) appear to be on the 60009-defined trend, the samples from the upper 12 centimeters lie off this trend. The upper four samples have increasing values of I_s/FeO and ^{36}Ar going towards the lunar surface. The solid line in Figure 5.32 is interpreted by Bogard and Hirsch (1977) as a trend produced by reworking after core deposition.

Elemental ratios of the surface-correlated noble gases were determined for <20 μm magnetic separates of the 60009 soils and some 60010 samples. The Ne/Ar ratios, but not the He/Ne or Ar/Xe ratios, were found to be consistently higher than for the <20 μm bulk soils. The ratio of gas concentration in the magnetic to non-magnetic sub-20 μm fraction for each noble gas element was calculated, and although the calculated concentration ratios varied, there was no obvious correlation with maturity, the FeO content or plagioclase contents (Bogard and Hirsch, 1976). This is surprising because higher noble gas concentrations have been found to be correlated directly to abundances of mafic minerals and magnetic agglutinates and anti-correlated to feldspar abundance (e.g., Charette and Adams, 1975; Signer et al., 1976). Incomplete separation of the sub-20 μm magnetic component for some of these soils because of clumping (McKay et al., 1976), may be the reason for the lack of correlation (Bogard and Hirsch, 1976, 1977).

The $^{40}Ar/^{36}Ar$ ratio varies from 0.83 to 2.69 for the samples analyzed from the soil column. This range probably reflects differences in ^{40}Ar implanted from the lunar atmosphere (e.g., Yaniv and Heymann, 1972; Bogard and Nyquist, 1973). Heymann (1975) and Bogard and Hirsch (1975) report $^{40}Ar/^{36}Ar$ ratios of more than about 4 for very old soils (or soil components) that have not been reworked in a near-surface environment for any length of time in the recent past. According to these two groups, this may

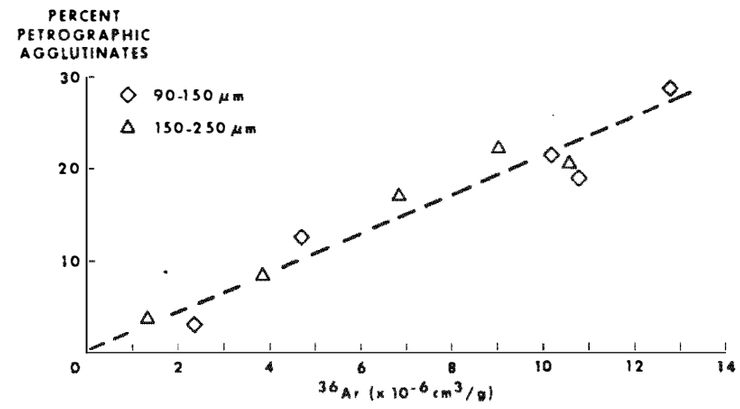

Figure 5.31. (Top) shows the correlation of petrographically-identified agglutinates (number percent) by McKay et al. (1976) with ^{36}Ar in two grain size separates of five 60009 soils. (Bottom) shows the correlation of the magnetic fraction separated by McKay et al. (1976) with ^{4}He in the 90-150 μm size fraction for the same five soils.

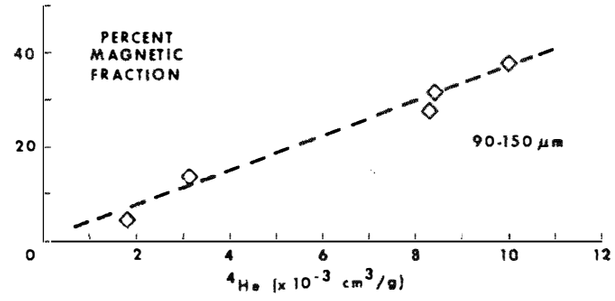

Figure 5.32 shows the two different relationships between ^{36}Ar and I_S/FeO for the 60009 and 60010 soils analyzed by Bogard and Hirsch (1976, 1977).

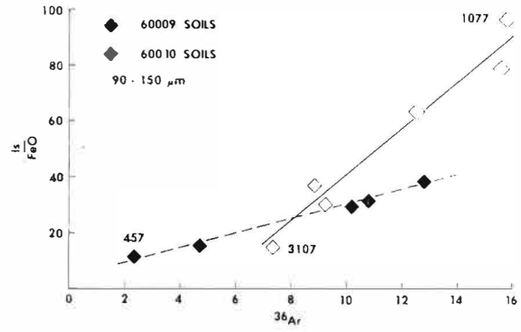

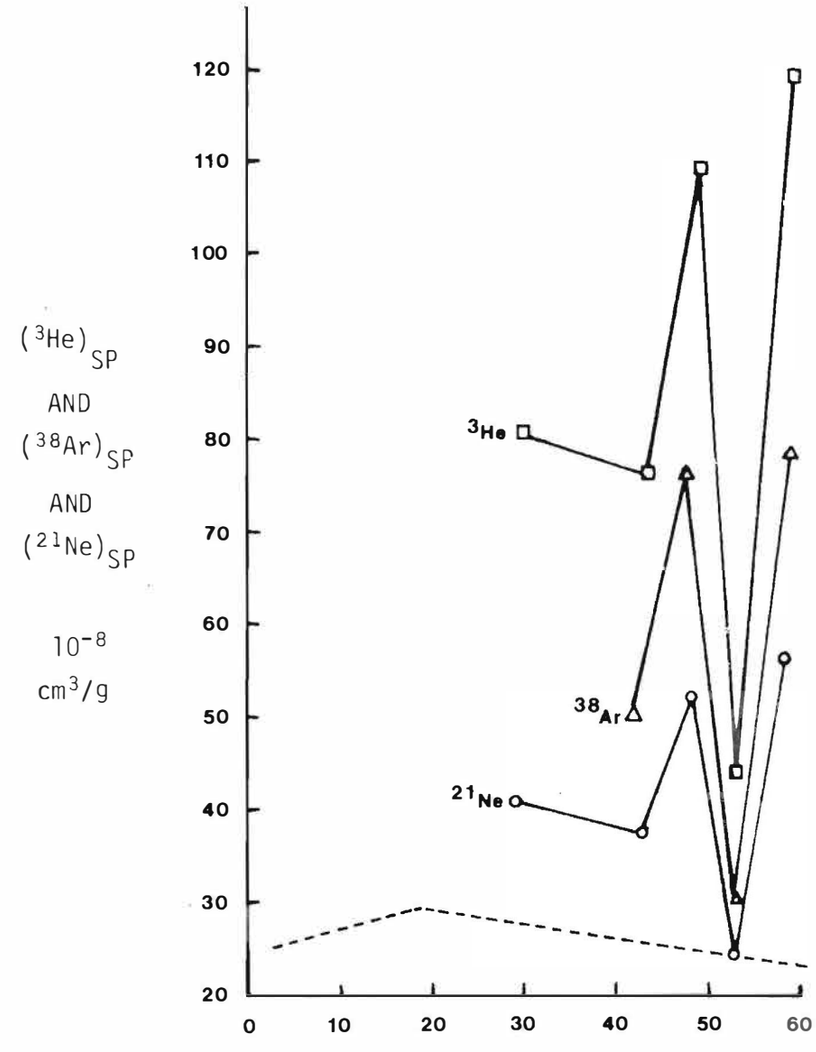

Figure 5.33

Cosmogenic ^{3}He (squares) and ^{38}Ar (triangles) of 60010-60009 drive tube samples as a function of core depth. Cosmogenic ^{21}Ne (circles) and the approximate ^{21}Ne production ratio normalized to 60009,457 (dashed line) as a function of depth.

reflect greater relative abundances of lunar atmosphere ^{40}Ar earlier in lunar history. Because soils associated with the approximately 50 m.y. old North Ray Crater have $^{40}Ar/^{36}Ar$ of about 0.9, Heymann et al. (1975) consider that the relative abundance of lunar atmosphere ^{40}Ar is lower in the recent past. In addition, as a soil is reworked at the lunar surface, the $^{40}Ar/^{36}Ar$ is apparently lowered so that there are very few mature soils with ratios above about 1.5.

5.7.2 Cosmogenic or Volume-Correlated Noble Gases

The volume-correlated noble gas components in lunar soils are produced primarily by cosmic ray irradiation although ^{4}He and ^{40}Ar may be produced by radioactive decay. Cosmogenic ^{3}He ($[^{3}He]_c$) is mainly produced from oxygen; ^{21}Ne is produced in roughly equal amounts from Mg, Al, and Si; over 90% $[^{38}Ar]_c$ is produced from Ca. Ba and La are the two major target elements of cosmogenic ^{126}Xe. Sr, Y, and Zr are the major target elements of cosmogenic ^{80}Kr. Although abundances of these source elements are not known for these core samples, the measured $^{80}Kr/^{126}Xe$ varies by only a factor of about 2 even though the $[^{126}Xe]_c$ varies by a factor of about 11, indicating that $[^{80}Kr]_c$ and $[^{126}Xe]_c$ are strongly correlated. In general, the concentrations of the cosmogenic gases ^{3}He, ^{21}Ne, ^{38}Ar, and ^{80}Kr vary by a factor of about 2 to 3 and are strongly correlated (Figure 5.33). Cosmogenic ^{3}He, ^{21}Ne, and ^{38}Ar data are plotted as a function of depth in Figure 5.33. The dotted line is the approximate shape of the ^{21}Ne production rate as a function of depth, after Reedy and Arnold (1972) and Wright et al. (1973) normalized to 60009,457, the least mature 60009 soil. The model line indicates where the data would fall if the soil column had been deposited suddenly without a previous irradiation history, or with soil of all equal amounts of pre-irradiation. It appears obvious from this that the soils received large and variable pre-irradiation before deposition in their present order.

Figure 5.34 illustrates by plotting cosmogenic ^{21}Ne versus maturity index I_s/FeO that, like the solar-wind-implanted surface-correlated gases, the cosmogenic gases correlate with soil maturity. This contrasts sharply with typical Apollo 16 surface soils, which show no such correlation. The correlation places a constraint on the predeposition irradiation conditions of the soils. Like McKay et al. (1976, 1977) and Blanchard et al. (1976), Bogard and Hirsch (1976) favor a mixing of at least two different components to explain the interbedded stratigraphy. Bogard and Hirsch (1977) found an inverse correlation between the near-surface I_s/FeO data and cosmogenic gases $^{3}He/^{38}Ar$ and $^{21}Ne/^{38}Ar$ and attributed the loss of ^{3}He and ^{21}Ne to micrometeorite reworking at and near the lunar surface.

A maximum time of deposition for most of the soil column is set by the exposure age of a plagioclase separate

Figure 5.34. Relationship of FMR data and cosmogenic ^{21}Ne contents for 60009 soils (solid circles), and several additional Apollo 16 soils (squares). All I_s/FeO data are from Morris (1976) and McKay et al. (1976). Cosmogenic ^{21}Ne data are from this work, Bogard and Hirsch (1975), Heymann et al. (1975), and Hintenberger and Weber (1973).

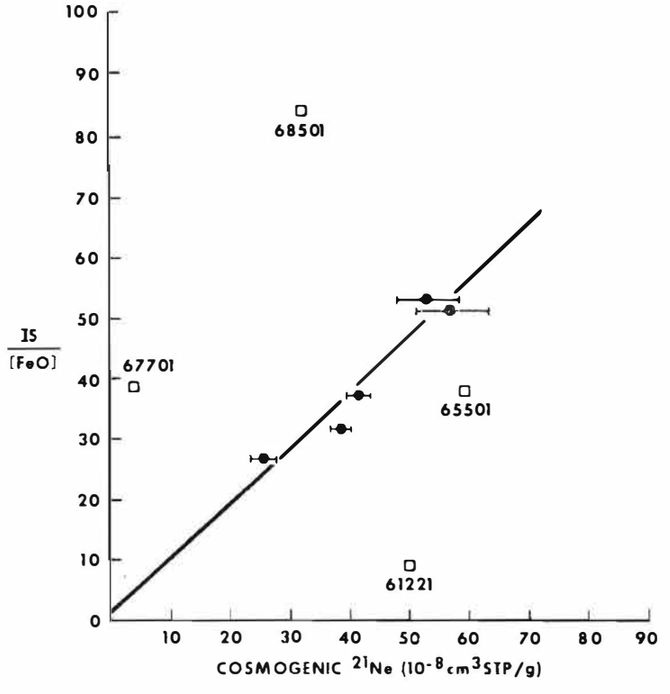

from 60009,457, which is from the coarse-grained, plagioclase-rich layer at 53 cm. The ^{38}Ar exposure age determined by Bogard and Hirsch (1976) for the plagioclase is 125 m.y. They conclude, based on this and previous evidence, that the core (at least to the 53 cm depth) was deposited by one event or sequence of closely spaced events approximately 125 m.y. ago; since then, the core was gardened to a depth of about 12.5 cm. Other investigators interpret the soil column as having been deposited in more discrete layers, as will be seen in the next section on particle track studies.

5.8 NUCLEAR PARTICLE TRACK STUDIES

There are essentially two main sources of energetic nuclear particles that create tracks in rocks and minerals on the lunar surface: low energy iron particles from solar flares, which penetrate on the order of a few millimeters and galactic cosmic ray iron-group particles, which penetrate up to about 20 centimeters. Grains with track densities greater or equal to 10^9 cm^{-2} have had significant exposure at the immediate lunar surface. Grains that have spent their entire history buried approximately 1 cm or greater beneath the surface can acquire only tracks from galactic cosmic rays; grains having track densities approximately 10^9 or less are in this class. A soil with most grains registering track densities greater than 10^9 cm^{-2} is considered mature; a soil with most grains registering track densities less than 10^9 cm^{-2} is considered immature; a more spreadout or transitional distribution of track densities indicates a submature soil that has undergone reworking (Bibring et al., 1975); and finally, a bimodal distribution is interpreted as a soil which has been mixed and contains both a mature and immature component (Blanford et al., 1979).

If un-irradiated grains are introduced into a soil, which then remains undisturbed at some depth below the lunar surface, the new grains will acquire tracks that follow the track production curve, or are related to it. If it was directly related to the absolute track production profile, the maximum exposure age for the soil layer could be determined (Crozaz et al., 1970). Minimum density grains connected by a simple curve would yield a track production curve with depth, or a track production profile. According to Blanford (1979), the relation to a Monte Carlo-produced production profile might yield a truer estimate of in situ residence time.

Track data have been collected from soil aliquots (Crozaz and Dust, 1977; Goswami et al., 1976; Blanford et al., 1977) and from continuous thick sections of the encapsulated soil column (Blanford et al., 1979). Appendix 10 presents the raw data of Crozaz and Dust (1977) as reproduced by Stew Nagle. Each point simply represents one [feldspar] grain with a particular track density (# of tracks/cm^2). Included in this diagram is a list of all of the sample numbers allocated for track studies. To the right of the raw data are two sets of track density histograms which compares the results of Blanford et al. (1977), left, with the results of Crozaz and Dust (1977), right. For this comparison, the Crozaz and Dust (1977) petrographic microscope data in Appendix 10 has been multiplied by two to make them comparable to the SEM-collected data (Blanford et al., 1977). The samples studied by Blanford et al. (1977) are the same as those studied by McKay et al. (1976, 1977) and Bogard and Hirsch (1976,

1977). The top three samples studied by Blanford et al. (1977) yield unimodal track density distributions characterized by high track densities (=mature soils), but all their remaining lower samples in the soil column yield bimodal distributions marked by a mode of high track densities and a mode with low track densities (=mixed soils). The correspondence with track density frequency/histograms of Crozaz and Dust (1977) is only fair. Blanford et al. (1979) attribute the differences to a bias against high track density grains in the data of Crozaz and Dust (1977) because the latter deliberately picked the clear or transparent plagioclase grains, thus avoiding brecciated (old, more irradiated) grains. (In addition, McKay et al., 1976, 1977 deduces the mature component is more mafic than the immature component). Both groups of minimum density grain data are in good agreement (Figure 5.35). Crozaz and Dust (1977) draw conclusions based on trends of the minimum track density grains, so the differences in high track density grain data are not reflected in their interpretations of core history. Goswami et al. (1976) only analyzed two "lithologies" in the 60009 soil column, but their results are in good agreement with Blanford et al. (1977) and Crozaz and Dust (1977).

Blanford et al. (1977) found such an excellent correlation between maturity index I_s/FeO and abundance of high track density grains that they consider the graph in Figure 5.36 depicts the mixing line and degree of mixing between a mature and immature component. They also note that the track density distributions for the three highest 60010 samples are essentially the same, and suggest that like agglutinates (Morris, 1976) the high density track grains saturate in mature soils before I_s/FeO does. Blanford et al. (1977) make an important point that for short-lived surfaces, I_s/FeO may not be a sensitive enough indicator, where the minimum density track grain distributions may be.

A very thorough track study, which provides excellent coverage through the entire soil column, is reported in Blanford et al. (1979), based on measurements made on thick continuous sections. Samples were taken at 1.2 cm intervals, the exceptions being where large rocks interfered, or the data of Crozaz and Dust (1977) were either absent or particularly interesting. (It is important to note that samples studied by Crozaz and Dust (1977) were from 2.5 cm across the diameter of the core from the encapsulated samples). The sampling area was a 1 mm wide swath across the thick section. Of 30 grains counted at each location, 1/3 were in the middle, and 1/3 were on each side. Feldspar grains (monomineralic and polymineralic) in the 50-175 μm size range were randomly selected.

Figure 5.35 summarizes the minimum density grain data results of both Blanford et al. (1979), derived from their continuous thin section work, and the same data from Crozaz

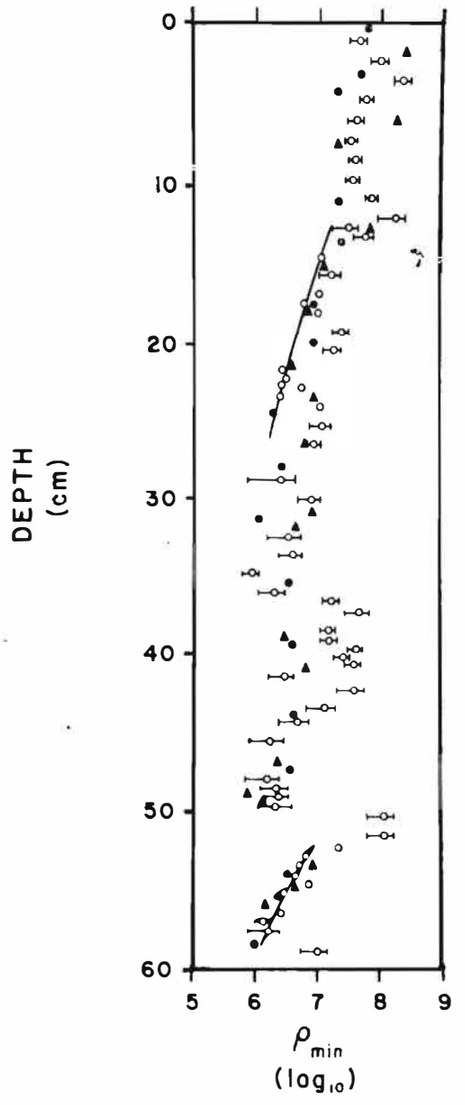

Figure 5.35. Depth in 60009/10 plotted against minimum density grains. Closed circles and triangles refer to measurements in plagioclase made by Crozaz and Dust (1977), and open circles are those reported here. The curves represent the track production profile of Blanford et al. (1975) for 2.5 x 10^8 y near the top and 9 x 10^6 y near the bottom. Crozaz and Dust (1977) measurements have been increased by a factor of two so that their optical measurements are normalized to our scanning electron micrograph measurements (cf. Crozaz et al., 1971), from Blanford et al. (1979).

and Dust (1977), derived from soil aliquot studies. What is interesting about these two papers is that although the data are relatively comparable, the interpretations are at variance. The differences can be attributed to one of three causes: semantics, as is probably the case for the upper 12 centimeters: lack of equivalent samples, as, for instance, occurs around the large broken rock fragment at about 42 centimeters; or quite simply different interpretations of the same data profiles, each with merit. A summary of the results, starting from the top, follows. At the top of the 60010 soil column, samples studied by Blanford et al. (1979) and Crozaz and Dust (1977) displayed similar trends and show a high abundance of track-rich grains, a spread in modality and a high track minimum. The highest track density and track minimum occurs between 2 and

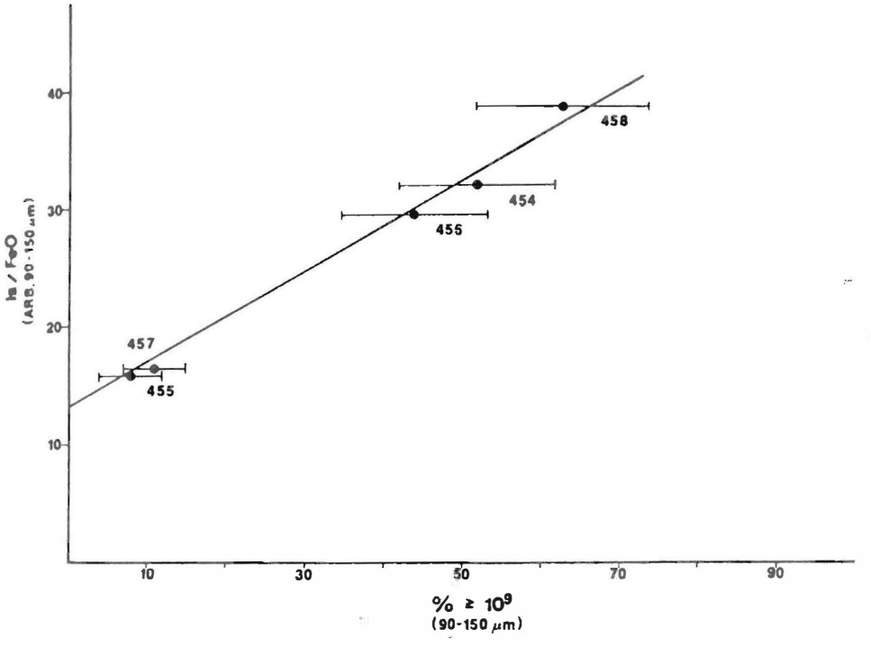

Figure 5.36. Normalized ferromagnetic resonance intensity in arbitrary units (McKay et al., 1976) versus percent grains with particle track densities $>10^9$ cm^{-2} both in the 90-150 μm sieve fraction for samples from drive tube 60009, from Blanford et al. (1977). Note that these are the same samples from 60009 as studied by McKay et al. (1976, 1977) and Bogard and Hirsch (1976, 1977).

3 cm. Both investigators correlate this with the ^{26}Al data of Fruchter et al. (1977) showing substantial mixing (=a local "recent" small cratering event) at 2 to 3 cm. It also correlates with the ^{53}Mn evidence of Nishiizumi et al. (1979).

Blanford et al. (1979) interpret a "reworking zone" in the top 12-13 cm of the soil column, which by their definition would include many small increments and some larger, as well as some small excavations. (They do not see 12 centimeters of continous accretion as probable). Crozaz and Dust (1977) interpret the interval from 11.5 cm up to have been accumulated in thin increments (accretion only). Between 12 and about 22 cm, the two groups obtained very similar results: a bimodal profile in which the minimum density increases towards the surface: Blanford et al. (1979) see one track production profile; Crozaz et al. (1977) see two. (Remember there is about a 2.5 cm lateral distance between the two sets of samples). Possible displacement of profiles may occur in the 22 to 27 cm interval as well; rock sample 60010,3016 (approximately 3 cm in diameter) was removed during the third dissection pass. The evidence that there may have been some distortion because of it comes from the fact that Blanford et al. (1979) found a bimodal grading to a unimodal high track density grain maximum going from 22 to 24 cm; the same profile was found by Crozaz and Dust (1977) between 25 and 27 cm. In the dark, fine-grained soil between 27 and 31 cm, track patterns discerned by the two groups were virtually identical: relatively invariant bimodal frequency histograms with one mode at 10^7 and another at $>10^9$ tracks/cm^2. Between 32 and 38 cm, track patterns are different probably largely because Crozaz and Dust (1977) have fewer data points than Blanford et al. (1979). Track abundances from light-colored soil in clasts are similar to each other (Crozaz and Dust, 1977) and comparable to the lower mode of the bimodal track frequencies of the bulk soil (Blanford et al., 1979). At 38 cm, just above a distinctive light layer, the lower mode is virtually absent (Blanford et al., 1979). Between 38 and 43 cm, data of Blanford et al. (1979) and Crozaz and Dust (1977) are not comparable because of the sampling disturbance caused by rock 60009,2069 discussed in Section 4.2.3. However, the data of Crozaz and Dust (1977) is comparable to the data of Goswami et al. (1976), and both sample sets came from the same "tilted" white soil layer. In the lower (60009) part of the soil column, bimodal distribtuions predominate. Blanford et al. (1979) see strong evidence for one track production profile, or buried surface, between about 52 and 58 cm (Figure 5.35). Crozaz and Dust (1977) see evidence for at least three buried surfaces or cycles of deposition in the lower soil column. These differences in interpretation are largely related to different coverage through the soil column. Blanford et al., (1979) presents an extremely thorough coverage: if the

data pointed to a trend, an intermediate level would be studied to check if that data would be consistent with the trend. In some cases, it is simply a matter of different interpreations. Crozaz and Dust (1977) interpret increasing upward low density grain gradient trends as track production profiles (=buried surfaces). Blanford et al. (1979) argue that it is not enough simply to have a trend, the curve the trend defines should have the shape of a track production profile and there should be no spurious data points within the trend. Figure 5.37 compares the results of Blanford et al. (1979) with the FMR data (Morris and Gose, 1976) and noble gas data (Bogard and Hirsch, 1977), each of which display similar trends.

5.9 PHYSICAL PROPERTIES

5.9.1 Secondary Electron Emission

The secondary electron emission characteristics of four soils from the lower half of the 60009/60010 soil column were measured by Gold et al. (1979) in an effort to understand the effects of ultra-violet photons and of solar wind electron bombardment on the charge distribution and electrostatic potential on the lunar surface. (Four samples from core 15005 were also studied). Previous studies of Gold and Williams (1973) had shown that under electron bombardment a homogeneous insulating powder moves because of differential charging of grains, a heterogeneous powder does not, and there is a tendency for two different powders not to mix, rather one flows over the other, retaining a sharp front. In this work, each soil sample was heated and outgassed in an Auger spectrometer before the measurements were made. The spectrometer was operated in a nonstandard manner in order to bombard the sample with primary electrons and to monitor the current due to elastically backscattered electrons as a function of the potential difference between the source and the grounded metal surfaces of the instrument. The "crossover voltage", at which effectively all the incident electrons are backscattered by surface charging effects, was measured as a function of beam current and of location on the soil sample. The "crossover voltage" varied from point to point on a sample, but the variation with beam current was roughly consistent among the points on any one sample. The samples exhibited distinct, parallel trends in voltage as a function of beam current. The investigators concluded that observed differences between soils was consistent with the hypothesis of soil layering influenced by electrostatic forces. However, the reason for the differences among the soils, each of which is a mixture of mineralogies, is not well understood.

Figure 5.37

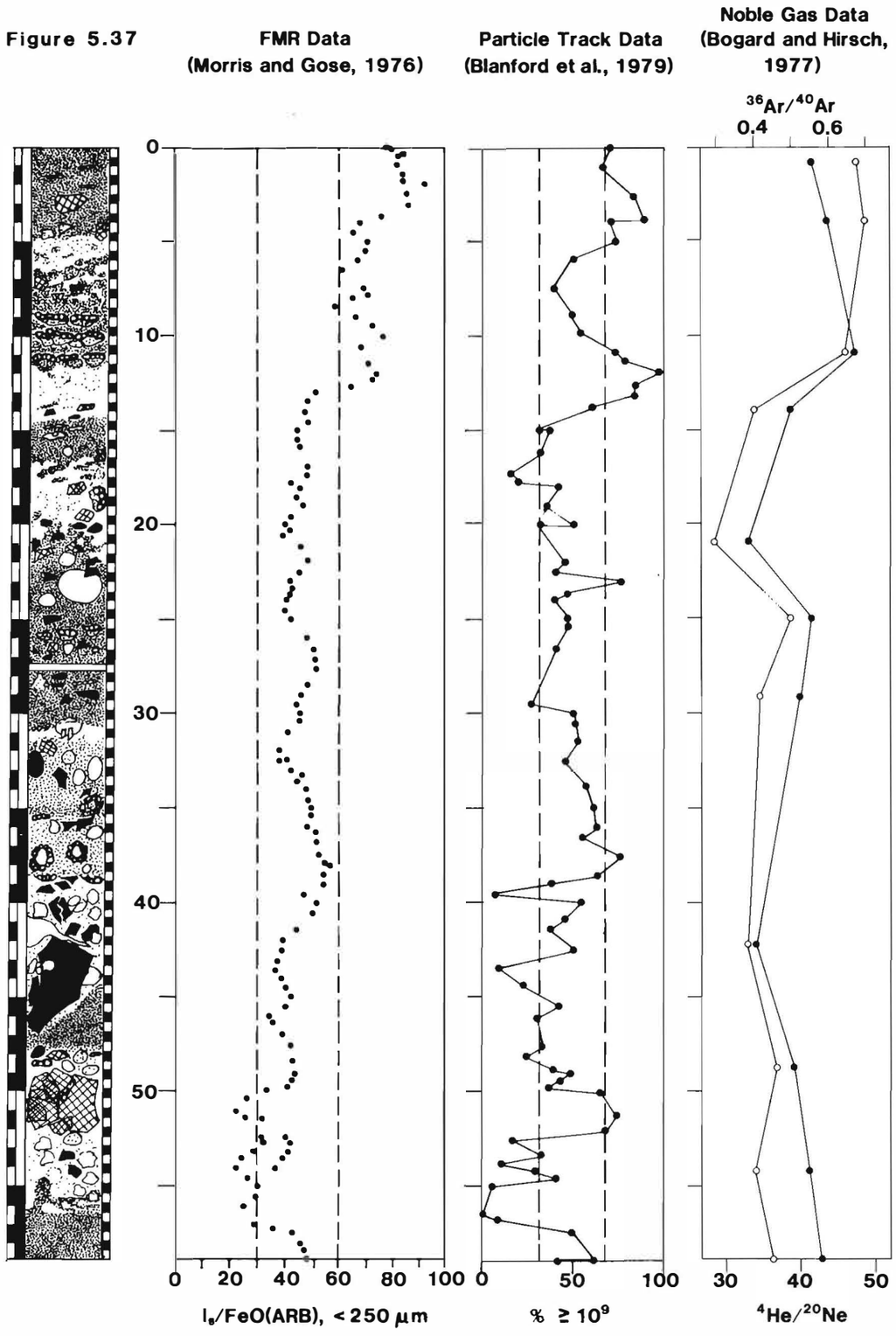
FMR Data
(Morris and Gose, 1976)
Particle Track Data
(Blanford et al., 1979)
Noble Gas Data
(Bogard and Hirsch, 1977)
$^{36}Ar/^{40}Ar$
0.4
0.6
0
10
20
30
40
50
0 20 40 60 80 100
$I_s/FeO(ARB)$, < 250 μm
0 50 100
% ≥ 10^9
30 40 50
$^4He/^{20}Ne$

5.9.2 Thermoluminescence

The low temperature thermoluminescence (TL) has been measured on samples from a number of soil columns including two samples from 60010 (Plachy et al., 1977). They found large scatter in the natural TL values, even after normalization, because, when measured, the TL properties were found to vary greatly from one individual grain to another. Measurements were then made on very fine-grained fractions (about 1 to 10 μm), which permitted averaging over a much larger number of grains and gave good reproducibilities (±2%). Unfortunately, the equilibrium TL values even for the fine-grained samples show large scatter as a function of depth, apparently related to physical, chemical, and/or mineralogical variations with depth. Therefore, the goal of obtaining a temperature gradient from which the outward heat flow could be calculated, was not possible (Plachy et al., 1977) because the scatter in the data essentially obliterates the gradual variation with depth (except for near the surface from the attenuation of the diurnal heat wave).

5.10 MISCELLANEOUS

This section includes several diverse studies that involved samples from 60009/60010. The objectives of these studies were not necessarily concerned with understanding the origin or history of the soil column.

5.10.1 Surface Carbon

Direct measurement of surface carbon concentrations for lunar soil breccias, including five from the 60009/60010 soil column, are reported in Filleux et al. (1977, 1978). Carbon in lunar soils has been attributed to solar wind implantation, impact vaporization of carbonaceous meteorites and subsequent condensation, and early outgassing of the moon. Knowledge of the surface vs. volume distributions of C and $^{13}C/^{12}C$ is necessary to understand the sources and sinks of C to the regolith (as opposed to bulk values). Filleux et al. (1977, 1978) made direct measurements of surface carbon concentrations by measuring the protons produced by the reaction of 1.07 MeV deuterons with ^{12}C. The measured proton energy spectrum can be related to the depth distribution of C, with lower energy protons associated with greater depths. Their 1978 paper presents the more refined results because of better background-corrected spectra and a more accurate evaluation of the effects of surface roughness on depth resolution.

Figure 5.38 is a graphical summary of their measured surface and volume C concentrations for the soil breccias (four) from 60010 and for the glass surface of the fragment from 60009. The latter contains similar surface C compared with the 60010 breccias (see also Figure 5.39), but its volume - correlated C component is negligible. Filleux et al. (1978) suggest the limited range of surface C concentrations for a wide range of volume C may mean the former represents a steady state value, and if so that the time scale to achieve this is short compared with the time scale to form volume-correlated C. They also consider their surface C concentrations to be upper limits to the amount of directly-implanted solar wind carbon, and that this is an important source of C in the lunar soil.

5.10.2 Small Particle Studies

Gibbons and Horz (1976) report on the microchemistry of some individual agglutinates from soil 60009,458.

Kempa and Papike (1979) compare the chemistry and petrography of the >20 and <20 μm soil fractions from three intervals in the core.

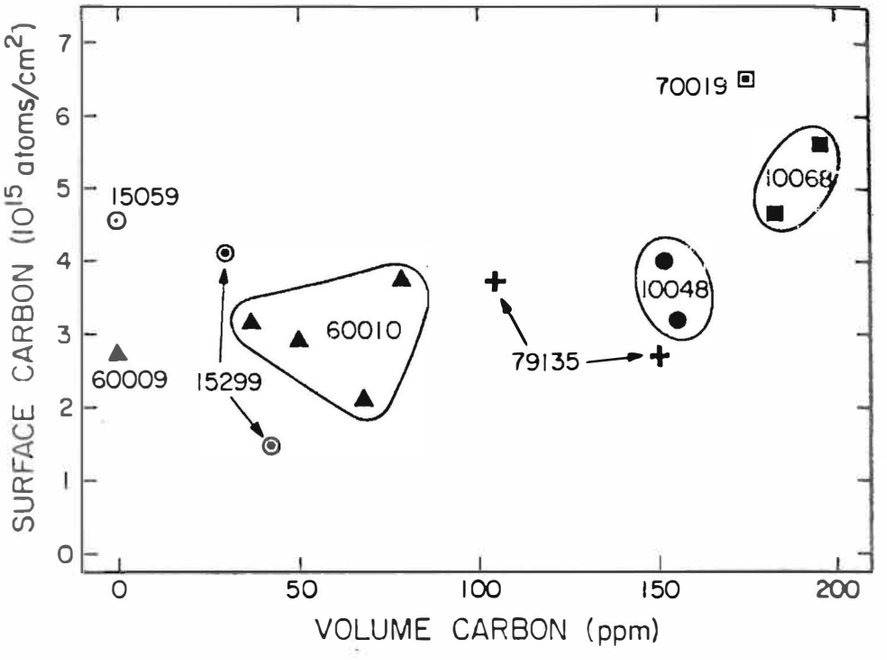

Figure 5.38. The measured surface and volume concentrations for carbon for each sample are compared. It is clear that there is no strong correlation between surface concentration and volume concentration for these samples.

Warren and Wasson (1980) report the chemistry of 4.3 g fragment 60010,3096.

5.10.3 Geological Processes

Heymann (1978) discusses the significance and possible sources of the light and dark soils at the Apollo 16 site.

Nagle et al. (1976) presents a stratigraphic thumbnail sketch of the 60009/60010 soil column, and suggest that three large craters, Gator (about 1 km diameter), Palmetto (about 1 km diameter), and Spook (about .5 km diameter), which should have penetrated to bedrock, lie approximately 1 crater diameter from the sampling site and could have contributed material to this soil column. Nagle (1977) adds the Eden Valley craters as another source of material (Figure 5.40). They are also the most degraded (=oldest) of the craters within reach of the LM/ALSEP station.

Nagle (1978) reports his observations of large (>1 mm) agglutinates from the dissection of the 60009/60010 soil column. Figure 5.41 summarizes his data. The agglutinate particles have glassy top sides and are soil-coated or have soil breccias underneath. The particles are considered

Figure 5.39. Measured surface and volume carbon concentrations.

Sample	Surface C concentration in 10^{15}/cm²		F-dose in 10^{16}/cm²	Volume C concentration (ppm)(e)
	Before sputtering	After sputtering		
60009,2066	3.7 ± 0.4(a)	2.8 ± 0.3	3.0	≤10
60010,1040	5.7 ± 0.5	2.1 ± 0.3	5.5	68 ± 22
60010,1042	3.4 ± 0.3	3.2 ± 0.3	3.0	36 ± 5
60010,1044	6.0 ± 0.5	2.9 ± 0.5	4.0	50 ± 14
60010,1060	3.8 ± 0.3	n.m.	—	78 ± 22
70019,17F	15 ± 1.3	6.5 ± 0.5	3.0	176 ± 30
70019,17F3	19 ± 1.6	n.m.	—	165 ± 30
70019,17B	19 ± 1.6	7.8 ± 0.7	3.0	158 ± 30,535(f)
10048,23A-2	8.7 ± 0.9	4.0 ± 0.4	1.8	151 ± 21
10048,23A-3	6.7 ± 0.7	3.1 ± 0.4	2.5	155 ± 25
10068,23A-1	9.7 ± 1.0	4.8 ± 0.4	6.0	181 ± 28
10068,23A-2	10.8 ± 1.0	5.6 ± 0.5	2.5	194 ± 16
15059,28	4.2 ± 0.4(b)	4.6 ± 0.4(b)	3.0	≤10
15299,191A	5.9 ± 0.5	4.1 ± 0.4	2.8	30 ± 9
15299,191B	3.9 ± 0.4	1.5 ± 0.2	3.5	42 ± 4
79135,59A	7.2 ± 0.6	3.7 ± 0.4	3.2	105 ± 16
79135,59B	5.7 ± 0.5	2.7 ± 0.3	3.0	149 ± 12
65315,7	2.5 ± 0.6(d)	≤0.1	1.5	≤12
terrestr. quartz	1.6 ± 0.2(c)	≤0.4	3.0	0
terrestr. quartz	1.2 ± 0.2(c)	≤0.5	1.0	0
terrestr. quartz	3.0 ± 0.3(c)	n.m.	—	0

(a)glass surface; approximately 50% dust covered.
(b)glass surface of unpitted lunar bottom.
(c)before handling: 0.6-1.0 × 10^{15}/cm².
(d)interior surface of unexposed anorthosite.
(e)errors are standard deviation of all measurements, both before and after sputtering.
(f)after sputtering.

authigenic (formed in place) if the glassy-side is clean of adhering dust and was up (facing the direction of the lunar surface). Zones of these authigenic agglutinates are interpreted to be buried surfaces by Nagle (1978), and these zones correspond in some instances, with the track studies and interpretations of Crozaz and Dust (1977). Arguments against the above interpretations are in the track data of Blanford et al. (1979), which does not reflect all the same "buried surface" zones, and the FMR data of Morris and Gose (1976), which do not reflect evidence of numerous buried surfaces either. Petrographic and track studies need to be performed on the coarse-grained agglutinates from the soil column to resolve these differences and understand the significance of these particles. All of the investigators who had been allocated samples (directly) from the 60009/60010 core to date are listed in Figure 5.42.

Figure 5.40 is after Nagle (1977) and shows craters which may have contributed material to the LM/ALSEP site. The dotted and dashed lines around the various craters indicate the one crater diameter distance, which is a reasonable estimate for the extent of ejecta from each respective crater. At the bottom of the figure, these craters are listed in increasing age, based on their state of relative degradation and crater counts compared with crater counts in North Ray Crater (Nagle, personal communication).

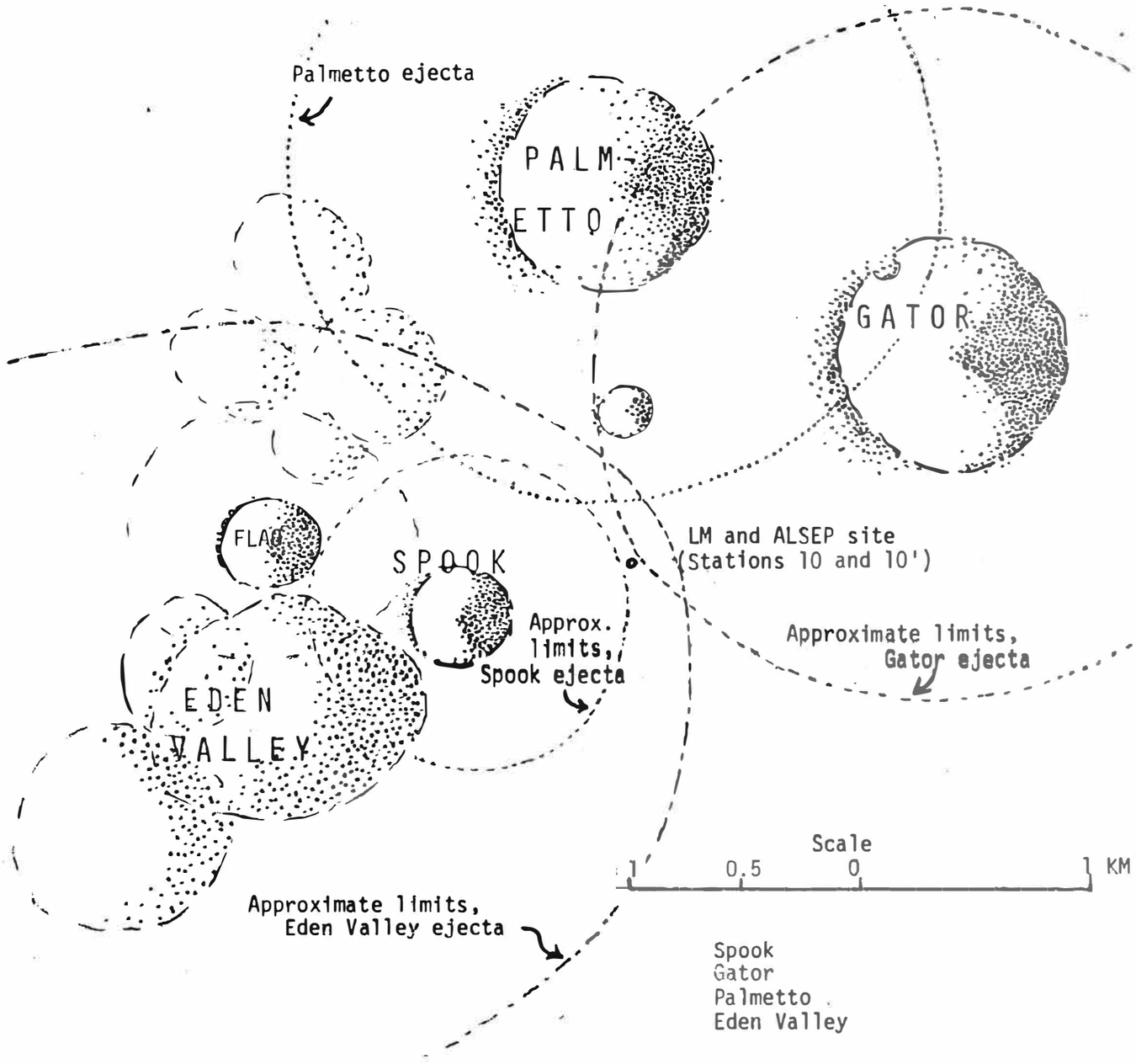

Figure 5.41 presents the abundance and distribution of oriented agglutinates ≥1 mm through the soil column. The calculated exposure time is based on an accumulation rate of 3.5%/my (Nagle, 1973).

60010

INTERVAL	DISSECTION 1 Sample No.	Aggl. No.	Aggl. Diameter	DISSECTION 3 Sample No.	Aggl. No.	Aggl. Diameter	DISSECTION 4 Sample No.	Aggl. No.	Aggl. Diameter	Agglutinate area (cm²)	Percent of Coverage	Calculated Exposure Time (m.y.)
0.5-0.0	178-9	Calculated on basis of entire core										7.6
1.0-0.5	176-7	5	1.5 mm	2105-6	2	2.5 mm	3105-6	7	2.5 mm	0.68	8.2	2.3
1.5-1.0	174-5	2	1 mm	2103-4	2	2 mm	3103-4	6	2 mm	0.34	4.1	1.2
2.0-1.5	172-3	2	1 mm	2101-2	0		3101-2	6	2 mm	0.26	3.1	0.9
2.5-2.0	170-1	2	1 mm	2099-0	2	1.5 mm	3099-0	4	1.5 mm	0.16	1.9	0.5
3.0-2.5	168-9	9	2.5 mm	2097-8	2	2 mm	3097-8	2	1.5 mm	0.68	8.2	2.3
3.5-3.0	165-7	2	1.5 mm	2095-6	2	2 mm	3095-6	3	1.5 mm	0.19	2.3	0.6
4.0-3.5	162-4	5	1.5 mm	2093-4	4	2.5 mm	3093-4	5	2.5 mm	0.67	8.0	2.3
4.5-4.0	160-1	6	1.5 mm	2091-2	0		3091-2	1	2 mm	0.15	1.8	0.5
5.0-4.5	158-9	1	1 mm	2089-0	2	2 mm	3089-0	2	2 mm	0.17	2.1	0.6
5.5-5.0	156-7	5		2087-8	2	2 mm	3087-8	9	2 mm	0.80	9.6	2.7
6.0-5.5	154-5	4	1.5 mm	2085-6	3	1.5 mm	3085-6	1	1.5 mm	0.17	2.1	0.6
6.5-6.0	152-3	5	1.5 mm	2083-4	4	2.5 mm	3083-4	4	1.5 mm	0.45	5.4	1.5
7.0-6.5	150-1	2	2 mm	2081-2	2	2 mm	3081-2	2	1.5 mm	0.20	2.4	0.7
7.5-7.0	148-9	1	1 mm	2079-0	0		3079-0	6	1.5 mm	0.15	1.8	0.5
8.0-7.5	145-7	5	2.5 mm	2077-8	0		3077-8	0		0.31	3.7	1.0
8.5-8.0	142-4	4	2 mm	2075-6	3	2 mm	3075-6	0		0.28	3.4	1.0
9.0-8.5	139-0	9	2-1 cm 7-2 mm	2073-4	5	2 mm	3073-4	5	1.5 mm	2.59	31.2	8.9
9.5-9.0	136-8	10	1-1.5 cm 9-2&3 mm	2071-2	5	2 mm	3071-2	6	2 mm	3.25	39.2	11.2
10.0-9.5	134-5	12	2-1 cm 10-2&3 mm	2069-0	3	2 mm	3069-0	5	2.5 mm	3.06	36.9	10.5
10.5-0.0	132-3	10	8 cm	2067-8	6	2 mm	3067-8	4	1.5 mm	6.73	81.2	23.2
11.0-11.5	130-1	5	5 mm	2065-6	4	1.5 mm	3065-6	3	2 mm	1.46	17.6	5.0
11.5-11.0	128-9	12	5 mm	2063-4	8	2.5 mm	3067-4	0		3.38	40.7	11.6
12.0-11.5	126-7	0		2061-2	0		3061-2	0				
14.5-4.0	114-5	0		2059-2	3	2.5 mm	3051-2	0		0.19	2.3	
15.0-4.5	112-3	0		2049-0	2	1 mm	3049-0	0		0.02	0.2	
15.5-5.0	110-1	2	2 mm	2047-8	0		3047-8	1	2 mm	0.12	1.4	
16.0-15.5	108-9	0		2045-6	0		3045-6	2	1.5 mm	0.05	0.5	2.3
16.5-6.0	106-7	2		2043-4	0		3043-4	3	1.5 mm	0.09	1.1	
17.0-10.5	104-5	0		2041-2	2	1 mm	3041-2	0		0.02	0.2	
17.5-7.0	102-3	3	1.5 mm	2039-0	0		3039-0	0		0.07	0.8	
18.0-17.5	100-01	5	1.5 mm	2037-8	0		3037-8	0		0.11	1.4	
18.5-8.0	98-9	1	1 mm	2035-6	0		3035-6	0		0.02	0.2	
19.0-18.5	95-97	2	1.5 mm	2033-4	0		3033-4	4	2 mm	2.41	29.1	8.3
23.0-22.5	74-5	1	2.5 mm	2014-5	0		3014-5	0		0.06	0.8	
23.5-3.0	72-3	5	1.5 mm	2013-4	0		3012-3	3	1.5 mm	0.18	2.2	
24.0-3.5	70-1	1	1 mm	2011-2	0		3010-1	1	1.5 mm	0.32	0.4	
24.5-4.0	68-9	1	1 mm	2008-0	6	2 mm	3008-9	3	2.5 mm	0.44	5.2	1.5
25.5-5.0	66-7	3	1 mm	2006-7	2	1 mm	3006-7	3	3 mm	0.31	3.7	
26.0-5.5	64-5	0		2004-5	0		3004-5	3	1.5 mm	0.07	0.8	
26.6-6.0	62-3	2	1.5 mm	2002-3	3	5 mm	3002-3	1	1.5 mm	0.25	3.0	
27.3-6.6	60-1	4	2.5 mm	2000-1			3000-1	8	1.5 mm	0.57	6.8	

60009

INTERVAL	DISSECTION 1 Sample No.	Aggl. No.	Aggl. Diameter	DISSECTION 2 Sample No.	Aggl. No.	Aggl. Diameter	DISSECTION 3 Sample No.	Aggl. No.	Aggl. Diameter	Agglutinate area (cm²)	Percent of Coverage	Calculated Exposure Time (m.y.)
1.0-0.5	41-2	1	1 mm	1000-1	1	2 mm	3000-1	6	2 mm	0.32	4.6	
1.5-1.0	42-3	0		1002-3	1	9 mm	3002-3	6	2 mm	1.05	15.2	5.6
4.5-4.0	57-8	4	3 mm	1014-7	3	2 mm	3017-8	7	1.5 mm	0.48	6.9	
5.0-4.5	62-3	3	2 mm	1019-0	1	2 mm	3019-0	0		0.16	2.3	
5.5-5.0	64-5	1	1 mm	1021-2	1	3 mm	3021-2	1	1.5 mm	0.12	1.7	4.9
6.0-5.5	68-9	1	2 mm	1024-5	1	2.5 mm	3023-4	4	2.5 mm	0.24	3.5	
6.5-6.0	70-1	2	2.5 mm	1026-7	1	1.5 cm	3025-6	2	2 mm	0.20	2.9	
8.5-8.0	80	0		1037-8	5	2.5 mm	3034-5	0		0.31	4.5	
9.0-8.5	82	3	2.5 mm	1039-0	1	1 mm	3036-7	8	2.5 mm	0.70	10.1	4.2
11.0-10.5	97-8	1	1 mm	1048-9	5	2 mm	3046-7	0				
11.5-11.0	100-1	2	1.5 mm	1052-3	5	2.5 mm	3048-9	2	1 mm	0.58	8.4	
12.0-11.5	104-5	3	2 mm	1054-5	5	2 mm	3050-1	5	2.5 mm	0.82	11.8	7.1
12.5-12.0	110-2	0		1057-8	2	2 mm	3052-3	4	2 mm	0.24	3.5	
13.0-12.5	113-4	0		1059-0	1	1.5 mm	3054-5	2	2 mm	0.07	1.0	
20.0-19.5	168-9	0		1091-2	1	1.5 mm	3085-6	1	1 mm	0.02	0.3	
20.5-20.0	170-1	0		1093-4	0		3087-8	0		0		5.2
21.0-20.5	173-3	0		1095-6	3	1.5 mm	3089-0	3	1.5 mm	0.135	1.9	
21.5-21.0	174-5	6	3 mm	1097-8	6	2 mm	3091-2	4	2 mm	1.00	14.5	
22.0-21.5	176	1	2 mm	1099-0	4	1.5 mm	3093-4	0		0.11	1.6	

Figure 5.42. Principal Investigators who have been allocated Core Samples as of Fall, 1981.

60009 -

1. Arnold, J.R.*
2. Banerjee, S.K.*
3. Blanchard, D.P.*
4. Blanford, G.E.*
5. Bogard, D.D.*
6. Clayton, R.N.*
7. Ehmann, W.D.*
8. Gold, T.*
9. Gose, W.A.*
10. Haskin, L.A.*
11. Horz, F.*
12. Housley, R.M.*
13. Maurette, M.*
14. McKay, D.S.*
15. Papike, J.J.*
16. Perkins, R.W.*
17. Price, P.B.*
18. Signer, P.*
19. Tatsumoto, M.*
20. Tombrello, T.A.*
21. Walker, R.M.*
22. Wasserburg, G.J.*

60010* -

1. Keil, K.
2. Wasson, J.T.

REFERENCES

Adams J.B., Charette M.P., and Rhodes J.M. (1975) Chemical fractionation of the lunar regolith by impact melting. Science 190, 380-381.

AFGIT (Apollo Field Geology Investigation Team) (1972) Documentation and environment of the Apollo 16 samples: A preliminary report. Interagency Report: Astrogeology 51. p. 21-22, 229.

AFGIT (1973) Apollo 16 exploration of Descartes: A geologic summary. Science 179, 62-69.

AFGIT Geology of the Apollo 16 area, central lunar highlands (G.E. Ulrich, C.A. Hodges and W.R. Muehlberger, eds.)(1981) U.S. Geol. Survey Open File Report No. 79-1091, 1128 pp. (To be published as U.S. Geol. Survey Prof. Paper No. 1048). In press.

Ali M.Z. and Ehmann W.D. (1976) Chemical characterization of lunar core 60009. Proc. Lunar Sci. Conf. 7th, p. 241-258.

Ali M.Z. and Ehmann W.D. (1977) Chemical characterization of lunar core 60010 (abstract). In Lunar Science VIII, p. 16-18. The Lunar Science Institute, Houston.

Ali M.Z. and Ehmann W.D. (1977) Chemical characterization of lunar core 60010. Proc. Lunar Sci. Conf. 8th, p. 2967-2981.

Ali M.Z., Stroube W.B., James W.D., Jr., and Ehmann W.D. (1976) Compositional studies of impact generated glasses and core sample 60009 (abstract). In Lunar Science VII, p. 10-12. The Lunar Science Institute, Houston.

Andre C.G. and El-Baz F. (1981) Regional chemical setting of the Apollo 16 landing site and the importance of the KANT plateau (abstract). In Workshop on Apollo 16, LPI Tech. Report No. 81-01, p. 33-35.

Arvidson R., Crozaz G., Drozd R.J., Hohenberg C.M., and Morgan C.J. (1975) Cosmic ray exposure ages of features and events at the Apollo landing sites. The Moon 13, p. 259-276.

Bailey N.G. and Ulrich G.E. (1975) Apollo 16 voice transcript. U.S.G.S. Report GD-74-030.

Banerjee S.K., Gingrich D., and Marvin J.A. (1977) Remanent magnetization stratigraphy of lunar cores (abstract). In Lunar Science VIII, p.53-55. The Lunar Science Institute, Houston.

Banerjee S.K., Gingrich D., and Marvin J.A. (1977) Remanent magnetization stratigraphy of lunar cores. Proc. Lunar Sci. Conf. 8th, p. 2953-2965.

Bansal B.M., Church S.E., Gast P.W., Hubbard N.J., Rhodes J.M., and Weismann H. (1972) The chemical composition of soils for the Apollo 16 and Luna 20 sites. Earth Planet. Sci. Lett. 17, 29-35.

Bibring J.P., Borg J., Burlingame A.L., Langevin Y., Maurette M., and Vassent B. (1975) Solar wind and solar flare maturation of the lunar regolith. Proc. Lunar Sci. Conf. 6th, p. 3471-3493.

Blanchard D.P. and Brannon J.C. (1977) Effects on composition of maturation in a well documented, isochemical suite of soils from drive tube 60009/10 (abstract). In Lunar Science VIII, p. 121-123. The Lunar Science Institute, Houston.

Blanchard D.P., Jacobs J.W., and Brannon J.C. (1976) Drive tube 60009: A chemical study of magnetic separates of size fractions from fine strata (abstract). In Lunar Science VII, p. 70-72. The Lunar Science Institute, Houston.

Blanchard D.P., Jacobs, J.W., Brannon J.C., and Brown R.W. (1976) Drive tube 60009: A chemical study of magnetic separates of size fractions from five strata Proc. Lunar Sci. Conf. 7th, p. 281-294.

Blanford G.E. (1980) Track production below reworking zones (abstract). In Lunar and Planetary Science XI, p. 85-87. The Lunar and Planetary Institute, Houston.

Blanford G.E. and Hawkins J.A. (1979) Irradiation stratigraphy in double tube 60009/10 (abstract). In Lunar and Planetary Science X, p. 137-139. The Lunar and Planetary Institute, Houston.

Blanford G.E. and Wood G.C. (1978a) Irradiation stratigraphy in Apollo 16 cores (abstract). In Lunar and Planetary Science IX, p. 106-108. Lunar and Planetary Institute, Houston.

Blanford G.E., Blanford J., and Hawkins J.A. (1979) Irradiation stratigraphy and depositional history of the Apollo 16 double drive tube 60009/10. Proc. Lunar Planet. Sci. Conf. 10th, p. 1333-1349.

Blanford G.E., McKay D.S., and Wood G.C. (1977) Particle track densities in double drive tube 60009 (abstract). In Lunar Science VIII, p. 127-129. The Lunar Science Institute, Houston.

Blanford G.E., McKay D.S., and Wood G.C. (1977) Particle track densities in double drive tube 60009/10. Proc. Lunar Sci. Conf. 8th, p. 3017-3025.

Bogard D.D. and Nyquist L.E. (1973) $^{40}Ar/^{36}Ar$ variations in Apollo 15 and 16 regolith. Proc. Lunar Sci. Conf. 4th, p. 1975-1985.

Bogard D.D., Nyquist L.E., Hirsch W.C., and Moore D.R. (1973) Trapped solar and cosmogenic noble gas abundances in Apollo 15 and 16 deep drill samples. Earth Planet. Sci. Lett. Vol. 21, 52-69.

Bogard D.D. and Hirsch W.C. (1975) Noble gas studies on grain size separates of Apollo 15 and 16 deep drill cores. Proc. Lunar Sci. Conf. 6th, p. 2057-2083.

Bogard D.D. and Hirsch W.C. (1976) Noble gases in 60009 drive tube samples: Trapped gases and irradiation history (abstract). In Lunar Science VII, p. 79-81. The Lunar Science Institute, Houston.

Bogard D.D. and Hirsch W.C. (1976) Noble gases in 60009/10 drive tube samples: Trapped gases and irradiation history. Proc. Lunar Sci. Conf. 7th, p. 259-279.

Bogard D.D. and Hirsch W.C. (1977) Noble gas evidence for the depositional and irradiational history of 60010-60009 core soils. Proc. Lunar Sci. Conf. 8th, p. 2983-2999.

Boynton W.V., Baedecker P.A., Chou C.L., Robin K.L., and Wasson J.T. (1975) Mixing and transport of lunar surface materials: Evidence obtained by the determination of lithophile, siderophile, and volatile elements. Proc. Lunar Sci. Conf. 6th, 2241-2259.

Boynton W.V., Chou C.L., Bild R.W., Baedecker P.A., and Wasson J.T. (1976) Element distributions in size fractions of Apollo 16 soils: Evidence for element mobility during regolith processes. Earth Planet. Sci. Lett. 29, 21-33.

Butler P., Jr. (1972) Apollo 16 Lunar Sample Information Catalog, p. 6, 37, 40, 43-44. MSC-03210, NASA Johnson Space Center, Houston.

Charette M.P. and Adams J.B. (1975) Agglutinates as indicators of soil maturity: The rare gas evidence at Apollo 16. Proc. Lunar Sci. Conf. 6th, p. 2281-2289.

Cirlin E.H., Housley R.M., Goldberg I.B., and Crowe H. (1976) Exposure age stratigraphy studies of lunar core samples by ferromagnetic resonance (abstract). In Lunar Science VII, p. 152-153. The Lunar Science Institute, Houston.

Crozaz G. and Dust S. (1977) Irradiation history of lunar cores and the accumulation of the regolith (abstract). In Lunar Science VIII, p. 215-217. The Lunar Science Institute, Houston.

Crozaz G. and Dust S. (1977) Irradiation history of lunar cores and the development of the regolith. Proc. Lunar Sci. Conf. 8th, p. 3001-3016.

Crozaz G., Haack U., Hair M., Maurette M., Walker R.M., and Woolum D. (1970) Nuclear track studies of ancient solar radiations and dynamic lunar surface processes. Proc. Apollo 11 Lunar Sci. Conf., p. 2051-2080.

Crozaz G. and Morrison D. (1975) Track studies of core 60009. Preliminary Examination Report circulated by Lunar Sample Curator, JSC unpublished.

Delano J.W. (1975) Petrology of the Apollo 16 mare component: Mare Nectaris. Proc. Lunar Sci. Conf. 6th, p. 15-47.

Duke M.B. and Nagle J.S. (1974) Lunar Core Catalog. NASA Publication JSC 09252.

Duke M.B. and Nagle J.S. (1976) Supplement to the Lunar Core Catalog. NASA Publication JSC 09252.

Duke M.B. and Nagle J.S. (1978) Lunar Core Catalog and Supplements, p. 4-5, 17-18, 21, 16-2 to 16-3, 16-8, 16-11 to 16-13, 16-17 to 16-18, 16-58 to 16-85, A60-9 and A60-10. JSC 09252, NASA Johnson Space Center, Houston.

Eberhardt P., Geiss J., Graf H., Grogler N., Krahenbuhl U., Schwaller H., Schwarzmuller J., and Stettler A. (1970) Trapped solar wind noble gases, exposure age and K/Ar-age in Apollo 11 fine material. Proc. Apollo 11 Lunar Sci. Conf., p. 1037-1070.

Ehmann W.D. and Chyi L.L. (1974) Abundances of the group IV B elements, Ti, Zr, and Hf and implications of their ratios in lunar materials. Proc. Lunar Sci. Conf. 5th, p. 1015-1024.

Elston D.P., Boudette E.L., Schafer J.P., Muehlberger W.R., and Sevier J.R. (1972) Apollo 16 field trips. Geotimes 17, 27-30.

Filleux C., Spear R.H., Tombrello T.A., and Burnett D.S. (1978) Direct measurement of surface carbon concentrations for lunar soil breccias. Proc. Lunar Sci. Conf. 9th, p. 1599-1617.

Filleux C., Tombrello T.A., and Burnett D.S. (1977) Direct measurement of surface carbon concentrations (abstract). In Lunar Science VIII, p. 296-298. The Lunar Science Institute, Houston.

Filleux C., Tombrello T.A., and Burnett D.S. (1977) Direct measurement of surface carbon concentrations. Proc. Lunar Sci. Conf. 8th, p. 3755-3772.

Folk R.L. (1968) Petrology of sedimentary rocks. Hemphill's Drawer University Station, Austin, Texas, 170 pp.

Fruchter J.S., Rancitelli L.A., and Perkins R.W. (1976) Recent and long-term mixing of the lunar regolith bases on ^{22}Na and ^{26}Al measurements in Apollo 15, 16, and 17 deep drill stems and drive tubes. Proc. Lunar Sci. Conf. 7th, p. 27-39.

Fruchter J.S., Rancitelli L.A., and Perkins R.W. (1977) Gardening of lunar regolith and distrubances in the upper portion of lunar regolith cores (abstract). In Lunar Science VIII, p. 334-336. The Lunar Science Institute, Houston.

Fruchter J.S., Rancitelli L.A., Laul J.C., and Perkins R.W. (1977) Lunar regolith dynamics based on analysis of the cosmogenic radionuclides ^{22}Na, ^{26}Al, and ^{53}Mn. Proc. Lunar Sci. Conf. 8th, p. 3595-3605.

Gibbons R.V., Horz F., Schaal R.B. (1976) The chemistry of some individual soil agglutinates. Proc. Lunar Sci. Conf. 7th, p. 405-422.

Gold T., Baron R.L., and Bilson E. (1979) Determination of secondary electron emission characteristics of lunar soil samples. Earth Planet. Sci. Lett. 45, 133-140.

Gose W.A. and Morris R.V. (1976) Ferromagnetic resonance and magnetic studies of 60003 and 60009: Compositional and exposure stratigraphy (abstract). In Lunar Science VII, p. 319-321. The Lunar Science Institute, Houston.

Gose W.A. and Morris R.V. (1977) Depositional history of the Apollo 16 deep drill core. Proc. Lunar Sci. Conf. 8th, p. 2909-2928.

Goswami J.N., Braddy D., and Price P.B. (1976) Microstratigraphy of the lunar regolith and compaction ages of lunar and meteoritic breccias (abstract). In Lunar Science VII, p. 328-330. The Lunar Science Institute, Houston.

Goswami J.N., Braddy D., and Price P.B. (1976) Microstratigraphy of the lunar regolith and compaction ages of lunar breccias. Proc. Lunar Sci. Conf. 7th, p. 55-74.

Hawke B.R., Spudis P.D., Head J.W., and McCord T.B. (1981) Remote sensing studies of the Apollo 16--Descartes region. In Workshop on Apollo 16, LPI Tech. Report No. 81-01, pp. 44-46.

Head J.W. and Goetz A.F.H. (1972) Descartes region--evidence for Copernican-age volcanism. J. Geophys. Res. 77, 1368-1374.

Heymann D. (1975) Argon-lead isotopic correlation in samples from lunar maria: Records from the ancient lunar regolith. Earth Planet. Sci. Lett. Vol. 27, 445-448.

Heymann D., Walton J.R., and Jordan L. (1975) Light and dark soils at the Apollo 16 landing site (abs.) In Lunar Science VI, p. 361-363. The Lunar Science Institute, Houston.

Heymann D. (1978) Light and dark soils at Apollo 16 revisited (abstract). In Lunar and Planet. Sci. IX, p. 506-508. Lunar and Planetary Institute, Houston.

Heymann D., Jordan J.L., Walker A., Dziczkaniec M., Ray J., and Palma R. (1978) Inert gas measurements in the Apollo 16 drill core and an evaluation of the stratigraphy and depositional history of this core. Proc. Lunar Planet. Sci. Conf. 9th, p. 1885-1912.

Heymann D., Ray J., Dziczkaniec M., and Palma R. (1978) Mixing of major soil components in the Apollo 16 drill core (abstract). In Lunar and Planetary Science IX, p. 512-514. Lunar and Planetary Institute, Houston.

Heymann D., Ray J., Dziczkaniec M., and Palma R. (1978) Test for buried regolith surfaces in Apollo 16 cores (abstract). In Lunar and Planet. Sci. IX, p. 515-517. Lunar and Planetary Institute, Houston.

Housley R.M., Cirlin E.H., Goldberg I.B., and Crowe H.E. (1976) Ferromagnetic resonance studies of lunar core stratigraphy. Proc. Lunar Sci. Conf. 7th, p. 13-26.

Hu H.N. and Taylor L.A. (1977) Agglutinate formation: Lack of chemical fractionation (abs.) In Lunar Science VIII, p. 463-465. The Lunar Science Institute, Houston.

Hubbard N.J., Rhodes J.M., Gast P.W., Bansal, B.M., Shih C.Y., Wiesmann H., and Nyquist L.E. (1973) Lunar rock types: The role of plagioclase in non-mare and highland rock types. Proc. Lunar Sci. Conf. 4th, p. 1297-1312.

Janghorbani M., Miller M.D., Ma M.S., Chyi L.L., and Ehmann W.D. (1973) Oxygen and other elemental abundance data for Apollo 14, 15, 16 and 17 samples. Proc. Lunar Sci. Conf. 4th, p. 1115-1126.

Laniv A. and Heymann D. (1972) Atmospheric ^{40}Ar in lunar fines. Proc. Lunar Sci. Conf. 3rd, p. 1967-1980.

Mahmood A., Mitchell J.K., and Carrier W.D. III (1974) Grain orientation in lunar soil. Proc. Lunar Sci. Conf. 5th, p. 2347-2354.

McKay D.S. and Heiken G.H. (1973) The South Ray Crater age paradox. Proc. Lunar Sci. Conf. 5th, p. 41-47.

McKay D.S., Dungan M.A., Morris R.V., and Fruland R.M. (1977) Grain size, petrographic, and FMR studies of the double core 60009/10: A study of soil evolution. Proc. Lunar Sci. Conf. 8th, p. 2929-2952.

McKay D.S., Fruland R.M., and Heiken G.H. (1974) Grain size and the evolution of lunar soils. Proc. Lunar Sci. Conf. 5th, p. 887-906.

McKay D.S., Morris R.V., and Dungan M.A. (1976) Comparative studies of grain size separates of 60009 (abstract). In Lunar Science VII, p. 524-526. The Lunar Science Institute, Houston.

McKay D.S., Morris R.V., Dungan M.A., Bogard D.D., and Fruland R.M. (1977) Maturity of soil in drive tube 60009/10 and implications for regolith evolution (abstract). In Lunar Science VIII, p. 646-648. The Lunar Science Institute, Houston.

McKay D.S., Morris R.V., Dungan M.A., Fruland R.M., and Fuhrman R. (1976) Comparative studies of grain size separates of 60009. Proc. Lunar Sci. Conf. 7th, p. 295-313.

Milton D.J. (1968) Geologic map of the Theophilus Quadrangle of the Moon. U.S. Geol. Survey Misc. Geol. Inv. Map I-546 (LAC78).

Milton D.J., and Hodges C.A. (1972) Geologic maps of the Descartes region of the Moon, Apollo 16 premission maps. U.S. Geol. Survey Misc. Geol. Inv. Map I-748 (2 sheets).

Mitchell J.K., Carrier W.D., III, Houston W.N., Scott R.F., Bromwell L.G., Durgunoglu H.T., Hovland H.J., Treadwell D.D., and Costes N.C. (1972) Soil mechanics. Apollo 16 Prelim. Sci. Rep. NASA SP-315, p. 8-1 to 8-29.

Mitchell J.K., Carrier W.D., III, Costes N.C., Houston W.N., and Scott R.F. (1973) Surface soil variability and stratigraphy at the Apollo 16 site (abstract). In Lunar Science IV, p. 525-527. The Lunar Science Institute, Houston.

Mitchell J.K., Carrier W.D., III, Costes N.C., Houston, W.N., Scott R.F. (1973) Surface soil variability and stratigraphy at the Apollo 16 site. Proc. Lunar Sci. Conf. 4th, p. 2437-2445.

Morris R.V. (1976) Surface exposure indices of lunar soils: A comparative FMR study. Proc. Lunar Sci. Conf. 7th, p. 315-335.

Morris R.V., (1977) Origin and evolution of the grain-size dependence of the concentration of fine-grained metal in lunar soils. The maturation of lunar soils to a steady-state stage. Proc. Lunar Sci. Conf. 8th, p. 3719-3747.

Morris R.V. (1978) In situ reworking (gardening of the lunar surface: Evidence from the Apollo cores (abstract). In Lunar and Planetary Science IX, p. 757-759. Lunar and Planetary Institute, Houston.

Morris R.V. (1978) In situ reworking (gardening of the lunar surface: Evidence from the Apollo cores. Proc. Lunar Planet. Sci. Conf. 9th, p. 1801-1811.

Morris R.V. and Gose W.A. (1976) Ferromagnetic resonance and magnetic studies of cores 60009/10 and 60003: Compositional and surface exposure stratigraphy. Proc. Lunar Sci. Conf. 7th, p. 1-11.

Morris R.V. and Gose W.A. (1977) Ferromagnetic resonance and magnetic studies of the Apollo 16 deep drill core: Surface exposure and compositional stratigraphy (abstract). In Lunar Science VIII, p. 688-690. The Lunar Science Institute, Houston.

Muehlberger W.R., Batson R.M., Bondette E.L., Duke C.M., Eggleton R.E., Elston D.P., England A.W., Reeman V.L., Hait M.H., Hall T.A., Head J.W., Hodges C.A., Holt H.E., Jackson E.D., Jordan J.A., Larson K.B., Milton D.J., Reed V.S., Rennilson J.J., Schaber G.G., Schafer J.P., Silver L.T., Stuart-Alexander D., Sutton R.L., Swann G.A., Tyner R.L., Ulrich G.E., Wilshire H.G., Wolfe E.W., and Young J.W. (1972) Preliminary investigation of the Apollo 16 landing site. Apollo 16 Prelim. Sci. Rep. NASA SP-315, p. 6-1 to 6-81.

Muehlberger W.R., Horz F., Sevier J.R., and Ulrich G.E. (1980) Mission objectives for geological exploration of the Apollo 16 landing site. Proc. Conf. Lunar Highlands Crust, p. 1-49.

Munsell Book of Color (1963).

Murrell M.T., Nishiizumi K., and Arnold J.R. (1979) ^{53}Mn profile in 74001/2: Comments on the recent history of the core (abstract). In Lunar and Planet. Science X, p. 881-883. Lunar and Planetary Institute, Houston.

Nagle J.S., (1977) Possible sources of immature soil at the Apollo 16 ALSEP site (abstract). In Lunar Science VIII, p. 709-711. The Lunar Science Institute, Houston.

Nagle J.S. (1978) The authigenic component in lunar cores (abstract). In Lunar and Planet. Science IX, p. 793-795. Lunar and Planetary Institute, Houston.

Nagle J.S. (1979) Drive tube 76001 - continuous accumulation with complications? Proc. Lunar Planet. Sci. Conf. 10th, p. 1385-1399.

Nagle J.S., Duke M.B., Morrison D.A., Blanford G.E., and Crozaz G. (1976) Stratification in drive tubes 60010/60009 (abstract). In Lunar Science VII, p. 599-601. The Lunar Science Institute, Houston.

Nakamura Y. (1981) Geophysical data on structure and tectonics of the Apollo 16 landing site (abstract). In Workshop on Apollo 16, LPI Tech. Report No. 81-01, p. 87-94.

Nishiizumi K., Imamura M., Honda M., Murrell M.T., and Arnold J.R. (1978) A study of gardening in the lunar regolith using ^{53}Mn (abstract). In Lunar and Planet. Science IX, p. 811-813. Lunar and Planetary Institute, Houston.

Nishiizumi K., Imamura M., Kohl C.P., Murrell M.T., Arnold J.R., and Russ G.P., III (1979) The extent of lunar regolith mixing. Earth Planet. Sci. Lett. 44, p. 409-419.

Nishiizumi K., Murrell M.T., Arnold J.R., and Imamura M. (1980) ^{53}Mn measurements in individual rocklet from 60010 and in lunar core 70009 (abstract). In Lunar and Planetary Science XI, p. 818-820. The Lunar and Planetary Institute, Houston.

Papike J.J., Vaniman D.T., Schweitzer E.L., and Baldwin K. (1978) Apollo 16 drive tube 60009/10 Part III: Total major element partitioning among the regolith components or chemical mixing models with petrologic credibility (abstract). In Lunar and Planetary Science IX, p. 862-864. The Lunar and Planetary Institute, Houston.

Pearce G.W., Gose W.A., and Strangway D.W. (1973) Magnetic studies on Apollo 15 and 16 lunar samples. Proc. Lunar Sci. Conf. 4th, p. 3045-3076.

Pepin R.O., Basford J.R., Dragon J.C., Coscio M.R., Jr., and Murthy V.R. (1974) Rare gases and trace elements in Apollo 15 drill core fines: Depositional chronologies and K-Ar ages and production rates of spallation-produced ^{3}He, ^{21}Ne, and ^{36}Ar versus depth. Proc. Lunar Sci. Conf. 5th, p. 2149-2184.

Plachy A.L., Walker R.M., and Zimmerman D.W. (1977) Thermoluminescence and lunar heat flow (abstract). In Lunar Science VIII, p. 779-780. The Lunar Science Institute, Houston.

Reedy R.C. and Arnold J.R. (1972) Interaction of solar and galactic cosmic ray particles with the moon. J. Geophys. Res. Vol 77, 537-555.

Rhodes J.M., Adams J.B., Blanchard D.P., Charette M.P., Rodgers K.V., Jacobs J.W., Brannon J.C., and Haskin L.A. (1975) Chemistry of agglutinate fractions in lunar soils. Proc. Lunar Sci. Conf. 6th, p. 2291-2307.

Rose H.J., Jr., Baedecker P.A., Berman S., Christian R.P., Dwornik E.J., Finkelman R.B., and Schnepee M.M. (1975) Chemical compositions of rocks and soils returned by the Apollo 15, 16, and 17 missions. Proc. Lunar Sci. Conf. 6th, p. 1363-1373.

Signer P., Bauer H., Derksen U., Etique P., Funk H., and Horn P. (1976) Correlations between trapped and spallogenic light noble gases in lunar soils and minerals (abs.) In Lunar Science VII, p. 806-808. The Lunar Science Institute, Houston.

Simon S.B., Papike J.J., and Vaniman D.T. (1978) Apollo 16 drive tube 60009/10. Part I: Modal petrology (abstract). In Lunar and Planetary Science IX, p. 1056-1058. The Lunar and Planetary Institute, Houston.

Simon S.B., Papike J.J., and Vaniman D.T. (1978) The Apollo 16 drive tube 60009/10. Part I: Modal petrology. Proc. Lunar Planet. Sci. Conf. 9th, p. 1813-1826.

Taylor S.R., Gorton M.P., Muir P., Nance W.B., Rudowski R., and Ware N. (1973) Composition of the Descartes region, lunar highlands. Geochim. Cosmochim. Acta 37, 2665-2683.

Trask N.J. and McCauley J.F. (1972) Differentiation and volcanism in the lunar highlands: Photogeologic evidence and Apollo 16 implications. Earth Planet. Sci. Lett. 14, 201-206.

Vaniman D.T., Lellis S.F., Papike J.J., and Cameron K.L. (1976) The Apollo 16 drill core: Modal petrology and characterization of the mineral and lithic component. Proc. Lunar Sci. Conf. 7th, p. 199-239.

Vaniman D.T. and Papike J.J. (1977) Very low Ti (VLT) basalt: a new mare rock type from the Apollo 17 drill core. Proc. Lunar Sci. Conf. 8th, p. 1443-1471.

Vaniman D.T., Papike J.J., and Schweitzer E.L. (1978) The Apollo 16 drive tube 60009/10. Part II: Petrology and major element partitioning among regolith components. Proc. Lunar Planet. Sci. Conf. 9th, p. 1827-1860.

Vaniman D.T., Schweitzer E.L., and Papike J.J. (1978) Apollo 16 drive tube 60009/60010. Part II: Characterization of the mineral, lithic and glass components (abstract). In Lunar and Planetary Science IX, p. 1186-1188. The Lunar and Planetary Institute, Houston.

Via W.N. and Taylor L.A. (1976) Chemical aspects of agglutinate formation: Relationships between agglutinate composition and the composition of the bulk soil. Proc. Lunar Sci. Conf. 7th, p. 393-402

Walker D., Longhi J., and Hays J.F. (1977) Experimental petrology and origin of Fra Mauro rocks and soil. Proc. Lunar Sci. Conf. 3rd, p. 797-817.

Walton J.R., Lakatos S., and Heymann D. (1973) Distribution of inert gases in fines from the Cayley-Descartes region. Proc. Lunar Sci. Conf. 4th, p. 2079-2096.

Wanke H., Palme H., Baddenhausen H., Dreibus G., Jagouty E., Kruse H., Palme C., Spettel B., Teschke F., and Thacker R. (1975) New data on the chemistry of lunar samples: Primary matter in the lunar highlands and the bulk composition of the moon. Proc. Lunar Sci. Conf. 6th, p.1313-1340.

Warren P.H. and Wasson J.T. (1980) Further foraging for pristine non-mare rocks (abstract). In Lunar Planet. Science XI, p. 1217-1219. The Lunar and Planetary Institute, Houston.

Wasson J.T., Chou C.L., Robinson K.L., and Baedecker P.A. (1975) Siderophiles and volatiles in Apollo 16 rocks and soils. Geochim. Cosmochim. Acta 39, 1475-1485.

Wilhelms D.E. and McCauley J.F. (1971) Geologic map of the nearside of the Moon. U.S. Geol. Survey Misc. Geol. Inv. Map I-703.

Wright R.J., Simms L.A., Reynolds M.A., and Bogard D.D. (1973) Depth variation of cosmogenic gases in the 120 kg Keyes chondrite. J. Geophys. Res. Vol. 78, 1308-1318.

APPENDICES

APPENDIX 1. Preliminary particle track studies prior to the dissection of the 60009/60010 soil column

Twelve small samples of about 10 mg each were removed for particle track studies prior to the dissection of each core section. The intent was to use the results as an aid for dissection and, if possible, to distinguish buried surfaces or depositional units. Figure A1.1 shows the sample locations and presents the raw track data.

The preliminary track counting and analysis was done by G. Crozaz, G. Blanford, and D. Morrison (unpublished work). Feldspar grains were selected from each of the 10 mg samples. These were etched, enlarging particle tracks and enabling easier and more accurate counting of the tracks. The number of tracks found on an individual grain was converted to tracks per square centimeter for tabulation. Track densities range from 10^4 to greater than $10^9/cm^2$.

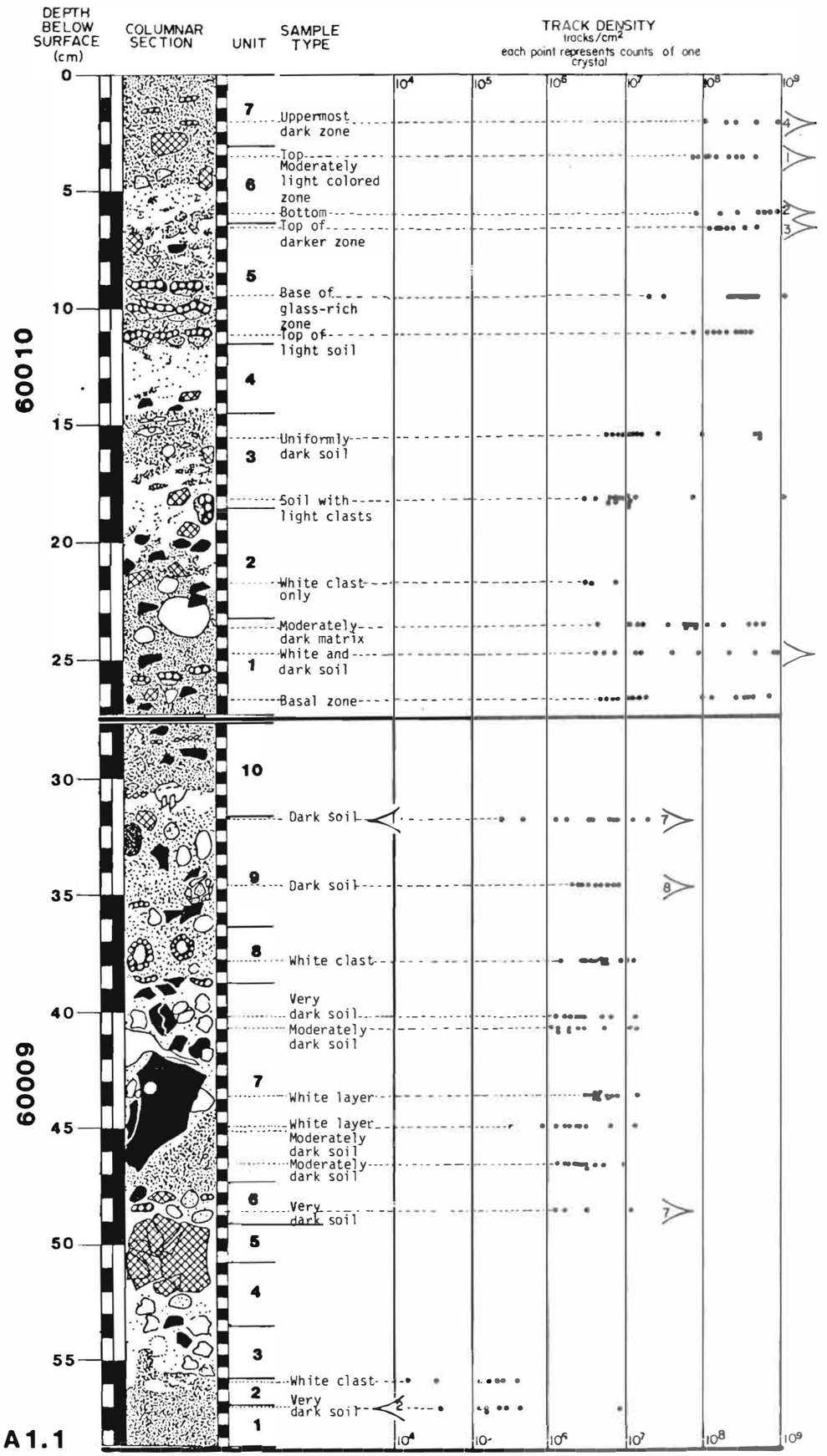
DEPTH BELOW SURFACE (cm)
COLUMNAR SECTION
UNIT
SAMPLE TYPE
TRACK DENSITY
tracks/cm²
each point represents counts of one crystal
60010
60009
Uppermost dark zone
Top
Moderately light colored zone
Bottom
Top of darker zone
Base of glass-rich zone
Top of light soil
Uniformly dark soil
Soil with light clasts
White clast only
Moderately dark matrix
White and dark soil
Basal zone
Dark soil
Dark soil
White clast
Very dark soil
Moderately dark soil
White layer
White layer
Moderately dark soil
Moderately dark soil
Very dark soil
White clast
Very dark soil

Figure A1.1

APPENDIX 2. Peel and continuous thin section samples

Peels

After the dissection passes through a core have been completed, the soil column remaining in the aluminum receptacle is stabilized in two ways. First, a thin layer of the soil column is removed, forming what is called a peel. Figure A2.1 shows the post-dissection 60009 soil column still in the nitrogen processing cabinet. The core is moved to the open air. A controlled thickness of poly-butyl methacrylate adhesive is spread onto a plexiglass strip, pre-cut to the length and width of the soil column. The methacrylate surface is then wet with a solvent (Krylon) and pressed against the relatively flat dissected surface of the soil column for less than five minutes. When lifted, the peel removes a layer of soil 1 or 2 mm thick, which is sprayed with Krylon to fix the particles in place.

The peels are a permanent record of grain orientations and relationships. Individual grains later can be removed for study by dissolving the methacrylate bond with acetone. Figure A2.2 shows the first peel, 60009,6002 on the left, next to the soil column on the right.

Encapsulation and Continuous Thin Sections

After the peel(s) is removed, the remaining soil column is stablized by encapsulating it in epoxy applied under vacuum. In essence one very long potted butt (PB) is made of each core section. The epoxy used is Araldite 506-Versamid 140 diluted 1:1 with its solvent, butyl glycidyl ether.

The soil column and diluted epoxy are placed in a vacuum chamber. The chamber is then evacuated overnight and held at vacuum (about 4 mm Hg) for another 1-2 hours to maximize outgassing of both the soil column and epoxy. A mechanical system allows the epoxy to be gently added, essentially simultaneously to the whole length of the soil column. When the mixture is slowly poured on the soil column in a vacuum chamber, very little bubbling from outgassing and particle displacement occurs. After encapsulation is complete, the chamber is slowly repressurized.

The encapsulated soil column is removed and cured at 30-35° C. The column is encapsulated a second time to make a rectangular block from which thin sections can be made. The epoxy used is stable in the hot caustic solutions employed for particle track studies. Figure A2.3 shows an encapsulated soil column. Figures A2.4 and A2.5 show the ways in which the encapsulated soil columns, 60009 and 60010, were sliced making three long potted butts from each. One of these long PB's from each soil column was then cut into shorter lengths from which polished sections subsequently were made.

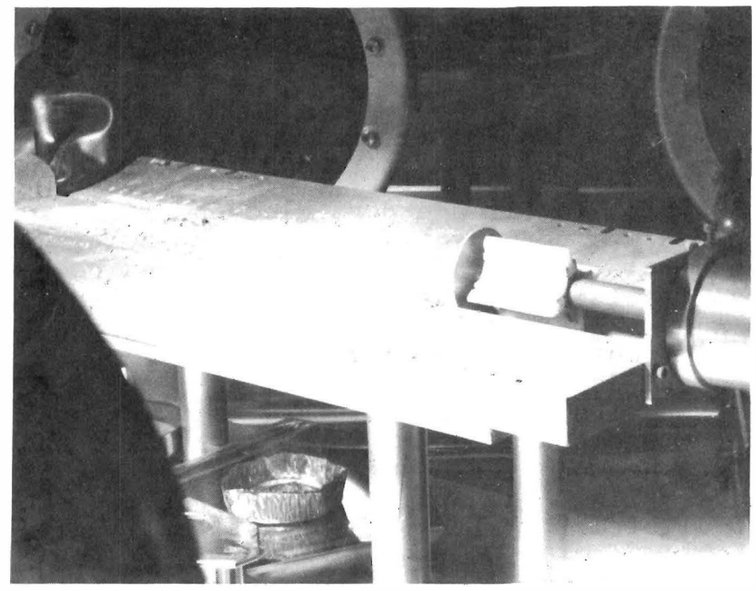

Figure A2.1. The 60009 soil column after five dissection passes and before the first peel was taken. Two peels were taken from this soil column.

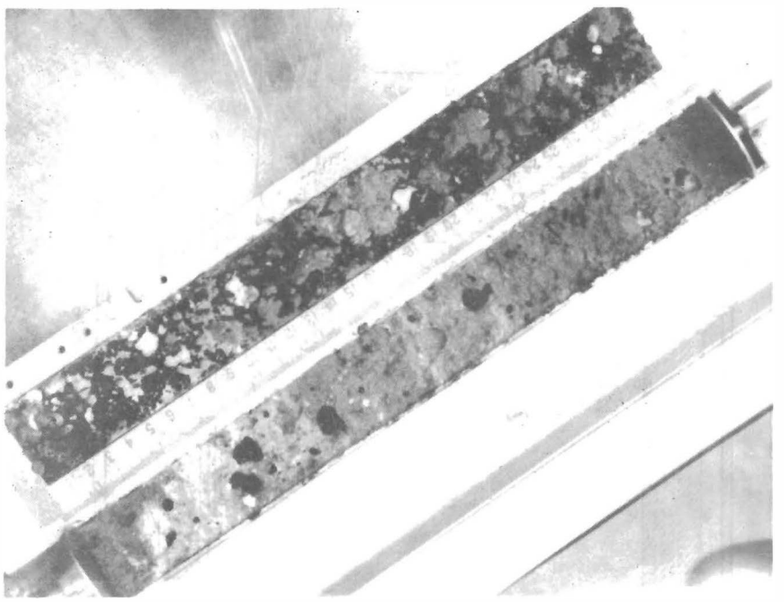

Figure A2.2 shows the first peel (60009,6001) that was removed from the soil column. The soil column is on the right and some of the glue has remained on its surface, appearing as black globs. This usually occurs when there is a fragment too large or too heavy to adhere to the plastic strip when it is removed. (Photo #S75-33765)

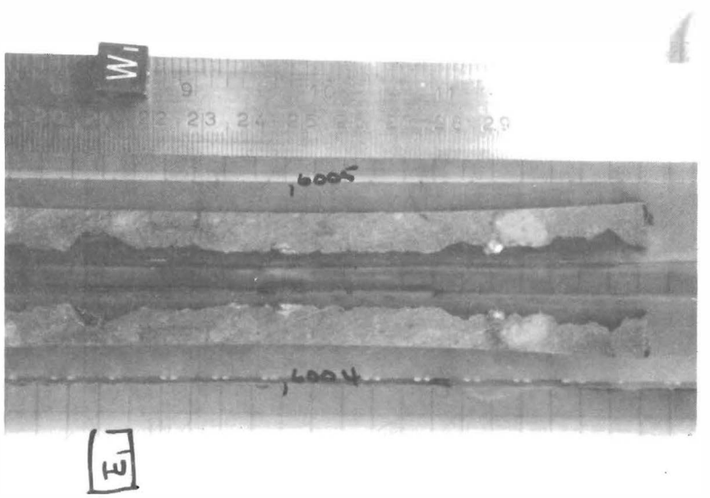

Figure A2.3 shows encapsulated soil column 60009 divided into sections, 6004 and 6005.

Figure A2.4

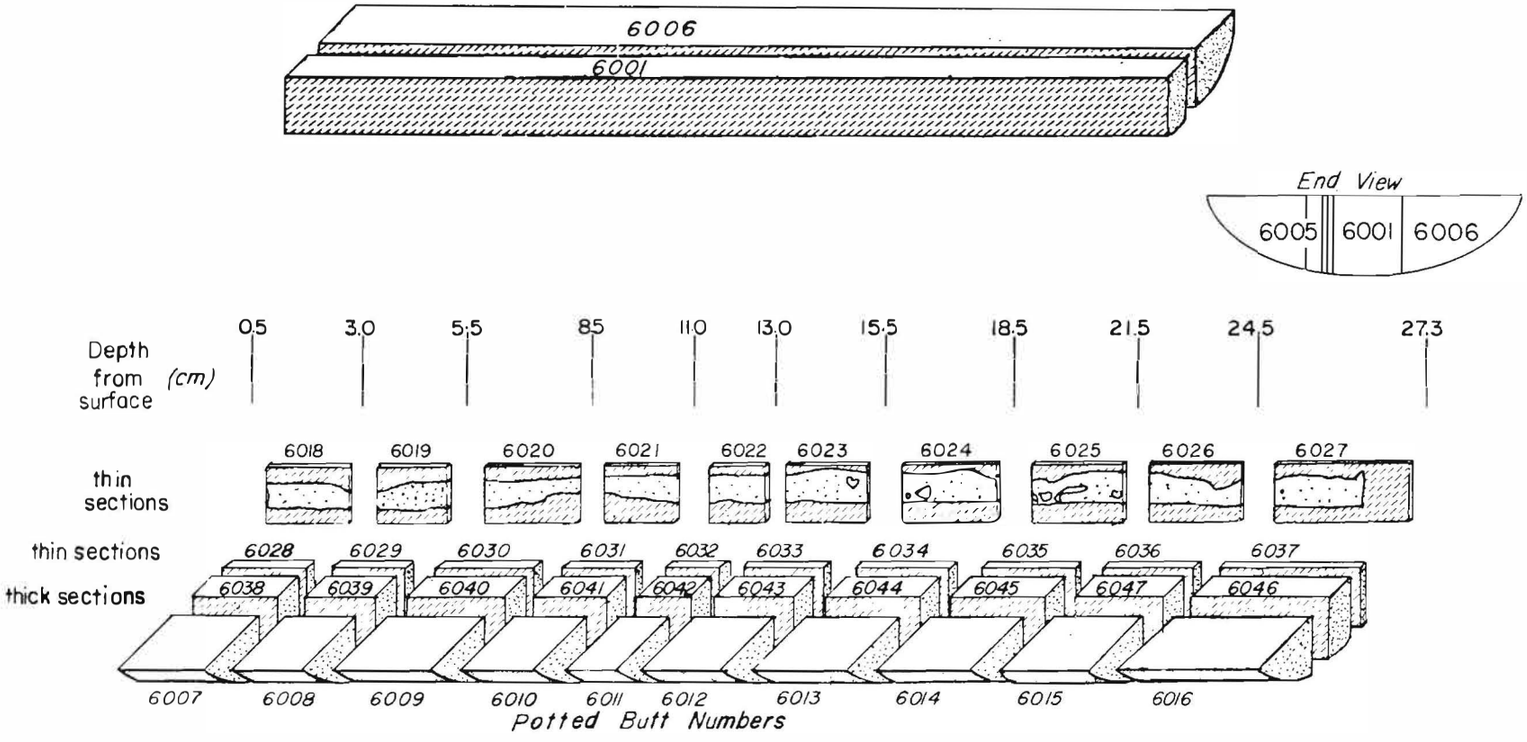

60010
,6005

Figure A2.5

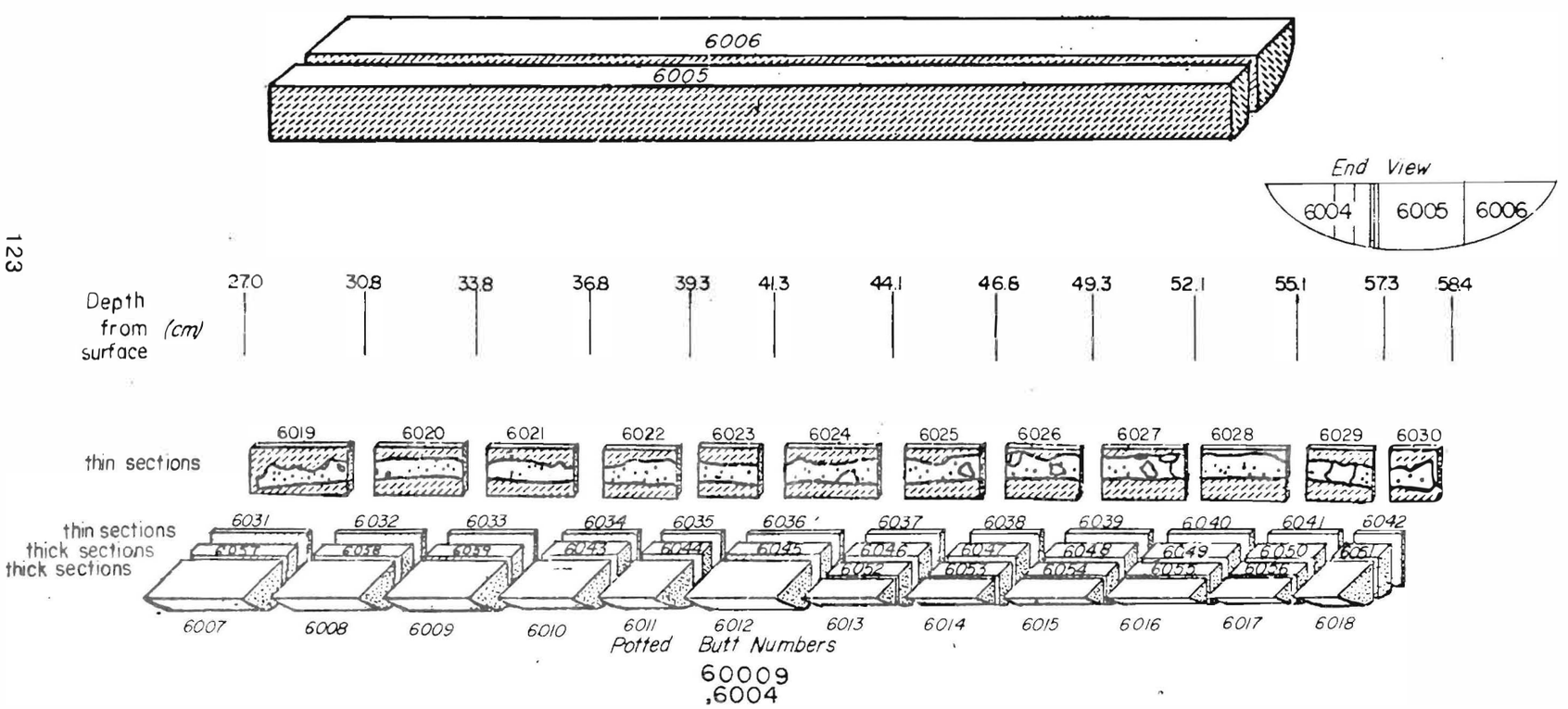
6006
6005
End View
6004
6005
6006
Depth from surface (cm)
27.0
30.8
33.8
36.8
39.3
41.3
44.1
46.6
49.3
52.1
55.1
57.3
58.4
thin sections
6019
6020
6021
6022
6023
6024
6025
6026
6027
6028
6029
6030
thin sections
thick sections
thick sections
6031
6032
6033
6034
6035
6036
6037
6038
6039
6040
6041
6042
6007
6008
6009
6010
6011
6012
6013
6014
6015
6016
6017
6018
Potted Butt Numbers
60009
,6004

APPENDIX 3. Continuous thin sections

This is one set of continuous polished thin sections, minus 5 mm from the top of each section (60009 & 60010), photographed through a petrographic microscope under three different lighting conditions, which emphasize different features. The far left column was taken in plane-polarized transmitted light. The middle column was taken with oblique light and the section itself over a white background. This tends to enhance darker features in the matrix of the soil column. The far right column was taken with oblique light and the section itself over a black background. This enhances the lighter features in the soil column.

Both thin sections and photographs are available for study through the Curator's Office.

The figures should be labelled A3.1 and A3.2, but they are incorrectly labelled A4.1 and A4.2.

Figure A4.1

60010
Continuous Polished Thin Sections

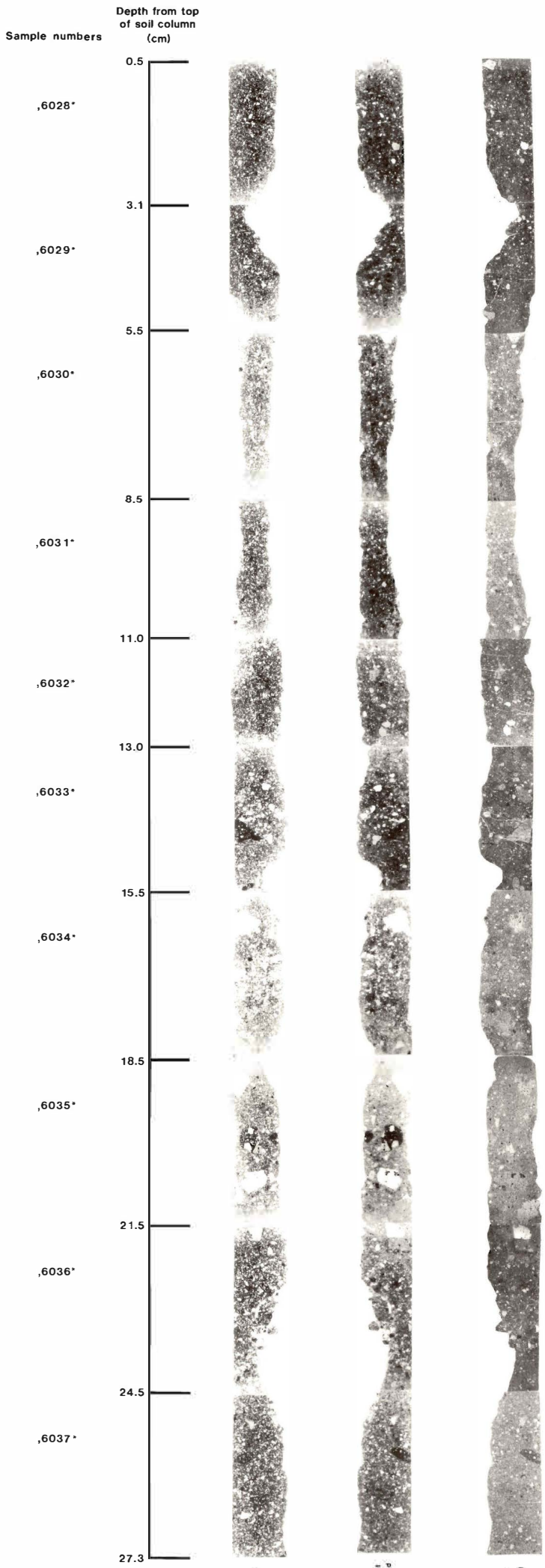

Figure A4.2

60009

Continuous Polished Thin Sections

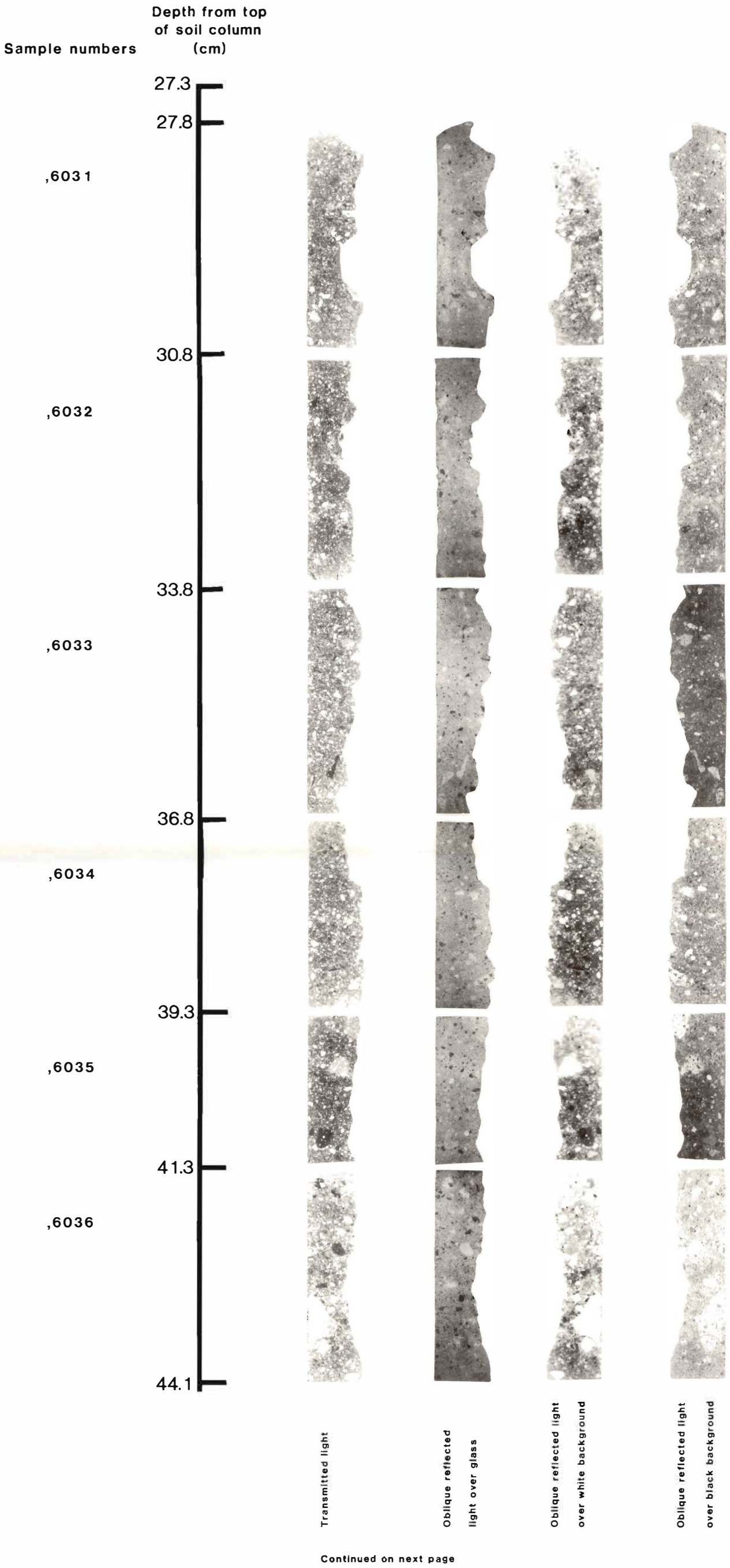

Continued on next page

APPENDIX 4. Grain size data

TABLE A4.1. GRAIN SIZE DATA FROM SELECTED INTERVALS IN 60010

This table shows the weights collected in each sieve interval for the analyzed samples. Data from 1 to 10 mm were furnished by the Curator's Office and were determined by measuring intermediate axes on individual grains rather than by sieving (S. Nagle, pers. comm.) All weights are in grams. (60010 data from McKay et al. 1977; 60009 data from McKay et al. 1976.)

Grain Size Fraction	0.5-1cm (60010,1077)	3.5-4.0cm (60010,1076)	11-11.5cm (60010,1075)	14-14.5cm (60010,1074)	20-20.5cm (60010,3107)	24.5-25cm (60010,1073)
4-10mm	0.00	0.00	0.159	0.269	0.517	1.017[1]
2-4mm	0.142	0.136	0.380	0.378	0.579	0.3330
1-2mm	0.3029	0.296	0.4537	0.600	0.384	0.4567
1mm	6.614	6.404	6.760	6.811	6.190	6.8567
500-1000µm	0.05102	0.04336	0.05046	0.06402	0.03318	0.05749
250-500µm	0.05212	0.05328	0.05342	0.05851	0.04405	0.05905
150-250µm	0.04795	0.05004	0.04735	0.04750	0.04128	0.04557
90-150µm	0.05201	0.05286	0.05510	0.05166	0.04818	0.05328
75-90µm	0.02124	0 02131	0.01908	0.01775	0.01831	0.01853
45-75µm	0.05413	0.06335	0.05951	0.05717	0.05991	0.05463
20-45µm	0.08501	0.09169	0.07741	0.09226	0.10914	0.06861
10-20µm	0.06933	0.07501	0.05128	0.06312	0.07633	0.05600
<10µm	0.03567	0.04242	0.06169	0.05331	0.09565	0 04545
Total	0.46848	0.49332	0.47530	0.50530	0.52603	0.45861

[1]Represents only one large fragment-not used in calculating M_z and σ_1.

TABLE A4.2. GRAIN SIZE DATA FROM SELECTED INTERVALS IN 60009

This table shows the weights collected in each sieve interval for the analyzed samples. Data from 1 to 10 mm were furnished by the Curator's Office and were determined by measuring intermediate axes on individual grains rather than by sieving (S. Nagle, pers. comm.) All weights are in grams. (60010 data from McKay et al. 1977; 60009 data from McKay et al. 1976.)

Grain Size Fraction	28.8-29.3cm (60009,454)	42.8-43.3cm (60009,455)	48.4-49.0cm (60009,456)	53.3-53.8cm (60009,457)	58.3-58.8cm (60009,458)
4-10mm	0.294	0.648	0.641	0.267	0.0
2-4mm	0.090	0.660	0.319	0 375	0.260
1-2mm	0.253	0.645	0.315	0.190	0.228
1mm	4.228	8.625	5.683	3.205	5.385
500-1000μm	0.3233	0.02303	0.03073	0.03394	0.02858
250-500μm	0.05186	0.03081	0.04465	0.04979	0.04929
150-250μm	0.04186	0.02315	0.04000	0.04051	0.03820
90-150μm	0.04558	0.02264	0.04341	0.04346	0.04364
75-90μm	0.01600	0.00715	0.01694	0.01493	0.01601
45-75μm	0.05914	0.02278	0.04965	0.04870	0.05298
20-45μm	0.11644	0.03135	0.07636	0.05706	0.08712
10-20μm	0.00615	0.00058	0.03283	0.01042	0.02894
10μm	0.01225	0.00096	0.03391	0.01027	0.02748
Total	0.45508	0.20196	0.49165	0.38158	0.50153

APPENDIX 5. Modal data based on continuous thin sections

TABLE A5.1. MODAL DATA BASED ON CONTINUOUS THIN SECTIONS OF 60010 SOIL COLUMN

		60010												LUNAR SURFACE →							
Stratigraphic Units:		1				2		3		4				5				6		7	
	60010,	6027		6026		6025		6024		6023		6022		6021		6020		6019		6018	
B = Bottom of section; T = Top of section		B	T	B	T	B	T	B	T	B	T	B	T	B	T	B	T	B	T	B	T
	Lithic Fragments																				
	Mare Component	0.2	--	0.1	3.1	0.5	--	--	--	--	0.6	--	--	--	--	0.4	--	--	--	--	--
	Highland Component																				
	Anorthosites	1.2	0.4	0.4	0.7	2.0	1.9	1.3	0.4	1.5	0.6	0.9	1.2	0.4	2.5	0.5	0.2	0.9	0.6	--	--
	Norite/Troctolite	--	--	--	1.1	--	--	2.0	--	--	--	--	--	--	1.0	0.5	0.4	--	--	--	--
	LMB	2.0	1.8	6.6	1.4	1.2	2.8	0.3	0.9	2.0	0.1	5.7	1.1	1.2	0.2	1.4	0.8	2.2	0.3	0.4	1.4
	Feldspathic Basalt	--	0.2	0.5	2.0	--	1.7	0.8	--	0.5	--	0.9	--	1.0	--	--	0.7	--	--	0.5	--
	RNB	--	1.0	--	0.4	2.3	1.6	--	--	--	0.4	0.4	--	0.5	--	--	--	0.3	0.8	--	--
	POIK	1.0	9.8	3.2	3.1	4.3	3.0	3.9	7.2	5.7	3.7	3.7	4.0	3.0	7.4	5.7	3.0	0.9	2.7	5.8	2.6
Large	Fused Soil Component																				
	DMB	3.0	1.3	3.1	2.0	2.1	0.6	0.6	3.9	1.8	3.1	1.2	0.7	--	0.5	3.9	0.7	3.8	1.6	3.1	0.8
Clasts	Agglutinate	5.3	1.2	0.1	1.9	0.7	0.5	2.6	4.7	1.3	2.5	3.1	3.8	2.8	4.4	1.9	3.1	3.6	2.4	4.0	6.1
0.2-2.0 mm	Mineral Fragments																				
	Olivine/Pyroxene	--	0.4	--	--	--	--	--	--	--	--	0.3	--	0.5	--	0.5	--	--	--	--	--
	Plagioclase	3.4	8.5	7.4	5.5	0.5	2.1	4.7	3.4	1.9	1.9	2.4	2.5	2.9	2.9	4.6	3.8	1.0	0.3	2.0	1.1
	Opaques	--	--	--	--	--	--	--	--	--	--	--	--	--	--	--	--	--	--	--	--
	Glass Fragments																				
	Orange	--	--	--	--	--	--	--	--	--	--	--	--	--	--	--	--	--	--	--	--
	Yellow	--	0.4	0.4	--	--	--	0.1	0.2	0.2	0.8	--	--	--	--	0.4	0.4	--	--	--	--
	Green	--	--	--	--	--	--	--	--	--	--	--	--	--	--	0.3	--	--	--	--	--
	Brown	--	--	--	--	--	--	--	--	--	--	--	--	--	--	--	--	--	--	--	--
	Gray	--	--	--	--	--	--	--	--	--	--	--	--	--	--	--	--	--	--	--	--
	Clear	0.4	--	0.3	--	--	--	--	0.1	--	--	0.7	--	0.8	--	--	--	--	0.4	--	--
	Miscellaneous																				
	Devitrified Glass	0.9	--	--	0.1	0.7	0.2	--	--	0.5	0.6	--	0.3	--	--	--	0.2	0.3	0.7	0.6	--
	Other	--	--	--	--	--	--	--	--	--	--	--	--	--	--	--	--	--	--	--	--

TABLE A5.1 (Continued)

		60010																			
		LUNAR SURFACE →																			
Stratigraphic Units:		1			2			3			4			5				6		7	
	60010,	6027		6026		6025		6024		6023		6022		6021		6020		6019		6018	
B = Bottom of section; T = Top of section		B	T	B	T	B	T	B	T	B	T	B	T	B	T	B	T	B	T	B	T
	Lithic Fragments																				
	Mare Component	--	--	--	--	--	--	--	--	--	--	--	--	--	--	--	--	--	--	--	0.1
	Highland Component																				
	Anorthosites	1.4	1.6	0.9	1.8	0.6	2.1	0.8	0.7	0.8	1.8	1.0	1.7	1.0	0.7	0.1	0.6	0.7	0.4	0.7	1.5
	Norite/Troctolite	0.1	--	--	--	--	0.2	--	0.8	--	--	0.5	--	1.2	0.5	--	--	--	--	--	--
	LMB	0.7	1.2	0.9	1.7	0.2	0.4	--	0.2	0.2	--	0.1	--	0.2	0.2	--	--	0.7	0.3	0.4	0.7
	Feldspathic Basalt	--	--	--	--	--	--	--	--	0.2	0.1	--	0.2	--	--	--	--	--	0.3	--	--
	RNB	--	--	--	--	0.5	0.2	--	--	--	--	0.1	--	--	--	--	--	--	0.1	--	--
	POIK	2.7	2.4	3.6	2.4	4.5	3.4	0.9	1.6	1.6	4.5	2.1	2.0	3.1	1.5	2.9	3.6	3.3	2.6	5.5	3.4
	Fused Soil Component																				
	DMB	2.8	3.2	2.5	4.5	2.8	3.7	3.3	3.9	5.5	3.7	2.0	4.5	4.2	3.2	4.2	3.2	5.8	6.2	4.6	3.6
Small	Agglutinate	3.7	4.5	2.4	3.1	1.9	2.2	3.2	3.2	2.5	4.7	3.9	5.6	8.6	7.0	4.3	8.1	5.7	8.0	7.3	8.2
Clasts	Mineral Fragments																				
	Olivine/Pyroxene	0.4	0.8	1.1	1.0	0.8	1.5	0.5	0.7	1.2	0.8	1.5	0.5	1.1	0.6	0.5	0.5	0.7	1.0	0.9	1.0
0.02-0.2 mm	Plagioclase	17.4	15.0	13.7	14.3	10.5	10.7	10.7	10.6	14.5	8.4	8.2	7.5	8.6	9.1	9.4	8.7	9.7	8.9	6.5	7.4
	Opaques	--	--	--	0.3	--	--	0.1	--	--	0.2	--	0.2	--	--	--	0.1	0.1	0.1	--	0.1
	Glass Fragments																				
	Orange	--	--	--	--	--	--	--	--	--	--	0.1	--	--	--	--	0.2	--	--	--	--
	Yellow	0.5	1.0	0.6	0.3	0.5	0.8	0.4	0.5	0.4	0.6	0.1	0.2	0.2	0.3	0.1	0.2	0.3	0.2	--	0.2
	Green	--	--	0.2	--	--	0.1	--	--	--	--	--	--	--	--	0.1	--	--	--	--	--
	Brown	--	--	--	--	0.1	--	--	--	--	--	--	--	--	--	--	--	--	--	--	--
	Gray	--	--	--	--	--	--	--	--	--	--	--	--	--	--	--	--	--	--	--	--
	Clear	0.2	0.5	0.1	0.4	0.2	0.8	0.5	0.3	0.2	0.5	0.9	0.5	0.6	0.5	0.5	0.2	0.2	0.8	0.5	0.9
	Miscellaneous																				
	Devitrified Glass	0.2	0.1	--	0.2	--	0.4	--	0.2	0.2	--	0.1	--	0.9	--	0.1	0.1	--	0.5	0.4	0.6
	Other	0.3	--	--	--	--	--	--	--	--	--	--	--	--	--	--	--	--	--	--	--
Totals	Large Clasts	17.4	25.0	22.1	21.3	14.3	14.4	16.3	20.8	15.4	14.3	19.3	13.6	13.1	19.0	20.1	13.3	13.0	9.8	16.4	12.0
	Small Clasts	30.4	30.3	26.0	30.0	22.6	26.5	20.4	23.7	27.3	25.3	20.6	22.9	28.7	23.6	22.2	25.5	27.2	29.4	26.8	27.8
	Matrix	52.2	44.7	51.9	48.7	63.1	59.1	63.3	55.5	57.3	60.4	60.1	53.5	58.2	57.4	57.7	61.2	59.8	60.8	56.8	60.2

from Simon et al. (1978)

TABLE A5.2. MODAL DATA BASED ON CONTINUOUS THIN SECTIONS OF 60009 SOIL COLUMN

		60009																									
		LUNAR SURFACE →																									
Stratigraphic Units:		1	2	3			4	5	6				7						8	9			10				
B= Bottom of PTS; T = Top of PTS	60009,	6030	6029			6028		6027	6026		6025		6024		6023		6022		6021	6020			6019				
M = Middle of PTS			B	M	T	B	T	B	T	B	T	B	T	B	T	B	T	B	T	B	T	B	T	B	T	B	T
	Lithic Fragments																										
	Mare Component	--	--	--	--	--	--	--	--	--	--	--	--	--	--	--	0.3	--	--	--	0.7	--	0.7	--	--		
	Highland Component																										
	Anorthosites	0.6	1.3	--	0.7	0.7	4.8	1.5	1.8	--	0.5	0.8	--	1.0	1.0	--	0.9	0.3	0.2	1.8	0.3	2.3	--	0.7	1.6		
	Norite/Troctolite	1.6	--	--	--	1.1	1.5	0.4	--	0.1	0.4	1.3	--	0.3	--	--	--	--	--	--	--	0.2	--	--	--		
	LMB	4.4	0.8	9.8	4.5	4.3	3.2	--	0.3	--	2.2	3.8	0.6	8.4	1.1	3.4	1.2	5.4	--	3.2	0.5	7.7	3.1	7.3	1.3		
	Feldspathic Basalt	0.2	1.1	--	1.5	0.3	0.5	0.5	3.1	--	--	1.4	1.2	--	0.7	--	2.5	--	0.8	--	--	--	--	--	0.5		
	RNB	1.4	0.1	0.7	--	2.1	--	--	0.3	0.7	0.9	0.4	2.3	--	0.6	4.7	--	0.3	1.3	--	0.3	4.4	--	1.2	--		
	POIK	2.4	7.1	1.7	2.6	5.3	2.3	2.7	5.3	4.4	3.4	3.0	6.6	5.2	4.7	3.9	2.1	4.4	1.9	2.8	2 2	5.0	7.5	5.3	7.0		
Large	Fused Soil Component																										
	DMB	0.8	0.9	5.3	0.2	0.9	1.7	--	5.1	1.6	0.7	4.3	5.6	1.6	0.6	1.8	1.0	0.5	0.6	--	5.0	0.4	0.7	6.0	1.9		
Clasts	Agglutinate	1.1	2.6	--	0.2	--	0.7	0.4	1.4	0.8	0.4	1.3	4.0	0.4	3.0	1.0	2.0	2.2	2.2	9.0	1.3	1.4	0.6	0.9	2.8		
0 2-2.0 mm	Mineral Fragments																										
	Olivine/Pyroxene	--	0.3	--	0.4	0.3	--	--	--	--	--	--	--	--	--	--	--	--	--	--	--	--	--	--	--		
	Plagioclase	0.9	3.0	3.0	12.2	11.5	7.8	3.5	3.5	7.2	4.8	1.0	4.1	9.5	7.7	3.9	7.7	3.2	4.5	3.4	5.6	2.6	3.0	4.2	3.4		
	Opaques	--	--	--	--	--	--	--	--	--	--	--	--	--	--	--	--	--	--	--	--	--	--	--	--		
	Glass Fragments																										
	Orange	--	--	--	--	--	--	--	--	--	--	--	--	--	--	--	--	--	--	--	--	--	--	--	--		
	Yellow	--	--	--	--	0.7	--	--	--	--	--	--	--	--	--	--	--	--	--	--	--	0.2	--	--	0.5		
	Green	--	--	--	--	--	--	--	--	--	--	--	--	--	--	--	--	--	--	--	--	--	--	--	--		
	Brown	--	--	--	--	--	--	--	--	--	--	--	--	--	--	--	--	--	--	--	--	--	--	--	--		
	Gray	--	--	--	--	--	--	--	--	--	--	--	--	--	--	--	--	--	--	--	--	--	--	--	--		
	Clear	0.2	--	--	--	--	--	--	--	--	--	--	1.1	--	--	--	0.1	--	1.0	1.3	0.3	--	--	1.3	--		
	Miscellaneous																										
	Devitrified Glass	--	--	--	--	--	--	--	--	2.1	--	1.4	--	0.9	0.2	0.2	0.6	--	--	1.5	1.3	1.1	1.5	1.1	--		
	Other	--	--	--	--	--	--	--	--	--	--	--	--	--	0.4	--	--	--	--	--	--	--	--	--	--		

TABLE A5.2 (Continued)

		60009	LUNAR SURFACE →																							
Stratigraphic Units:			1	2	3		4	5	6			7						8	9		10					
B= Bottom of PTS; T = Top of PTS		60009,	6030	6029		6028		6027	6026		6025	6024		6023		6022		6021	6020		6019					
M = Middle of PTS				B	M	T	B	T	B	T	B	T	B	T	B	T	B	T	B	T	B	T	B	T	B	T
	Lithic Fragments																									
	Mare Component		--	--	--	--	--	--	--	--	--	--	--	--	--	--	--	--	--	--	--	--	--	--	--	--
	Highland Component																									
	Anorthosites		1.1	1.9	0.3	--	0.2	0.5	0.5	0.6	1.5	1.1	1.8	0.6	0.6	0.8	0.6	0.2	0.5	1.3	1.0	1.5	1.3	1.0	0.4	0.3
	Norite/Troctolite		0.3	0.2	0.9	1.0	0.4	0.3	0.3	0.2	0.2	0.4	1.4	1.0	0.6	0.4	--	0.7	0.3	0.6	0.1	0.4	0.4	0.3	0.1	--
	LMB		1.1	1.7	2.1	0.6	0.7	0.5	0.6	0.4	0.3	0.3	0.6	0.5	0.2	0.4	--	0.6	0.6	0.4	0.3	0.2	0.7	0.5	0.6	0.5
	Feldspathic Basalt		0.4	0.3	0.1	--	0.3	0.2	0.1	0.1	0.1	--	0.1	0.2	0.5	0.1	--	--	--	0.7	0.2	0.3	--	0.3	--	--
	RNB		0.4	0.7	0.3	--	0.5	--	0.1	0.3	0.4	1.0	--	0.2	0.4	0.1	0.3	--	0.2	0.1	--	--	0.1	0.1	--	--
	POIK		1.2	1.5	0.6	1.2	1.3	2.3	2.6	1.7	2.3	2.4	0.8	2.4	1.8	1.7	2.7	2.3	3.1	3.1	1.3	1.3	1.4	1.9	3.8	3.7
	Fused Soil Component																									
	DMB		4.4	2.9	1.7	1.6	1.1	1.3	2.8	2.5	2.5	3.0	2.4	2.9	2.7	2.3	3.1	3.5	4.8	3.4	3.4	4.4	2.8	2.5	1.3	1.6
Small	Agglutinate		5.9	2.0	0.6	1.7	1.5	2.3	2.8	2.8	2.7	3.9	3.3	3.9	2.6	2.8	4.1	3.7	4.6	6.7	4.1	4.6	3.2	3.3	2.8	4.7
Clasts	Mineral Fragments																									
	Olivine/Pyroxene		0.7	1.0	0.9	0.8	1.4	1.0	0.8	1.6	0.9	0.9	1.1	1.3	0.9	1.1	1.2	1.0	1.6	1.1	1.6	0.9	0.8	0.3	--	0.5
0.02-0.2 mm	Plagioclase		8.7	8.3	19.8	23.7	18.5	17.1	12.2	6.1	14.7	9.1	7.9	7.7	13.7	15.6	10.5	14.0	13.3	12.1	12.4	10.8	9.5	10.5	12.9	14.1
	Opaques		0.1	--	0.1	--	--	--	0.5	0.1	0.1	0.1	--	--	--	--	--	--	0.1	0.1	--	--	--	--	0.3	0.1
	Glass Fragments																									
	Orange		--	0.1	--	--	--	0.1	--	--	--	0.4	--	--	--	--	--	--	--	--	--	--	--	--	--	--
	Yellow		0.5	0.1	--	0.1	--	--	0.2	--	0.1	0.1	0.1	0.6	0.1	0.1	0.9	0.2	--	0.5	0.3	0.1	--	0.3	0.5	0.7
	Green		--	0.2	--	--	--	--	--	--	--	--	--	--	--	--	--	--	0.2	--	--	0.2	--	--	0.1	0.1
	Brown		--	--	--	--	--	--	--	0.2	0.1	0.5	--	--	--	--	--	--	--	--	--	--	--	--	--	--
	Gray		--	--	--	--	--	--	0.1	--	--	--	--	--	--	--	--	--	--	--	--	--	--	--	--	--
	Clear		0.9	0.9	--	0.2	0.1	0.2	1.0	0.2	0.5	0.7	1.6	0.4	0.2	0.4	0.5	0.2	0.1	0.6	0.9	0.9	1.0	0.4	0.6	0.3
	Miscellaneous																									
	Devitrified Glass		0.7	0.1	0.4	0.3	--	--	--	--	0.6	0.7	0.5	0.1	--	--	0.1	0.2	0.7	--	0.6	--	0.6	0.1	0.3	--
	Other		--	--	--	--	0.1	--	--	--	--	--	--	0.1	--	--	--	--	--	--	--	--	--	--	--	--
Totals	Large Clasts		13.6	17.2	20.5	22.3	27.2	22.5	9.0	20.8	14.8	13.3	18.7	25.5	27.3	20.0	18.9	18.4	16.3	12.5	23.0	17.5	25.3	17.1	28.0	19.5
	Small Clasts		26.4	31.9	27.8	30.3	26.1	25.8	24.6	26.8	27.0	24.6	21.6	21.9	24.3	25.8	24.0	26.6	30.1	30.8	26.2	25.6	21.8	21.5	23.7	26.1
	Matrix		60.0	50.9	51.7	47.4	46.7	51.7	66.4	52.4	58.2	62.1	59.7	52.6	48.4	54.2	57.1	55.0	53.6	56.7	50.8	56.9	52.9	61.4	48.3	54.4

from Simon et al. (1978)

APPENDIX 6. Modal data based on sieved size fractions

TABLE A6.1. MODAL DATA FROM SELECTED INTERVALS IN 60010 BASED ON SIEVED SIZE FRACTIONS

60010 Particle types and relative amounts from petrographic analysis of polished grain mounts -- all values are in percent.

Sample (Parent)	60010,1077 (60010,176)			60010,1076 (60010,162)			60010,1075 (60010,128)			60010,1074 (60010,114)			60010,3107 (60010,89)			60010,1073 (60010,68)		
Depth from top of core	0.5-1 cm			3.5-4 cm			11-11.5 cm			14-14.5 cm			20-20.5 cm			24.5-25 cm		
Grain size	250-500µm	150-250µm	90-150µm	250-500µm	150-250µm	90-150µm	250-500µm	150-250µm	90-150µm	250-500µm	150-250µm	90-150µm	250-500µm	150-250µm	90-150µm	250-500µm	150-250µm	90-150µm
Agglutinates	31.1	34.0	88.6	33.9	37.8	38.5	26.8	28.8	26.4	10.8	21.4	18.2	7.0	13.6	12.1	17.6	22.4	14.2
Plutonic metamorphic rocks	--	--	--	0.4	--	0.3	1.2	--	--	0.4	0.1	--	1.0	--	--	0.2	0.2	--
Plutonic igneous rocks	--	--	--	--	--	--	--	--	--	--	--	--	--	--	--	--	--	--
Crushed ANT-suite	7.1	3.3	3.0	4.8	4.3	3.7	4.7	4.7	3.8	8.8	4.6	6.3	7.0	7.4	5.6	6.5	3.8	4.5
Light matrix breccia	0.3	0.7	0.1	0.9	--	0.5	1.6	0.7	1.6	1.8	2.8	1.2	1.7	1.0	0.6	1.5	0.6	1.7
Metamorphosed breccia	10.6	6.9	5.4	9.7	8.0	6.5	7.1	9.2	5.6	8.6	10.4	8.3	12.0	10.4	10.6	7.0	6.6	7.0
Poikilitic rocks	18.6	18.9	16.3	19.9	18.9	11.7	16.5	15.5	15.6	19.6	14.3	14.7	34.6	26.9	23.3	15.6	14.9	12.5
Subophitic melt rocks	0.6	2.0	0.7	2.3	1.5	0.5	1.8	0.8	0.2	2.2	1.0	0.7	1.0	1.7	1.4	2.2	1.9	0.7
Olivine-porphyritic melt rock	0.6	--	--	--	--	0.3	0.2	--	--	--	--	--	0.7	0.1	--	0.2	--	--
Mare basalt	--	--	--	--	--	--	--	--	--	0.2	0.2	--	--	--	--	--	--	--
Brown matrix breccia	10.6	7.4	7.6	9.7	8.3	11.2	18.5	10.2	13.2	7.8	5.8	6.3	8.3	8.0	7.9	8.1	3.5	10.5
Feldspathic melt rock	1.1	0.6	--	1.8	--	0.3	0.4	1.2	0.4	1.8	1.6	0.2	1.7	2.6	1.4	0.9	0.6	0.3
Mesostasis-rich melt rocks	2.9	4.1	1.9	1.6	2.3	3.7	4.5	2.8	1.0	3.8	2.9	2.2	5.3	3.6	2.7	3.5	1.8	2.5
Melt matrix breccia	--	--	--	0.2	--	--	0.2	--	--	0.4	--	--	0.6	--	--	--	--	--
Plagioclase single crystal	7.1	11.4	13.1	8.6	7.8	10.7	8.1	13.0	18.2	26.8	25.1	29.8	7.6	11.9	14.6	31.7	35.8	36.7
Polycrystalline plagioclase	1.7	1.1	1.4	0.4	0.8	1.2	0.8	1.0	2.0	1.0	1.4	2.2	2.3	2.0	2.9	0.2	1.6	1.8
Pyroxene crystals	0.6	0.7	1.4	0.2	--	0.8	--	1.3	1.8	0.8	1.9	4.2	0.7	1.3	5.1	0.2	0.6	0.8
Olivine crystals	--	0.3	0.4	--	--	0.3	--	0.2	--	0.2	1.0	1.0	0.3	0.3	0.6	--	--	0.3
Opaque	--	0.6	--	0.7	--	0.3	0.4	--	--	0.2	0.3	--	0.3	0.3	0.6	--	--	0.5
Yellow-orange glass	0.3	0.1	0.1	--	0.3	1.3	--	0.7	0.4	0.2	0.4	0.7	0.7	1.6	0.4	--	0.3	0.3
Colorless glass	1.4	1.4	4.4	0.9	2.3	2.7	2.0	2.8	4.0	0.4	1.2	2.5	1.7	1.7	5.0	1.1	0.6	1.7
Quench crystallized glass	5.7	5.7	5.4	3.8	6.3	5.7	5.3	7.0	5.6	4.4	3.5	1.7	5.7	5.6	5.9	3.7	4.6	3.3
Total grains counted	350	700	700	442	600	600	492	600	500	500	700	600	300	700	700	540	625	600

from McKay et al. (1977)

TABLE A6 2 MODAL DATA FROM SELECTED INTERVALS IN 60009 BASED ON SIEVED SIZE FRACTIONS

60009 Particle types and relative amounts in three grain sizes of the fine analyzed samples from 60009. All values are percent.

Sample (Parent)	60009,454 (60009,45)			60009,455 (60009,123)			60009,456 (60009,174)			60009,457 (60009,209)			60009,458 (60009,246)		
Depth from top of drive tube	28.8 - 29.3 cm			42.8 - 43.3 cm			48.4 - 49.0 cm			53.3 - 53.8 cm			58.3 - 58.8 cm		
Grain size	250-500 m	150-250 m	90-150 m	250-500 m	150-250 m	90-150 m	250-500 m	150-250 m	90-150 m	250-500 m	150-250 m	90-150 m	250-500 m	150-250 m	90-150 m
Agglutinates	9.5	17.0	19.2	9.2	8.4	12.5	14.9	22.4	21.5	8.3	3.6	2.2	26.4	20.5	28.8
Plutonic metamorphic rocks	1.5	1.1	0.4	--	0.3	0.2	1.9	1.5	--	--	--	0.4	2.0	0.6	--
Plutonic igneous rocks	0.5	0.9	--	2.5	0.3	0.2	0.6	--	--	--	--	--	0.7	0.4	--
Crushed ANT-suite	4.0	2.7	1.1	13.3	12.7	6.8	4.3	3.3	2.7	1.7	0.8	3.8	2.7	3.7	2.1
Light matrix breccia	3.5	1.4	0.8	3.3	7.9	3.8	1.2	2.8	1.7	--	0.8	0.8	--	3.1	3.6
Metamorphosed breccia	14.0	8.6	12.0	11.7	5.1	10.0	19.3	11.1	13.8	6.6	2.0	5.0	14.3	11.2	9.3
Poikilitic rocks	14.5	12.6	13.2	6.7	3.8	4.0	18.0	9.2	10.3	--	5.2	4.4	13.6	13.7	10.1
Subophitic melt rocks	1.5	1.7	--	0.8	0.6	0.8	2.5	1.3	1.2	--	--	--	1.4	2.6	1.4
Olivine-porphyritic melt rock	1.0	0.3	--	--	--	--	--	0.2	0.2	--	--	--	0.7	--	0.1
Mare basalt	0.5	--	--	0.8	0.3	--	1.2	0.2	0.3	--	--	--	0.7	0.1	--
Brown matrix breccia	8.5	9.4	7.1	5.0	5.7	8.5	10.6	10.9	7.3	3.3	2.8	1.0	14.2	14.2	13.1
Melt matrix breccia	4.5	2.2	--	2.5	0.3	--	--	0.5	0.2	--	--	--	0.7	1.2	0.4
Feldspathic melt rock	1.0	1.7	3.4	--	0.3	0.8	5.0	0.8	1.2	--	--	1.2	1.4	1.3	1.4
Mesostasis-rich melt rocks	4.0	5.1	1.5	0.8	2.9	0.7	3.7	3.0	2.3	--	2.8	1.4	1.4	3.1	1.4
"Black and white" breccia	1.0	--	--	0.8	--	--	--	--	--	--	--	--	--	--	--
Plagioclase single crystals	22.5	26.2	24.4	34.4	44.1	44.5	11.2	17.7	22.7	71.7	76.0	74.2	6.9	11.9	15.2
Polycrystalline plagioclase	0.5	2.5	2.1	3.3	2.2	2.5	--	3.0	2.3	--	0.8	2.0	2.0	2.8	4.4
Pyroxene crystals	0.5	0.3	0.8	0.8	1.0	0.7	--	1.8	2.5	1.7	0.8	1.4	0.7	0.6	0.1
Olivine crystals	1.0	0.3	3.0	--	1.3	1.5	--	1.2	0.8	--	2.4	0.6	--	0.4	0.3
Opaque	--	1.1	0.4	--	--	0.2	--	0.3	0.2	--	--	0.2	--	--	0.6
Yellow-orange glass	--	0.5	1.5	--	--	0.3	--	0.2	1.3	--	--	--	0.7	0.9	1.1
Colorless glass	--	2.2	1.5	--	--	1.0	--	2.5	2.5	--	0.1	0.4	0.7	1.9	2.0
Clear glass fragments	--	1.9	--	--	--	0.7	1.0	--	--	--	--	--	--	--	--
Agglutinitic glass	0.5	--	0.8	--	--	0.5	--	2.3	1.0	--	--	0.2	0.7	0.4	0.6
Maskeleynite	0.5	0.3	--	--	0.3	--	0.6	0.2	--	--	--	--	--	0.3	--
Quench crystallized glass	2.5	1.1	3.4	0.8	1.9	0.3	0.6	1.3	2.5	3.3	1.2	0.4	5.4	2.2	2.4
Devitrified glass	2.5	0.8	3.0	3.3	0.6	0.8	3.1	2.8	1.5	3.3	0.4	0.4	2.7	2.9	2.0
Total grains counted	200	300	266	119	315	600	161	400	600	60	250	500	148	680	700

from McKay et al. (1976)

APPENDIX 7. Major, minor, and trace element abundances

TABLE A7.1. MAJOR AND MINOR ELEMENTAL ABUNDANCES IN THE 60010 SOIL COLUMN

60010 sub-sample #	O%	Si%	Al%	Ca%	Mg%	Fe%	Ti%	Na%	K%	Cr%	Mn%
239	43.8	20.2	15.1	12.0	3.8	3.75	0.316	0.301	0.090	0.086	0.069
40	41.1	21.5	14.7	12.1	3.9	6.42	0.414	0.326	0.087	0.088	0.069
224	44.8	20.4	14.2	11.3	3.7	3.67	0.269	0.309	0.086	0.079	0.059
219	42.7	22.4	14.5	11.5	3.7	3.74	0.378	0.313	0.092	0.085	0.067
203	44.0	21.4	14.4	11.6	3.9	4.70	0.457	0.308	0.089	0.083	0.068
199	43.5	22.0	14.8	11.1	3.4	3.99	0.278	0.331	0.094	0.080	0.059
191	43.5	22.6	14.2	11.1	3.5	3.72	0.351	0.318	0.095	0.087	0.066
242	43.0	21.0	15.8	12.9	3.1	3.14	0.346	0.296	0.076	0.066	0.054
179	43.0	22.5	15.5	12.2	3.3	3.43	0.486	0.303	0.078	0.070	0.058

from Ali and Ehmann (1977)

TABLE A7.2. TRACE ELEMENT ABUNDANCES IN 60010

60010 sub-sample #	Sc ppm	Co ppm	Ba* ppm	La ppm	Ce ppm	Nd* ppm	Sm ppm	Eu ppm	Tb ppm	Dy* ppm	Yb ppm	Lu ppm	Hf ppm	Th* ppm	V ppm	Ta ppm	Ni ppm
239	8.13	29.9	120.	12.3	26.	20.	5.5	1.10	0.81	3.1	3.09	0.59	4.1	0.9	19.4	0.50	550.
40	9.54	142.	180	13.0	36.	15	6.2	1.23	1.44	4.8	3.17	0.64	4.1	1.0	25.2	0.70	10600
224	8.07	31.5	120.	11.7	28.	11.	5.2	1.14	0.77	4.0	3.20	0.60	3.6	1.0	15.4	0.56	440.
219	8.96	26.8	120.	11.5	27.	15.	5.3	1.05	0.70	3.2	2.90	0.63	3.8	1.6	35.4	0.60	200.
203	8.87	63.2	160.	10.8	30.	19.	5.2	1.16	0.82	3.4	3.22	0.60	3.1	1.3	24.4	0.46	1160.
199	8.42	49.2	110.	11.9	26.	17.	5.3	1.10	0.78	3.0	3.00	0.58	3.6	0.8	24.0	0.43	710.
191	8.33	22.7	140.	12.3	23.	15.	5.7	1.09	0.74	3.0	2.82	0.63	3.6	1.7	21.0	0.49	470.
242	6.96	31.7	100.	9.8	21.	14.	4.3	1.07	0.67	2.6	2.21	0.48	2.8	1.0	17.9	0.42	390.
179	7.94	28.7	160.	11.3	22.	14.	5.0	1.11	0.71	2.6	2.61	0.56	3.5	1.0	35.5	0.37	370.

*Estimated accuracy for most trace-element determinations is ±5–10%, relative. Due to poor counting statistics for this irradiation unit, data for Ba, Nd, Dy, and Th are assigned error limits of ±15–20%.

from Ali and Ehmann (1977)

TABLE A7.3. MAJOR AND MINOR ELEMENTAL ABUNDANCES IN THE 60009 SOIL COLUMN

60009 Subsample #	0%	Si%	Al%	Ca%	Mg%	Fe%	Ti%	Na%	K%	Cr%	Mn%
302	44.6	21.6	14.8	10.9	3.97	3.78	0.394	0.31	0.092	0.083	0.058
307	42.8	21.9	14.7	10.1	4.76	3.76	0.435	0.30	0.098	0.084	0.062
310	42.1	22.1	14.3	11.3	(4.38)	3.64	0.425	0.29	0.084	0.078	0.060
315	44.3	21.8	14.6	11.4	3.93	3.59	0.405	0.29	0.082	0.080	0.060
319	43.7	21.4	14.5	12.7	4.63	3.71	0.307	0.30	0.099	0.080	0.059
322	43.5	21.9	14.8	12.2	4.68	3.88	0.395	0.31	0.096	0.079	0.059
334	43.4	20.9	14.8	12.2	3.65	3.42	0.337	0.29	0.108	0.078	0.058
341	45.4	21.9	15.3	11.9	—	3.08	0.340	0.32	0.102	0.050	0.057
344	45.2	21.8	15.1	(11.0)	3.22	3.03	0.246	0.31	0.046	0.047	0.048
347	44.1	21.9	15.4	12.3	3.41	2.81	0.247	0.31	0.065	0.049	0.045
377	43.8	21.2	16.6	12.8	2.98	2.59	0.309	0.29	0.041	0.039	0.042
380	42.6	20.9	14.9	13.6	3.74	3.04	0.421	0.30	0.052	0.049	0.050
363	43.9	21.2	15.4	12.5	3.77	2.80	0.221	0.29	0.067	0.046	0.046
373	44.0	21.1	15.9	11.9	4.35	3.46	0.349	0.31	0.058	0.059	0.052
385	44.8	21.5	14.5	11.4	4.46	3.60	0.376	0.31	0.102	0.079	0.058
391	45.3	21.7	14.2	13.7	4.35	3.94	0.511	0.31	0.108	0.089	0.060
394	44.1	20.8	15.2	—	—	3.48	—	0.30	0.089	0.077	0.056
402	45.0	21.0	15.2	(11.2)	3.85	2.98	0.210	0.30	0.090	0.066	0.055
406	44.7	20.8	15.2	14.0	4.08	2.91	0.436	0.27	0.082	0.060	0.048
409	44.0	19.9	17.7	13.3	2.41	1.80	0.256	0.28	0.037	0.035	0.031
413	46.9	19.7	17.5	12.3	2.53	1.49	0.230	0.29	—	0.023	0.028
419	45.2	20.8	17.4	13.7	2.60	1.84	0.258	0.29	0.040	0.027	0.032
416	45.2	20.9	18.0	11.0	2.21	1.33	0.184	0.29	0.033	0.018	0.026
422	44.5	21.0	17.0	13.0	2.29	1.69	0.284	0.28	0.040	0.025	0.030
425	44.8	21.1	16.7	14.3	2.41	1.79	0.224	0.30	0.032	0.025	0.030
432	44.9	21.4	16.9	13.1	2.23	1.61	0.228	0.29	0.026	0.029	0.030
441	45.4	22.5	14.1	11.1	4.53	4.18	0.432	0.32	0.122	0.093	0.068

Note: Values in parenthesis calculated only by difference. Ca data are preliminary and may be 5–10% relative too high, due to analytical problems in the determination of this element.

from Ali and Ehmann (1976)

TABLE A7.4. TRACE ELEMENT ABUNDANCES IN 60009

60009 Subsample #	Sc ppm	Co ppm	Cl ppm	Ba ppm	La ppm	Ce ppm	Nd ppm	Sm ppm	Eu ppm	Tb ppm	Yb ppm	Lu ppm	Hf ppm	Th ppm	V ppm	Ta ppm
302	7.7	23.2	410	139	11.7	35.9	20.6	4.9	1.19	0.94	3.91	0.43	3.4	1.69	24	0.57
307	7.7	20.7	69	166	12.4	30.8	23.7	4.8	1.16	0.79	3.94	0.42	3.4	2.01	31	0.74
310	7.4	21.7	—	134	11.6	29.8	20.8	4.2	1.10	0.87	3.65	0.39	3.3	1.44	—	0.68
315	7.4	22.8	57	90	11.4	28.2	15.5	4.0	1.10	0.73	3.48	0.40	3.4	1.20	19	0.54
319	7.4	24.2	190	136	12.2	28.6	25.5	4.8	1.10	0.83	3.59	0.40	3.8	1.91	27	0.58
322	7.4	27.9	250	120	13.6	32.1	30.7	4.7	1.17	0.88	3.79	0.46	3.8	1.50	20	0.69
334	6.9	20.7	170	157	12.7	30.4	24.0	4.9	1.17	0.90	3.86	0.42	3.4	2.27	22	0.58
341	6.0	25.9	—	124	11.7	27.2	20.8	4.0	0.99	0.78	3.75	0.42	3.1	1.74	—	0.52
344	6.0	23.3	170	196	13.0	24.8	12.6	3.6	1.28	0.79	3.27	0.40	3.0	1.12	20	0.37
347	5.7	17.2	220	151	10.8	26.0	17.0	4.6	1.05	0.87	3.34	0.36	2.6	1.42	20	0.62
377	5.1	17.8	380	102	98.7	133.0	45.9	3.3	1.28	0.61	2.97	0.38	2.0	1.07	23	0.47
380	6.1	18.8	260	122	11.4	24.3	11.4	4.8	1.13	0.78	3.53	0.42	3.4	1.40	21	0.51
362	5.6	19.0	200	122	9.3	19.7	10.0	3.3	1.16	0.57	3.26	0.34	2.6	1.24	19	0.48
373	7.1	20.6	250	120	12.0	39.2	12.8	4.1	1.18	0.84	3.64	0.48	3.2	1.11	34	0.57
385	7.4	19.5	200	96	11.6	30.6	17.6	4.3	1.21	0.79	3.32	0.40	2.9	1.55	24	0.46
391	8.4	22.7	60	146	12.9	32.6	22.5	5.2	1.25	0.85	3.77	0.46	4.1	2.24	24	0.48
394	6.6	16.6	—	64	9.8	25.6	20.9	3.9	1.17	0.68	2.92	0.34	2.7	1.07	—	—
402	5.7	18.9	120	110	10.0	25.4	20.4	4.0	1.14	0.71	3.12	0.34	3.1	1.23	16	0.50
406	5.5	21.6	23	88	9.7	24.0	23.5	3.5	1.15	0.62	2.92	0.32	2.5	1.20	25	0.38
409	3.1	10.5	42	46	5.0	12.0	11.8	1.9	1.00	0.35	1.26	0.15	1.3	0.57	13	—
413	3.2	7.0	500	66	5.6	11.6	7.2	1.6	1.14	0.36	2.14	0.16	0.96	0.62	6.3	0.25
419	3.3	9.7	200	89	6.7	12.0	5.5	2.0	0.89	0.40	1.67	0.19	1.2	0.75	—	0.31
416	2.5	6.9	350	53	3.9	6.4	3.8	1.3	0.94	0.22	1.41	0.14	1.0	0.46	7.4	0.15
422	3.0	10.5	180	55	3.5	11.1	7.0	1.8	0.80	0.29	1.52	0.17	0.97	0.70	25	0.26
425	3.2	9.5	120	59	4.3	15.9	4.9	1.7	1.14	0.33	1.55	0.18	1.4	0.58	10	0.19
432	3.0	7.1	35	55	4.3	9.8	7.3	1.4	0.88	0.31	1.60	0.14	1.1	0.55	10	0.22
441	8.6	27.1	32	124	13.8	34.3	28.6	5.5	1.24	1.00	4.27	0.50	4.2	2.40	38	0.60

*Estimated accuracy for most trace element determinations is ±5-10% relative.

from Ali and Ehmann (1976)

APPENDIX 8. Chemical compositions

TABLE A8.1. COMPOSITIONS OF BULK SOIL SAMPLES AND SIZE FRACTIONS OF SOILS FROM 60010

Sample	Size	Depth (cm)	I_s/FeO <250mm	% FeO	% Na_2O	Sc	Cr	Co	Ni	Hf	Ta	Th	La	Ce	Sm	Eu	Tb	Yb	Lu
60010,1077	Unsieved	0.5-1.0	90	5.27	0.47	9.3	840	23.5	320	4.2	0.63	1.9	12.1	32.9	5.9	1.16	1.26	4.4	0.62
	90-150μm			5.27	0.47	9.1	830	29.2	410	4.3	0.62	2.1	12.1	33.1	5.9	1.16	1.30	4.3	0.61
	<20μm			5.25	0.47	9.2	930	23.2	410	4.4	0.62	2.0	13.3	34.6	6.2	1.17	1.39	4.3	0.63
60010,1076	Unsieved	3.5-4.0	92	5.40	0.47	9.4	860	29.2	410	4.6	0.66	2.3	13.6	36.2	6.5	1.17	1.46	4.6	0.65
	90-150μm			5.91	0.47	9.5	800	44.8	650	4.4	0.73	2.2	12.1	32.4	5.8	1.16	1.27	4.4	0.61
	<20μm			5.30	0.46	9.3	990	24.4	530	4.4	0.69	2.2	13.1	35.0	6.1	1.15	1.25	4.5	0.62
60010,1075	Unsieved	11.0-11.5	67	6.10	0.46	9.4	800	61.0	970	4.6	0.53	1.9	12.0	31.7	5.7	1.13	1.32	4.3	0.60
	90-150μm			5.41	0.48	9.4	930	29.5	530	4.5	0.63	2.0	11.7	30.6	5.6	1.15	1.27	4.2	0.59
	<20μm			5.30	0.46	9.2	890	25.1	2190	5.0	0.59	2.0	12.9	33.2	6.0	1.13	1.24	4.1	0.59
60010,1074	Unsieved	14.0-14.5	47	5.00	0.48	8.7	830	20.6	260	4.2	0.57	2.1	12.3	32.7	5.8	1.09	1.17	4.4	0.59
	90-150μm			4.77	0.45	7.9	660	22.1	270	3.7	0.43	1.7	9.5	26.8	4.6	1.07	0.95	3.4	0.46
	<20μm			5.34	0.49	8.9	940	26.0	420	4.3	0.54	2.1	12.6	33.7	5.9	1.12	1.20	4.2	0.56
60010,3107	Unsieved	20.0-20.5	26	6.40	0.51	13.2	970	26.3	340	7.2	0.91	3.1	17.2	46.3	8.5	1.28	1.84	6.6	0.91
	90-150μm			5.65	0.50	10.5	890	33.6	470	4.7	0.73	2.3	13.5	36.1	6.6	1.20	1.50	4.9	0.70
	<20μm			5.45	0.53	10.1	1170	20.7	460	6.0	0.83	3.0	18.4	48.0	8.7	1.27	1.94	5.5	0.81
60010,1073	Unsieved	24.5-25.0	53	4.47	0.45	7.9	650	18.9	270	3.7	0.57	1.8	10.3	28.3	4.9	1.10	1.14	3.6	0.51
	90-150μm			4.01	0.46	6.7	560	23.8	370	3.1	0.38	1.4	10.2	25.9	4.3	1.02	0.95	3.1	0.43
	<20μm			4.66	0.46	8.2	730	21.3	1280	4.8	0.51	2.0	12.0	31.8	5.7	1.10	1.19	3.9	0.52

from Blanchard et al. (1977)

TABLE A8.2. COMPOSITIONS OF BULK SOIL SAMPLES AND SIZE FRACTIONS OF SOILS FROM 60009

Sample	Size	Fraction	Weight fraction	% FeO	% Na_2O	Sc	Cr	Co	Ni	Hf	Ta	Th	La	Ce	Sm	Eu	Tb	Yb	Lu
60009,454	Unsieved	Total		5.17	0.52	8.3	740	32.0	450	4.9	0.66	2.0	13.4	34.5	6.1	1.19	1.59	4.5	0.59
	90–150	Total		4.56	0.49	8.1	660	18.8	240	3.8	0.55	1.5	10.7	28.5	5.1	1.12	1.35	3.8	0.52
	<20	Total		5.13	0.70	8.8	880	24	420	4.6	0.66	2.3	13.6	35.5	6.3	1.22	1.64	4.5	0.60
	90–150	Magnetic	0.279	6.80	0.51	11.1	940	49	730	5.6	0.81	2.3	15.6	42.1	7.4	1.24	1.96	5.5	0.73
	90–150	Nonmagnetic	0.721	3.70	0.48	7.0	550	7.1	50	3.1	0.45	1.1	8.9	23.2	4.2	1.08	1.11	3.2	0.44
	<20	Magnetic	0.461	6.44	0.86	10.3	1140	37	690	5.2	0.84	2.3	13.6	35.7	6.4	1.21	1.66	4.7	0.62
	<20	Nonmagnetic	0.539	4.01	0.56	7.4	660	13.0	190	4.1	0.51	2.3	13.6	35.3	6.2	1.23	1.62	4.2	0.58
60009,455	Unsieved	Total		3.54	0.41	5.6	470	14.0	200	2.4	0.36	1.1	7.1	18.4	3.16	0.94	0.62	2.3	0.31
	90–150	Total		3.34	0.42	5.5	430	14.4	170	2.1	0.29	0.9	6.2	16.5	2.83	0.95	0.49	2.1	0.29
	<20	Total		4.66	0.44	7.7	740	16.9	250	3.2	0.47	1.4	9.8	25.4	4.21	1.00	0.78	3.2	0.43
	90–150	Magnetic	0.134	7.83	0.49	10.9	920	80	1120	5.9	0.88	2.3	16.2	43.5	7.4	1.23	1.35	5.8	0.77
	90–150	Nonmagnetic	0.866	2.65	0.41	4.6	350	4.2	30	1.5	0.20	0.65	4.61	12.4	2.13	0.91	0.36	1.5	0.21
	<20	Magnetic	0.353	6.77	0.44	10.5	1040	34.0	530	4.5	0.66	1.8	13.3	34.1	5.4	1.03	1.03	4.3	0.59
	<20	Nonmagnetic	0.647	3.51	0.43	6.2	570	7.6	100	2.5	0.36	1.2	7.9	20.7	3.57	0.98	0.65	2.6	0.34
60009,456	Unsieved	Total		5.06	0.49	9.4	770	19.0	220	4.5	0.49	2.3	12.8	33.2	6.1	1.16	1.08	4.5	0.63
	90–150	Total		5.19	0.48	9.7	800	23.3	290	4.6	0.48	1.9	11.6	31.4	5.6	1.18	1.06	4.4	0.60
	<20	Total		5.20	0.50	9.2	850	22.0	360	4.6	0.58	2.2	13.7	35.8	6.3	1.17	1.16	4.5	0.61
	90–150	Magnetic	0.316	7.20	0.51	11.6	990	56	770	5.4	0.77	2.8	16.2	42.3	7.8	1.25	1.42	5.8	0.81
	90–150	Nonmagnetic	0.684	4.26	0.47	6.8	710	8.2	60	4.3	0.34	1.5	9.5	26.4	4.5	1.15	0.88	3.7	0.50
	<20	Magnetic	0.467	7.05	0.49	11.4	1120	37.0	630	5.1	0.90	2.2	15.0	39.1	6.8	1.11	1.30	5.0	0.67
	<20	Nonmagnetic	0.533	3.58	0.52	7.2	620	8.9	120	4.2	0.30	2.2	12.6	32.9	5.9	1.22	1.04	4.1	0.56
60009,457	Unsieved	Total		1.95	0.42	3.24	270	9.8	90	1.4	0.15	0.54	4.08	11.0	1.85	0.92	0.31	1.39	0.19
	90–150	Total		1.58	0.41	2.60	190	4.7	50	1.7	0.13	0.40	2.94	7.6	1.39	0.90	0.25	1.2	0.17
	<20	Total		2.64	0.44	4.38	420	10.6	180	2.0	0.24	0.83	6.16	17.6	2.71	0.98	0.48	2.0	0.27
	90–150	Magnetic	0.041	7.42	0.52	11.2	890	58	850	5.8	1.0	2.5	16.3	41.8	7.7	1.24	1.43	5.7	0.75
	90–150	Nonmagnetic	0.959	1.33	0.41	2.23	160	2.5	10	3.6	0.09	0.31	2.37	6.1	1.12	0.88	0.20	1.0	0.14
	<20	Magnetic	0.262	4.92	0.44	7.62	800	26.9	470	3.4	0.47	1.3	9.65	27.2	4.18	1.02	0.76	3.1	0.47
	<20	Nonmagnetic	0.738	1.83	0.44	3.23	280	4.8	70	1.5	0.16	0.67	4.92	14.2	2.19	0.97	0.38	1.6	0.20
60009,458	Unsieved	Total		5.20	0.50	9.56	760	22	280	4.7	0.60	1.9	12.7	35.2	5.8	1.19	1.07	4.4	0.59
	90–150	Total		5.95	0.50	10.2	820	37.5	500	6.2	0.65	1.8	12.3	32.4	5.7	1.18	1.32	4.7	0.64
	<20	Total		5.70	0.53	9.8	890	27.7	460	4.8	0.74	2.6	14.7	40.3	6.9	1.25	1.18	4.5	0.66
	90–150	Magnetic	0.373	7.81	0.50	11.5	930	85	1210	5.6	0.66	2.3	15.7	41.9	7.2	1.23	1.98	5.7	0.77
	90–150	Nonmagnetic	0.627	4.85	0.50	9.5	750	9.2	70	6.6	0.64	1.5	10.3	26.8	4.8	1.15	0.92	4.1	0.56
	<20	Magnetic	0.539	7.08	0.52	11.5	1050	41	710	5.3	0.89	2.9	15.1	39.3	7.4	1.22	1.26	5.9	0.75
	<20	Nonmagnetic	0.461	4.09	0.54	7.9	700	12	160	4.2	0.56	2.3	14.2	41.5	6.4	1.28	1.08	2.9	0.56
Standard values		BCR-1		12.2	3.35	31.6		36.0		5.2	0.91	6.0	25.2	54.2	6.80	1.97	1.15	3.48	0.526
		DTS-1					4580		2390										
Relative uncertainties				2%	2%	2%	2%	4%	10–50%	8%	11%	10%	2%	8%	3%	4%	9%	5%	5%

from Blanchard et al. (1976)

APPENDIX 9. Noble gas data

Tables A9.1 through A9.8 are from Bogard and Hirsch (1976, 1977).

TABLE A9.1

Isotopic concentrations (cm^3 STP/g) of noble gases in grain size separates of core 60010. Abundance uncertainties are estimated as ±5% for He, Ne, Ar, and Xe and ±10% for Kr. Relative uncertainties for isotopic ratios are one sigma of the mean of multiple measurements of individual ratios plus one-half the applied blank corrections. Absolute isotopic ratios have an additional uncertainty of ±0.1%/mass unit. Blank corrections were generally <1%, except for some data on the coarsest grain sizes where blanks were 1–3% for soils and ~6–8% for plagioclase separates. Approximate subsurface soil depths and sample parent numbers are indicated.

Sample	Wt.(mg)	$^{3}He \times 10^{-6}$	$^{4}He \times 10^{-2}$	$^{22}Ne \times 10^{-8}$	$^{20}Ne/^{22}Ne$	$^{22}Ne/^{21}Ne$	$^{36}Ar \times 10^{-5}$	$^{36}Ar/^{38}Ar$	$^{40}Ar/^{36}Ar$	$^{84}Kr \times 10^{-8}$	$^{132}Xe \times 10^{-8}$
60010,1077 (.5–1 cm) parent .1066											
250–150 μm	25.08	3.56	.84	1.76	12.32 ± .03	22.27 ± .11	13.4	5.14 ± .01	1.56 ± .01	8.66	1.31
150–90 μm	9.11	4.81	1.13	2.22	12.33 ± .03	23.70 ± .13	15.8	5.17 ± .01	1.46 ± .01	10.4	1.60
90–75 μm	9.97	5.18	1.24	2.49	12.36 ± .05	24.09 ± .31	18.1	5.17 ± .01	1.38 ± .02	12.2	1.82
75–45 μm	16.20	6.59	1.62	3.13	12.40 ± .03	25.15 ± .18	21.6	5.19 ± .01	1.32 ± .01	13.9	1.91
45–20 μm	10.66	10.9	2.67	4.79	12.46 ± .03	27.39 ± .21	27.9	5.22 ± .01	1.23 ± .01	19.0	2.89
20–10 μm	6.04	22.3	5.66	10.4	12.55 ± .03	29.46 ± .21	59.8	5.23 ± .01	1.17 ± .01	35.6	5.36
60010,1076 (3.5–4 cm) parent .1058											
250–150 μm	28.13	3.04	.696	1.36	12.32 ± .15	21.76 ± .35	12.5	5.16 ± .01	1.48 ± .01	7.50	1.06
150–90 μm	11.14	4.92	1.16	2.13	12.48 ± .04	22.91 ± .11	15.7	5.15 ± .01	1.42 ± .01	9.15	1.30
90–75 μm	10.31	5.42	1.32	2.47	12.37 ± .03	23.82 ± .46	18.8	5.17 ± .01	1.38 ± .01	11.4	1.96
75–45 μm	17.74	7.06	1.71	3.09	12.41 ± .03	25.16 ± .38	22.3	5.19 ± .01	1.24 ± .01	14.2	2.07
45–20 μm	9.77	11.2	2.83	4.99	12.47 ± .04	27.25 ± .14	33.8	5.20 ± .01	1.23 ± .01	20.9	3.43
20–10 μm	6.36	23.3	5.91	10.1	12.51 ± .03	29.21 ± .38	55.6	5.22 ± .01	1.09 ± .01	42.3	5.00
<10 μm	10.27	46.4	11.6	18.7	12.71 ± .03	31.25 ± .49	111	5.23 ± .01	1.07 ± .01	66.6	8.35
Plagioclase	4.66	.310	.0685	.120	11.56 ± .07	11.19 ± .46	1.19	4.65 ± .01	3.08 ± .10	1.78	.432
60010.1076 Magnetic separate											
500–250 μm	5.97	3.94	.92	1.95	12.35 ± .04	22.47 ± .24	16.1	5.160 ± .005	1.71 ± .01	10.4	1.56
150–90 μm	4.13	6.92	1.74	3.38	12.36 ± .03	25.19 ± .17	26.6	5.178 ± .005	1.39 ± .01	16.9	2.36
75–45 μm	6.05	—	—	—	—	—	30.1	5.185 ± .010	1.25 ± .01	21.9	3.32
45–20 μm	5.00	14.3	3.62	6.30	12.41 ± .03	27.36 ± .21	39.5	5.204 ± .005	1.18 ± .01	24.8	3.68
20–10 μm	2.82	23.9	6.23	10.6	12.44 ± .05	29.30 ± .27	59.2	5.218 ± .005	1.09 ± .01	38.8	5.48
<10 μm	1.39	36.6	9.65	14.0	12.64 ± .03	31.05 ± .34	108.6	5.238 ± .005	1.089 ± .005	68.5	8.85
60010.1075 (11–11.5 cm) parent .1038											
250–150 μm	19.12	4.29	.983	1.72	12.28 ± .05	20.45 ± .13	13.0	5.14 ± .01	1.61 ± .01	7.60	1.11
150–90 μm	11.48	4.89	1.14	1.97	12.36 ± .03	22.37 ± .30	12.5	5.16 ± .01	1.50 ± .01	7.18	1.17
90–75 μm	8.19	5.81	1.34	2.51	12.34 ± .03	22.52 ± .27	17.6	5.16 ± .01	1.41 ± .01	11.8	1.77
75–45 μm	16.13	8.22	1.98	3.53	12.44 ± .03	24.68 ± .17	22.6	5.18 ± .01	1.32 ± .01	15.7	2.30
45–20 μm	12.92	9.53	2.41	4.65	12.45 ± .03	26.41 ± .16	28.5	5.19 ± .01	1.24 ± .01	18.7	2.92
20–10 μm	4.89	17.7	4.58	8.60	12.51 ± .04	28.83 ± .17	47.2	5.16 ± .06	1.15 ± .01	30.3	4.27
<10 μm	4.49	44.8	11.5	16.7	12.63 ± .08	30.62 ± .27	91.7	5.24 ± .02	1.15 ± .01	64.5	8.38

TABLE A9.1 (Continued)

60010,1074 (14–14.5 cm) parent ,1031											
250–150 μm	20.87	2.78	.528	1.21	11.91 ± .07	14.65 ± .17	6.93	5.04 ± .01	2.70 ± .02	3.78	.734
150–90 μm	9.79	3.72	.757	1.63	12.00 ± .07	17.11 ± .28	9.22	5.17 ± .01	2.42 ± .03	5.09	1.04
90–75 μm	7.19	4.02	.820	1.89	11.94 ± .09	17.60 ± .43	10.3	5.18 ± .01	2.39 ± .04	5.31	1.02
75–45 μm	13.12	5.10	1.10	2.37	12.09 ± .06	19.27 ± .13	12.7	5.12 ± .01	2.31 ± .01	6.58	1.22
45–20 μm	11.51	8.04	1.83	4.09	12.24 ± .04	23.58 ± .13	21.1	5.15 ± .01	2.18 ± .01	10.4	1.99
20–10 μm	7.09	15.0	3.58	8.15	12.31 ± .03	26.94 ± .11	—	—	—	—	—
< 10 μm	3.04	36.9	8.87	16.5	12.56 ± .03	29.53 ± .25	73.1	5.25 ± .01	2.17 ± .01	37.6	6.20
Plagioclase	12.61	.0673	.0121	.0401	4.72 ± .24	1.87 ± .08	.0776	2.48 ± .03	17.8 ± .6	.637	.218
60010,3107 (20–20.5 cm) parent ,3027											
250–150 μm	22.00	2.87	.421	1.12	11.33 ± .03	9.44 ± .06	5.81	4.87 ± .01	3.61 ± .01	3.29	.581
150–90 μm	10.65	3.39	.528	1.42	11.55 ± .04	11.29 ± .10	7.34	4.96 ± .01	3.27 ± .02	4.27	.733
90–75 μm	7.39	3.57	.543	1.46	11.54 ± .07	11.23 ± .28	7.52	4.99 ± .01	3.25 ± .01	5.67	1.13
75–45 μm	14.45	3.96	.612	1.71	11.65 ± .04	12.38 ± .12	7.99	5.02 ± .06	3.30 ± .02	5.99	1.22
45–20 μm	9.25	6.46	1.32	3.35	12.05 ± .05	18.17 ± .09	13.9	5.10 ± .01	2.97 ± .01	8.20	1.54
20–10 μm	5.87	5.36	1.26	4.50	12.27 ± .03	22.01 ± .08	20.5	5.15 ± .01	2.80 ± .01	11.8	2.20
< 10 μm	2.64	20.0	5.19	11.3	12.43 ± .07	27.54 ± .31	51.0	5.23 ± .01	2.94 ± .01	29.3	4.91
60010,1073 (24.5–25 cm) parent ,1004											
250–150 μm	21.40	2.21	.457	.943	11.98 ± .03	14.94 ± .13	6.18	5.07 ± .01	2.22 ± .01	3.93	.613
150–90 μm	10.76	3.26	.711	1.41	12.15 ± .06	17.87 ± .18	8.86	5.11 ± .01	2.00 ± .01	5.86	.832
75–45 μm	19.18	5.77	1.37	2.54	12.32 ± .03	21.51 ± .18	14.6	5.16 ± .01	1.74 ± .01	8.86	1.36
45–20 μm	10.23	9.10	2.20	3.87	12.46 ± .06	24.39 ± .10	15.6	5.19 ± .01	1.71 ± .01	15.1	2.38
20–10 μm	6.88	16.1	4.07	7.71	12.45 ± .04	27.56 ± .18	38.0	5.21 ± .01	1.57 ± .01	23.0	3.29
<10 μm	6.16	34.2	8.66	14.3	12.60 ± .03	30.90 ± .32	72.9	5.24 ± .01	1.57 ± .01	44.0	5.71
Plagioclase	11.15	.108	.0236	.0553	8.16 ± .23	3.23 ± .13	.331	3.98 ± .01	3.77 ± .17	.568	.165
60010,1211 (22–22.5 cm) parent ,1											
White clast	10.59	.0779	.00829	.0416	5.32 ± 1.34	2.13 ± .55	1.54	3.23 ± .40	19.3 ± 3.8	.712	.203
60009,456											
Plagioclase	8.61	.137	.0200	.0683	5.96 ± .21	2.23 ± .11	.236	3.03 ± .01	8.31 ± .34	.983	.315

TABLE A9.2

Isotopic ratios of Kr in selected grain size fractions of 60010. Very small hydrocarbon corrections have been applied to ^{78}Kr and ^{80}Kr based on mass 79, and to ^{78}Kr for $(^{40}Ar)_2$. Relative uncertainties given are one sigma of the mean of multiple measurements, plus one-half the magnitude of the above corrections for ^{78}Kr and ^{80}Kr. Absolute ratios have an additional uncertainty of ±0.1%/mass unit.

Sample	$^{78}Kr/^{86}Kr$	$^{80}Kr/^{86}Kr$	$^{82}Kr/^{86}Kr$	$^{83}Kr/^{86}Kr$	$^{84}Kr/^{86}Kr$
60010.1077					
250–150 μm	.0225 ± .0005	.1379 ± .0010	.6692 ± .0020	.6733 ± .0020	3.270 ± .005
75–45 μm	.0215 ± .0008	.1350 ± .0008	.6661 ± .0016	.6687 ± .0011	3.266 ± .007
60010.1076					
250–150 μm	.0233 ± .0005	.1373 ± .0006	.6692 ± .0015	.6726 ± .0010	3.266 ± .006
150–90 μm	.0220 ± .0005	.1360 ± .0011	.6660 ± .0037	.6692 ± .0022	3.257 ± .010
<10 μm	.0200 ± .0001	.1296 ± .0005	.6567 ± .0012	.6570 ± .0007	3.266 ± .003
60010.1075					
250–150 μm	.0250 ± .0013	.1379 ± .0009	.6632 ± .0028	.6690 ± .0030	3.247 ± .011
150–90 μm	.0228 ± .0003	.1394 ± .0010	.6712 ± .0024	.6739 ± .0022	3.276 ± .011
<10 μm	.0203 ± .0001	.1307 ± .0014	.6596 ± .0015	.6576 ± .0016	3.260 ± .005
60010.1074					
250–150 μm	.0263 ± .0007	.1771 ± .0015	.7077 ± .0046	.6970 ± .0016	3.282 ± .013
75–45 μm	.0254 ± .0017	.1750 ± .0021	.6962 ± .0048	.6829 ± .0024	3.271 ± .015
<10 μm	.0265 ± .0041	.1349 ± .0031	.6628 ± .0033	.6609 ± .0025	3.268 ± .011
60010,3107					
250–150 μm	.0344 ± .0009	.1773 ± .0016	.7238 ± .0018	.7441 ± .0029	3.309 ± .008
150–90 μm	.0323 ± .0016	.1659 ± .0011	.7068 ± .0057	.7191 ± .0029	3.292 ± .012
<10 μm	.0230 ± .0007	.1374 ± .0017	.6670 ± .0032	.6670 ± .0026	3.275 ± .011
60010.1073					
250–150 μm	.0258 ± .0007	.1460 ± .0009	.6800 ± .0026	.6865 ± .0032	3.267 ± .008
150–90 μm	.0242 ± .0009	.1416 ± .0010	.6755 ± .0025	.6791 ± .0037	3.272 ± .012
<10 μm	.0202 ± .0001	.1300 ± .0012	.6572 ± .0014	.6576 ± .0009	3.254 ± .002
60010.1211					
White clast	—	.1317 ± .0090	.6692 ± .0166	.6613 ± .0121	3.257 ± .035

TABLE A9.3

Isotopic ratios of Xe in selected grain size fractions of 60010. Relative uncertainties given are one sigma of the mean of multiple measurements. Absolute ratios have an additional uncertainty of ±0.1%/mass unit.

Sample	$^{124}Xe/^{136}Xe$	$^{126}Xe/^{136}Xe$	$^{128}Xe/^{136}Xe$	$^{129}Xe/^{136}Xe$	$^{130}Xe/^{136}Xe$	$^{131}Xe/^{136}Xe$	$^{132}Xe/^{136}Xe$	$^{134}Xe/^{136}Xe$
60010,1077								
250–150 μm	.0233 ± .0010	.0291 ± .0005	.2970 ± .0031	3.456 ± .022	.5547 ± .0041	2.776 ± .013	3.314 ± .017	1.231 ± .007
75–45 μm	.0218 ± .0008	.0262 ± .0025	.2928 ± .0020	3.449 ± .013	.5531 ± .0064	2.762 ± .011	3.313 ± .012	1.230 ± .005
60010,1076								
250–150 μm	.0239 ± .0008	.0299 ± .0004	.2981 ± .0015	3.447 ± .015	.5542 ± .0026	2.769 ± .013	3.312 ± .016	1.227 ± .005
150–90 μm	.0221 ± .0007	.0282 ± .0009	.2941 ± .0029	3.433 ± .022	.5504 ± .0032	2.761 ± .014	3.306 ± .022	1.231 ± .009
<10 μm	.0172 ± .0003	.0172 ± .0003	.2801 ± .0019	3.436 ± .008	.5451 ± .0020	2.709 ± .007	3.298 ± .007	1.224 ± .003
60010,1075								
250–150 μm	.0258 ± .0006	.0339 ± .0011	.3047 ± .0060	3.443 ± .017	.5519 ± .0028	2.778 ± .011	3.296 ± .012	1.223 ± .009
150–90 μm	.0230 ± .0014	.0277 ± .0014	.2896 ± .0026	3.389 ± .023	.5434 ± .0047	2.725 ± .015	3.273 ± .007	1.218 ± .006
<10 μm	.0160 ± .0003	.0162 ± .0004	.2684 ± .0019	3.362 ± .012	.5305 ± .0024	2.670 ± .012	3.269 ± .011	1.222 ± .005
600010,1074								
250–150 μm	.0246 ± .0020	.0342 ± .0056	.2942 ± .0093	3.227 ± .026	.5222 ± .0060	2.682 ± .019	3.166 ± .020	1.204 ± .013
75–45 μm	—	.0309 ± .0008	.2824 ± .0027	3.215 ± .016	.5209 ± .0035	2.645 ± .014	3.163 ± .017	1.200 ± .006
<10 μm	.0170 ± .0012	.0196 ± .0012	.2778 ± .0063	3.396 ± .018	.5379 ± .0101	2.680 ± .013	3.273 ± .021	1.221 ± .009
60010,3107								
250–150 μm	.0505 ± .0011	.0779 ± .0017	.3709 ± .0031	3.545 ± .023	.5989 ± .0060	2.985 ± .020	3.322 ± .016	1.222 ± .012
150–90 μm	.0411 ± .0015	.0626 ± .0019	.3462 ± .0039	3.500 ± .030	.5789 ± .0070	2.909 ± .021	3.308 ± .026	1.225 ± .013
<10 μm	.0206 ± .0012	.0242 ± .0011	.2833 ± .0045	3.429 ± .021	.5395 ± .0049	2.702 ± .019	3.267 ± .013	1.222 ± .008
60010,1073								
250–150 μm	.0303 ± .0027	.0413 ± .0009	.3085 ± .0046	3.390 ± .024	.5547 ± .0050	2.779 ± .027	3.269 ± .030	1.219 ± .015
150–90 μm	.0257 ± .0009	.0314 ± .0025	.2947 ± .0028	3.401 ± .020	.5465 ± .0036	2.754 ± .017	3.276 ± .018	1.220 ± .012
<10 μm	.0173 ± .0006	.0182 ± .0004	.2767 ± .0013	3.405 ± .013	.5363 ± .0047	2.695 ± .007	3.282 ± .007	1.226 ± .004
60010,1211								
White clast	—	—	.2203 ± .0104	3.030 ± .064	.4613 ± .0141	2.415 ± .041	3.063 ± .079	1.195 ± .031
60010,1076 Magnetic separate								
250–500 μm	.0242 ± .0008	.0310 ± .0012	.2965 ± .0037	3.409 ± .024	.5503 ± .0067	2.756 ± .013	3.292 ± .026	1.220 ± .010
<10 μm	.0159 ± .0013	.0161 ± .0012	.2720 ± .0026	3.373 ± .019	.5329 ± .0049	2.670 ± .016	3.260 ± .015	1.210 ± .007

TABLE A9.4

Isotopic ratios of the surface-correlated component and concentrations of the cosmogenic component (cm^3 STP/g) as determined by the ordinate-intercept technique. Cosmogenic data for plagioclase separates and 60010.1211 were calculated directly. Uncertainties given for isotopic ratios and abundances are one sigma of the ordinate intercept and of the slope, respectively, as derived by a first order regression. Normalized cosmogenic [^{126}Xe] have been corrected for differences in soil chemistry. Values of I_s/FeO are from McKay *et al.* (1976, 1977). Iron concentrations are from Blanchard *et al.* (1976) and Blanchard and Brannon (1977 and pers. comm.). Cosmogenic noble gas data for 60009.457 is reproduced from Bogard and Hirsch (1976).

Sample	$\frac{^4He}{^3He}$	$\frac{^{20}Ne}{^{22}Ne}$	$\frac{^{22}Ne}{^{21}Ne}$	$\frac{^{36}Ar}{^{38}Ar}$	$\frac{^{40}Ar}{^{36}Ar}$	$\frac{^3He}{10^{-8}}$	$\frac{^{21}Ne}{10^{-8}}$	$\frac{^{38}Ar}{10^{-8}}$	$\frac{^{80}Kr}{10^{-11}}$	$\frac{^{126}Xe}{10^{-11}}$	$\frac{^{126}Xe}{\text{Norm } 10^{-11}}$	$\frac{I_s}{FeO}$	[Fe] %
60010.1077	2546	12.57	31.5	5.26	.926	54.7	24.4	67.2	27.8	5.87	5.68	90	4.1
	±32	±.03	±.3	±.01	±.014	±6.2	±1.1	±9.1	±2.6	±.20			
60010.1076	2555	12.56	31.6	5.25	1.01	56.8	26.2	59.5	22.9	5.03	4.86	92	4.2
	±27	±.03	±.1	±.01	±.03	±5.1	±3.8	±4.7	±1.1	±.13			
Plagioclase						—	7.0	33.7	—	—			
60010.1076	2662	12.47	31.9	5.26	.83	72.1	27.6	88.3	—	7.95	7.68	—	—
Magnetic	±26	±.03	±7	±.01	±.04	±6.0	±3.5	±3.6	—	±.38			
60010.1075	2632	12.60	32.3	5.25	.960	82.8	33.1	65.9	24.8	6.62	6.62	67	4.8
	±41	±.03	±.4	±.01	±.024	±8.8	±1.6	±5.7	±1.9	±.37			
60010.1074	2478	12.39	31.1	≥5.25	2.1	93.5	45.9	61.9	57.2	4.62	5.69	47	3.9
	±20	±.03	±.5		±.1	±3.4	±1.9	±1.2	±1.7	±1.30			
Plagioclase						—	20.8	18.9	—	—			
60010.3107	2811	12.53	35.6	5.27	2.69	174	90.2	97.5	49.7	111	9.62	26	5.0
	±243	±.04	±1.1	±.02	±.10	±17	±4.9	±6.6	±1.5	±.3			
60010.1073	2565	12.58	32.0	5.25	1.46	69.6	36.2	48.9	22.3	5.07	5.82	53	3.5
	±19	±.03	±.8	±.01	±.03	±2.3	± 3	±4.7	±.2	±.17			
Plagioclase						—	15.8	23.0	—	—			
60010.1211	—	—	—	—	—	—	40.1	45.1	3.0	—	—	—	—
Clast							±.8	±1.0	±2.1				
60009.456	Plagioclase					—	29.3	38.4	—	—			
60009.457						45	21.5	29.0	6.85	0.79	+.0		
						±2.3	±3.0	±1.1	±1.45	± 28			
Plagioclase						4.5	17.8	24.3	—	—	—		

TABLE A9.5

Isotopic concentrations (cm^3 STP/g) of noble gases in grain size separates of Apollo 16 soils. Abundance uncertainties are estimated as ±5% for He, Ne, Ar, and Xe and ±10% for Kr. Relative uncertainties for isotopic ratios are one sigma of the mean of multiple measurements of individual ratios plus one-half the applied blank corrections. Absolute isotopic ratios have an additional uncertainty of ±0.1%/mass unit. Blank corrections were generally <1%, except for some data on the coarsest grain sizes. Approximate subsurface soil depths are indicated. The 250–500 μm sample of 60009,457 is a >99% plagioclase separate.

Sample	Wt.(mg)	^{3}He $\times10^{-6}$	^{4}He $\times10^{-2}$	^{22}Ne $\times10^{-5}$	$^{20}Ne/^{22}Ne$	$^{22}Ne/^{21}Ne$	^{36}Ar $\times10^{-4}$	$^{36}Ar/^{38}Ar$	$^{40}Ar/^{36}Ar$	^{84}Kr $\times10^{-8}$	^{132}Xe $\times10^{-8}$
60009,454 (~29 cm)											
250–150 μm	25.5	2.72	0.547	1.15	12.09 ± .03	15.44 ± .12	0.685	5.17 ± .01	2.26 ± .01	1.65	—
150–90 μm	4.96	3.91	0.831	1.71	12.16 ± .05	17.86 ± .28	1.08	5.04 ± .12	2.33 ± .01	6.93	1.49
90–75 μm	10.6	3.91	0.786	1.70	12.17 ± .05	17.81 ± .19	0.912	5.22 ± .03	—	4.92	0.96
75–45 μm	14.5	5.43	1.23	2.27	12.48 ± .04	20.58 ± .13	0.914	5.28 ± .01	—	7.88	1.38
45–20 μm	9.67	12.4	2.99	5.53	12.58 ± .05	26.12 ± .22	1.45	5.36 ± .03	—	16.0	2.76
<20 μm	5.01	30.5	7.65	13.0	12.51 ± .06	28.74 ± .15	6.30	5.31 ± .01	1.780 ± .005	32.0	4.61
<20 magnetic	2.32	33.3	8.35	13.7	12.43 ± .04	28.81 ± .17	5.68		1.695 ± .005	34.0	4.98
60009,455 (~43 cm)											
250–150 μm	11.06	1.26	0.242	0.536	11.71 ± .04	12.02 ± .28	0.386	5.09 ± .01	2.60 ± .02	2.59	0.42
90–75 μm	2.72	1.95	0.377	0.950	11.87 ± .03	15.07 ± .30	0.557	5.12 ± .01	2.71 ± .03	4.34	1.01
75–45 μm	9.61	3.24	0.663	1.40	12.03 ± .06	18.08 ± .22	0.745	5.19 ± .01	2.08 ± .01	3.89	0.70
45–20 μm	11.74	5.14	1.195	2.43	12.17 ± .03	21.83 ± .17	1.26	5.24 ± .03	1.98 ± .01	6.97	1.01
<20 μm	6.85	16.35	4.06	7.89	12.40 ± .03	28.18 ± .16	3.81	5.32 ± .01	1.94 ± .01	18.8	3.15
<20 magnetic	1.79	19.4	4.89	9.73	12.29 ± .05	28.24 ± .62	4.29	5.29 ± .01	1.78 ± .02	25.8	3.64
60009,456 (~48 cm)											
250–150 μm	19.73	3.26	0.626	1.36	11.92 ± .03	14.80 ± .09	0.902	5.15 ± .01	2.24 ± .01	4.08	0.49
150–90 μm	5.21	4.16	0.843	1.86	11.99 ± .03	16.22 ± .19	1.02	5.17 ± .01	2.17 ± .01	7.94	1.47
90–75 μm	10.74	6.06	1.28	2.52	12.14 ± .04	18.16 ± .16	1.44	5.21 ± .01	1.97 ± .01	7.71	1.30
75–45 μm	13.50	5.11	1.12	2.49	12.17 ± .03	19.32 ± .11	1.45	5.21 ± .01	1.86 ± .01	2.13	0.68
45–20 μm	10.19	8.26	1.93	4.01	12.30 ± .03	22.38 ± .10	2.14	5.26 ± .01	1.92 ± .01	11.9	2.09
<20 μm	7.83	28.1	6.59	12.4	12.54 ± .05	27.87 ± .27	5.99	5.31 ± .01	1.72 ± .01	28.1	4.57
<20 magnetic	2.38	34.3	8.54	14.9	12.42 ± .05	28.13 ± .35	6.49	5.32 ± .01	1.71 ± .01	35.0	5.47

TABLE A9.5 (Continued)

60009,457 (~53 cm)											
500–250 μm	13.63	.045	.009	.041	5.51 ± .44	2.18 ± .15	.014	2.92 ± .20	4.96 ± .11	.14	.034
250–150 μm	23.71	0.655	0.111	0.257	11.12 ± .07	8.60 ± .17	0.135	4.86 ± .01	2.84 ± .03	0.85	0.164
150–90 μm	5.49	0.93	0.182	0.404	11.89 ± .10	11.56 ± .60	0.234	5.04 ± .01	2.92 ± .03	1.88	—
90–75 μm	8.72	0.96	0.184	0.424	11.79 ± .08	12.41 ± .31	0.220	5.04 ± .03	2.52 ± .03	1.49	0.34
75–45 μm	15.30	1.20	0.267	0.62	12.06 ± .03	16.98 ± .22	0.400	5.17 ± .01	2.08 ± .02	2.25	0.34
45–20 μm	8.00	2.05	0.486	1.01	12.16 ± .06	20.49 ± .24	0.516	5.23 ± .01	2.00 ± .01	2.55	0.63
<20 μm	5.99	9.67	2.43	4.25	12.43 ± .04	27.31 ± .45	2.04	5.31 ± .01	1.91 ± .02	11.2	1.91
<20 magnetic	2.13	19.4	4.95	8.73	12.32 ± .03	27.86 ± .38	3.70	5.28 ± .01	1.80 ± .01	22.9	3.33
60009,458 (~58 cm)											
250–150 μm	14.11	3.83	0.76	1.64	11.93 ± .03	15.87 ± .15	1.06	5.15 ± .01	2.42 ± .01	5.81	1.02
150–90 μm	6.23	4.92	1.00	2.00	11.99 ± .13	16.88 ± .55	1.28	5.18 ± .01	2.20 ± .01	4.57	1.31
90–75 μm	6.72	5.37	1.16	2.09	12.16 ± .07	20.00 ± .38	0.81	5.27 ± .01	2.36 ± .01	4.77	0.80
75–45 μm	12.68	7.76	1.65	3.06	12.26 ± .03	22.15 ± .13	1.18	5.29 ± .01	2.10 ± .01	4.89	0.63
45–20 μm	11.77	9.87	2.32	4.85	12.22 ± .05	23.19 ± .38	2.33	5.24 ± .01	1.93 ± .01	12.8	2.20
<20 μm	7.25	26.9	6.85	12.7	12.46 ± .04	28.37 ± .12	5.81	5.30 ± .01	1.94 ± .01	35.7	5.13
<20 magnetic	2.31	37.5	9.11	15.8	12.46 ± .03	28.67 ± .07	6.60	5.31 ± .01	1.90 ± .01	41.6	6.13
60010,17 (~1 mm)											
>45 μm	3.95	6.52	1.56	2.76	12.28 ± .03	24.35 ± .28	1.70	5.29 ± .01	1.396 ± .006	11.4	1.40
<45 μm	1.71	21.4	5.36	8.37	12.43 ± .03	28.72 ± .26	5.66	5.30 ± .01	1.170 ± .005	34.6	4.06
60010,24 (~2 mm)											
>45 μm	5.40	4.92	1.22	2.16	12.24 ± .06	23.76 ± .10	1.60	5.25 ± .01	1.370 ± .005	11.36	1.68
<45 μm	0.78	13.4	3.39	5.65	12.33 ± .04	27.20 ± .37	3.06	5.29 ± .01	1.25 ± .02	22.8	3.23
60010,31 (~3 mm)											
>45 μm	7.35	7.75	1.84	3.19	12.34 ± .05	25.38 ± .16	2.21	5.26 ± .01	1.295 ± .005	14.5	2.00
<45 μm	2.72	19.5	4.93	8.19	12.41 ± .05	29.31 ± .31	4.96	5.30 ± .01	1.145 ± .005	28.6	3.81
60010,38 (~4 mm)											
>45 μm	7.71	6.79	1.62	2.78	12.30 ± .06	25.28 ± .31	1.85	5.265 ± .005	1.305 ± .005	12.3	1.41
<45 μm	4.76	24.8	6.27	9.77	12.43 ± .04	29.53 ± .11	5.56	5.30 ± .01	1.118 ± .006	34.7	4.41

TABLE A9.6

Isotopic ratios of Kr in selected grain size fractions of Apollo 16 soils. Small hydrocarbon corrections have been applied to ^{78}Kr and ^{80}Kr based on mass 79, and even smaller corrections for $(^{40}Ar)^{++}$ have been applied to ^{80}Kr. Relative uncertainties given are one sigma of the mean of multiple measurements, plus one-half the magnitude of the above corrections for ^{78}Kr and ^{80}Kr. Absolute ratios have an additional uncertainty of ±0.1%/mass unit.

Sample	$^{78}Kr/^{84}Kr$	$^{80}Kr/^{84}Kr$	$^{82}Kr/^{84}Kr$	$^{83}Kr/^{86}Kr$	$^{84}Kr/^{86}Kr$
60009,454					
<20 μm	—	.1318 ± .0017	.6628 ± .0018	.6630 ± .0039	3.262 ± .009
<20 mag.	.0187 ± .0050	.1315 ± .0017	.6624 ± .0036	.6605 ± .0037	3.260 ± .015
60009,455					
250–150 μm	—	.1451 ± .0062	.6881 ± .0066	.6968 ± .0078	3.291 ± .022
<20 μm	.0264 ± .0009	.1331 ± .0009	.6643 ± .0028	.6644 ± .0015	3.267 ± .011
<20 mag.	.0223 ± .0088	.1330 ± .0020	.6644 ± .0040	.6634 ± .0045	3.269 ± .012
60009,456					
250–150 μm	.0285 ± .0061	.1450 ± .0043	.6902 ± .0035	.6980 ± .0037	3.281 ± .012
<20 μm	.0274 ± .0008	.1332 ± .0010	.6638 ± .0018	.6642 ± .0023	3.262 ± .006
<20 mag.	.0203 ± .0061	.1327 ± .0009	.6644 ± .0023	.6650 ± .0036	3.273 ± .011
60009,457					
250–150 μm	—	.1541 ± .0076	.7029 ± .0061	.7195 ± .0056	3.303 ± .020
<20 μm	—	.1321 ± .0014	.6627 ± .0028	.6623 ± .0030	3.260 ± .005
<20 mag.	.0279 ± .0010	.1334 ± .0010	.6633 ± .0041	.6643 ± .0055	3.264 ± .012
60009,458					
250–150 μm	.0240 ± .0068	.1461 ± .0015	.6843 ± .0035	.6937 ± .0048	3.286 ± .014
<20 μm	.0232 ± .0003	.1329 ± .0007	.6640 ± .0014	.6650 ± .0018	3.270 ± .022
<20 mag.	.0204 ± .0029	.1321 ± .0010	.6648 ± .0017	.6634 ± .0018	3.268 ± .007
60010,17					
>45 μm	.0213 ± .0080	.1283 ± .0048	.6663 ± .0032	.6672 ± .0034	3.267 ± .010
<45 μm	.0205 ± .0049	.1321 ± .0011	.6622 ± .0035	.6631 ± .0028	3.267 ± .011
60010,31					
>45 μm	.0217 ± .0024	.1351 ± .0014	.6662 ± .0031	.6680 ± .0029	3.259 ± .012
<45 μm	.0184 ± .0040	.1317 ± .0020	.6602 ± .0025	.6605 ± .0037	3.262 ± .010
60010,38					
>45 μm	.0275 ± .0007	.1323 ± .0020	.6658 ± .0027	.6672 ± .0031	3.264 ± .007
<45 μm	.0214 ± .0011	.1304 ± .0007	.6592 ± .0013	.6602 ± .0013	3.262 ± .005

TABLE A9.7

Isotopic ratios of Xe in selected grain size fractions of Apollo 16 soils. Relative uncertainties given are one sigma of the mean of multiple measurements. Absolute ratios have an additional uncertainty of ±0.1%/mass unit.

Sample	$^{124}Xe/^{136}Xe$	$^{126}Xe/^{136}Xe$	$^{128}Xe/^{136}Xe$	$^{129}Xe/^{136}Xe$	$^{130}Xe/^{136}Xe$	$^{131}Xe/^{136}Xe$	$^{132}Xe/^{136}Xe$	$^{134}Xe/^{136}Xe$
60009,454								
<20 μm	.0199	.0214	.2833	3.451	0.5492	2.729	3.304	1.226
	±.0011	±.0006	±.0027	±.022	±.0039	±.018	±.018	±.009
<20 mag.	.0186	.0208	.2795	3.409	.5394	2.697	3.273	1.218
	±.0012	±.0013	±.0039	±.020	±.0037	±.014	±.014	±.012
60009,455								
250–150 μm	.0273	.0369	.2928	3.316	.5363	2.703	3.212	1.211
	±.0024	±.0023	±.0040	±.033	±.0073	±.030	±.028	±.014
<20 μm	.0187	.0207	.2816	3.418	.5393	2.708	3.282	1.222
	±.0008	±.0011	±.0028	±.027	±.0039	±.020	±.019	±.010
<20 mag	.0192	.0224	.2817	3.408	.5409	2.704	3.284	1.223
	±.0016	±.0016	±.0033	±.003	±.0061	±.025	±.023	±.015
60009,456								
90–75 μm	.0284	.0374	.3080	3.445	.5587	2.799	3.302	1.225
	±.0010	±.0016	±.0039	±.033	±.0071	±.027	±.029	±.013
<20 μm	.0195	.0225	.2885	3.477	.5507	2.745	3.311	1.227
	±.0007	±.0003	±.0022	±.017	±.0034	±.015	±.012	±.007
<20 mag.	.0181	.0206	.2786	3.407	.5355	2.697	3.275	1.217
	±.0009	±.0009	±.0030	±.018	±.0037	±.017	±.013	±.019
60009,457								
250–150 μm	.0227	.0296	.2901	3.290	.5343	2.702	3.200	1.204
	±.0021	±.0052	±.0032	±.038	±.0092	±.030	±.030	±.014
<20 μm	.0163	.0159	.2723	3.345	.5281	2.663	3.234	1.217
	±.0012	±.0017	±.0045	±.022	±.0054	±.019	±.016	±.012
<20 mag.	.0179	.0185	.2757	3.382	.5387	2.688	3.266	1.217
	±.0014	±.0010	±.0039	±.024	±.0075	±.018	±.017	±.012
60009,458								
250–150 μm	.0287	.0396	.3076	3.410	.5499	2.781	3.269	1.217
	±.0013	±.0006	±.0044	±.021	±.0037	±.016	±.016	±.009
<20 μm	.0193	.0212	.2845	3.458	.5472	2.732	3.304	1.228
	±.0006	±.0005	±.0020	±.018	±.0030	±.014	±.013	±.008

TABLE A9.7 (Continued)

< 20 mag.	.0184	.0203	.2776	3.403	.5381	2.691	3.266	1.218
	±.0010	±.0005	±.0036	±.025	±.0070	±.020	±.019	±.013
60010,17								
>45 μm	.0236	.0285	.2970	3.468	.5591	2.771	3.320	1.228
	±.0028	±.0024	±.0061	±.056	±.0146	±.042	±.048	±.025
<45 μm	.0186	.0231	.2857	3.439	.5499	2.733	3.289	1.214
	±.0036	±.0058	±.0057	±.038	±.0080	±.032	±.035	±.015
60010,31								
>45 μm	.0216	.0265	.2968	3.489	.5584	2.782	3.336	1.234
	±.0012	±.0012	±.0029	±.014	±.0033	±.011	±.008	±.007
<45 μm	.0163	.0182	.2840	3.452	.5484	2.754	3.307	1.231
	±0041	±.0059	± .0049	±.035	±.0085	±.040	±.032	±.014
60010,38								
>45 μm	.0213	.0255	.2923	3.439	.5485	2.748	3.306	1.222
	±.0013	±.0016	±.0036	±.022	±.0063	±.018	±.021	±.009
<45 μm	.0183	.0201	.2832	3.434	.5455	2.728	3.302	1.227
	±.0005	±.0011	±.0024	±.019	±.0034	±.015	±.016	±.008
60007,243								
150–250 μm	.0231	.0291	.2921	3.407	.5477	2.739	3.285	1.223
	±.0008	±.0005	±.0036	±.024	±.0076	±.019	±.021	±.010
<20 μm	.0174	.0177	.2783	3.427	.5440	2.719	3.308	1.226
	±.0004	±.0002	±.0019	±.011	±.0021	±.010	±.009	±.005
60007,217								
150–250 μm	.0254	.0310	.2935	3.417	.5473	2.754	3.287	1.225
	±.0006	±.0013	±.0026	±.024	±.0060	±.020	±.020	±.013
<20 μm	.0179	.0192	.2837	3.461	.5490	2.740	3.321	1.230
	±.0005	±.0006	±.0025	±.018	±.0041	±.015	±.016	±.007
65501,4								
1–.5 μm	.0796	.1327	.4684	3.682	.6598	3.358	3.402	1.240
	±.0021	±.0028	±.0101	±.050	±.0135	±.048	±.041	±.017
<20 μm	.0200	.0225	.2902	3.488	.5497	2.747	3.308	1.228
	±.0002	±.0004	±.0022	±.018	±.0038	±.014	±.015	±.009

TABLE A9.8

Isotopic ratios of the surface-correlated component and concentrations of the cosmogenic component (cm^3 STP/g) as determined by the ordinate-intercept technique. Uncertainties given for isotopic ratios and abundances are one sigma of the ordinate intercept and of the slope, respectively, as derived by a first order linear regression. Derivation of chemistry-corrected abundances for 60009 soils is described in the text. Data for 60010 soils were determined from only two grain size separates each. (a) These ^{3}He data are highly uncertain because of a large solar wind component and because of a greater relative uncertainty in ^{3}He/^{4}He measurements.

Sample	^{4}He/^{3}He	^{20}Ne/^{22}Ne	^{22}Ne/^{21}Ne	^{36}Ar/^{38}Ar	^{40}Ar/^{36}Ar	^{3}He 10^{-8}	^{21}Ne 10^{-8}	^{38}Ar 10^{-8}	^{80}Kr 10^{-11}	^{126}Xe 10^{-11}	Chemistry-Corrected ^{21}Ne.10^{-8}	Chemistry-Corrected ^{126}Xe.10^{-11}
60009,454	2535	12.63	31.6	—	≤1.78	83.4	41.2	—	—	—	41.2	—
	±25	±.08	±.6			±3.0	±2.2					
60009,455	2520	12.44	31.8	5.35	1.89	73	34.5	52.6	13.9	2.99	38.0	5.4
	±95	±.06	±.4	±.01	±.03	±8	±1.2	±4.0	±3.7	±.43		
60009,456	2585	12.56	31.0	5.34	1.64	112	52.9	73.2	34.0	9.08	≡52.9	≡9.08
	±65	±.05	±1.2	±.01	±.03	±9	±5.4	±3.2	±5.4	±1.11		
60009,457	2350	12.56	32.7	5.35	1.78	45	21.5	29.8	6.95	0.79	25.0	4.0
	±120	±.09	±2.4	±.01	±.06	±2.3	±3.0	±1.1	±1.25	±.28		
Plagioclase	—	—	—	—	—	4.5	17.8	24.3	—	—	25.0	—
60009,458	2565	12.50	31.8	5.33	1.80	119	57	78.1	33.1	7.94	57	8.0
	±90	±.08	±1.2	±.01	±.11	±15	±6	±6.7	±4.0	±.82		
60010,17	2555	12.50	31.5	5.30	1.07	(65)[a]	27	—	—	6.0 ± 1.2		
60010,24	2545	12.39	29.9	5.32	1.11	(40)[a]	19	44	—	—		
60010,31	2635	12.45	32.5	5.33	1.02	(99)[a]	28	62	—	7.2 ± 1.0		
60010,38	2570	12.48	31.6	5.32	1.02	(71)[a]	23	44	—	4.7 ± .8		
60007,243	2680	12.48	31.9	5.32	0.96	75	25.0	45	—	6.25		
	±36	±.04	±.6	±.02	±.01	±7.5	±2.5	±19		±.66		
60007,217	2560	12.41	31.4	5.33	1.11	52	20.3	50	18	3.81		
	±44	±.05	±.2	±.02	±.05	±5	±.6	±9	±4	±.48		
65501,4	≥2630	12.57	33.4	5.42	2.54	119 ± 14	59 ± 20	96 ± 15	—	—		
< 125 μ		±.06	±.3	±.02	±.04							
500–1000 μ		—	—	—	—	104 ± 2	59 ± 11	70 ± 5	35 ± 4	10.0 ± 1.0		

APPENDIX 10. Particle track data

The data points represent track densities found on individual plagioclase crystals (one point = one grain with a particular track density that has been converted to number of tracks per square centimeter) from Crozaz and Dust (1977). These counts were made using a light microscope. This data has been converted to frequency histograms on the far right. Histograms compiled from the data of Blanford et al. (1977) are presented to the left of the Crozaz and Dust histograms. The differences are discussed in Section 5.8 in the text.

Figure A10.1

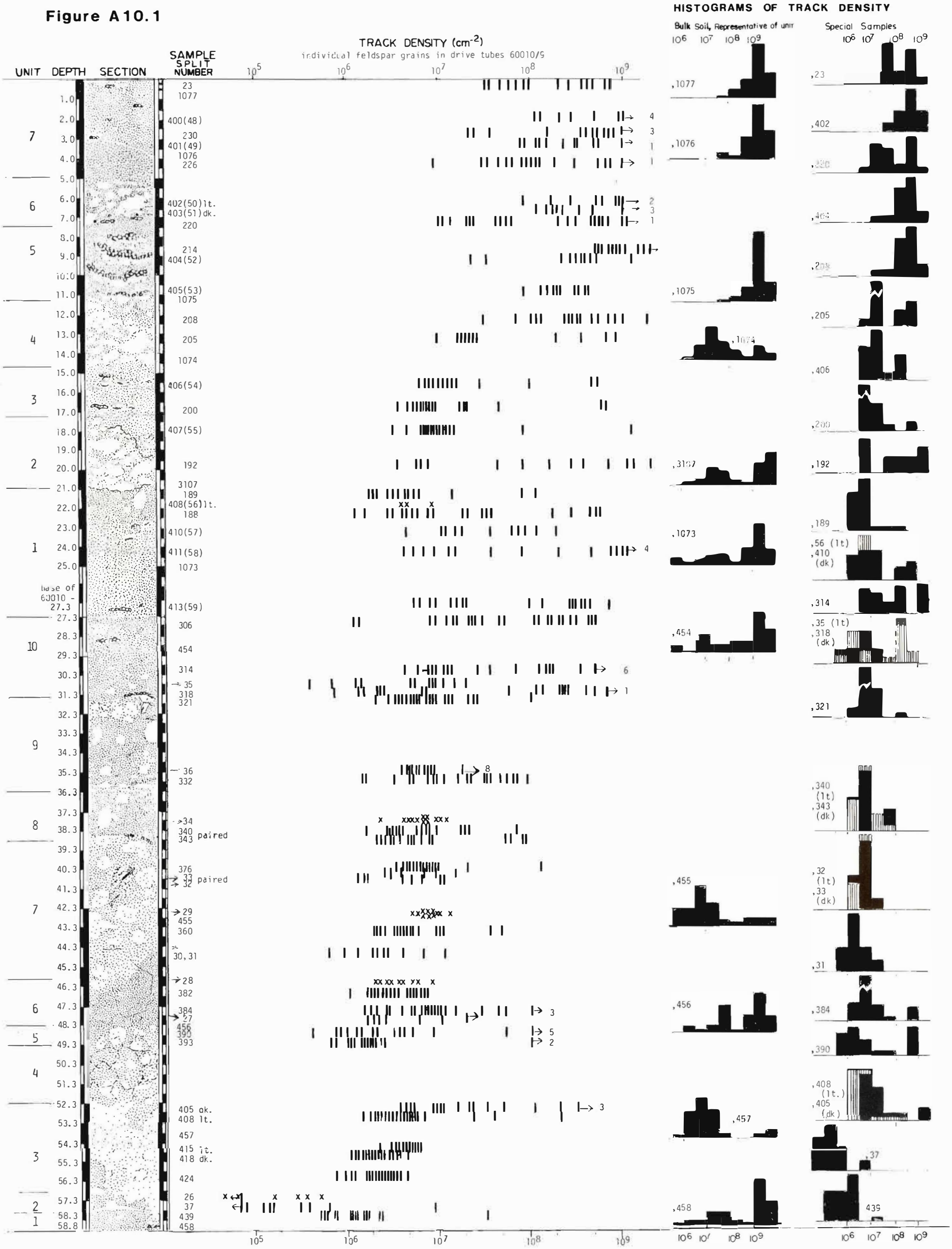
HISTOGRAMS OF TRACK DENSITY
Bulk Soil, Representative of unit
Special Samples
TRACK DENSITY (cm⁻²)
individual feldspar grains in drive tubes 60010/9
UNIT
DEPTH
SECTION
SAMPLE SPLIT NUMBER
base of 60010 - 27.3
paired
,1077
,1076
,1075
,1073
,3107
,454
,455
,456
,457
,458
,23
,402
,205
,192
,189
,56 (lt)
,410 (dk)
,314
,35 (lt)
,318 (dk)
,321
,340 (lt)
,343 (dk)
,32 (lt)
,33 (dk)
,31
,384
,390
,408 (lt.)
,405 (dk)
,37
439